uOttawa

L'Université canadienne
Canada's university

FACULTÉ DES ÉTUDES SUPÉRIEURES ET POSTOCTORALES

uOttawa

L'Université canadienne
Canada's university

FACULTY OF GRADUATE AND POSDOCTORAL STUDIES

Dmitrij Zelo

AUTEUR DE LA THÈSE / AUTHOR OF THESIS

M.Sc. (Mathematics)

GRADE / DEGREE

Department of Mathematics and Statistics

FACULTÉ, ÉCOLE, DÉPARTEMENT / FACULTY, SCHOOL, DEPARTMENT

Analysis and computation of fluid dynamics in a coupled free air porous domain

TITRE DE LA THÈSE / TITLE OF THESIS

A. Novruzi

DIRECTEUR (DIRECTRICE) DE LA THÈSE / THESIS SUPERVISOR

CO-DIRECTEUR (CO-DIRECTRICE) DE LA THÈSE / THESIS CO-SUPERVISOR

EXAMINATEURS (EXAMINATRICES) DE LA THÈSE / THESIS EXAMINERS

Y. Bourgault

L. Campbell

Gary W. Slater

LE DOYEN DE LA FACULTÉ DES ÉTUDES SUPÉRIEURES ET POSTDOCTORALES /
DEAN OF THE FACULTY OF GRADUATE AND POSTDOCORAL STUDIES

Analysis and computation of fluid dynamics in a coupled free air porous domain

D. Zelo

Thesis submitted to the
Faculty of Graduate and Postdoctoral Studies
In partial fulfillment of the requirements
For M.Sc. degree in mathematics

Department of Mathematics and Statistics
Faculty of Science
University of Ottawa

Your file Votre référence
ISBN: 0-494-11470-3
Our file Notre référence
ISBN: 0-494-11470-3

Contents

List of Figures

List of Tables

Acknowledgments

I would like to express my gratitude to all professors of the University of Ottawa and Carleton University who taught me during my studies. I am very indebted to my supervisor, professor Arian Novruzi, for his support, helpful suggestions and general direction of my research.

I am very thankful to all members of the Ottawa-Carleton Institute of Mathematics and Statistics for recommending me and to the board of the Faculty of Graduate and Postdoctoral studies for admitting me to the MSc program, for giving me financial support and the opportunity to study and work at the Department of Mathematics and Statistics.

I am very thankful to Stephane Gauthier for his help with Linux OS.

Ottawa, November 2004

Dmitrij Zelo

Abstract

We present analysis and computations of a 2D steady-state fluid dynamics in a coupled free air and porous domain. The 2D model is a simplification of the Hydrogen Fuel Cell (HFC) fluid dynamics for the case of one gas component and constant temperature.

The problem involves the Stokes equation and the mass conservation equation in the cathode channel and the Darcy equation with the mass conservation equation in the porous gas diffusive layer (GDL). On the interface are imposed the Saffman's condition, continuity of the pressure and the normal velocity.

Our main concern here is to find and implement an efficient computational method for solving the problem with a real data and a coupled domain with large aspect ratio.

For this purpose we implement the finite element method with the classical MINI finite element space for the velocity in the channel and the P1 finite element space for the pressure in the channel and GDL.

The resulting linear system is solved by using the iterative Gauss-Seidel overlapping block method and alternatively with the direct Gaussian Elimination method.

Existence and uniqueness of the weak solution is proved only for the problem with the reduced Saffman's condition on the interface.

1

Introduction

There are many important problems involving coupling of processes in two or more different media with common boundaries. These media can have different qualities and those processes can be governed by different laws. The dynamics in different media are coupled to each other by some conditions which are imposed on the common boundaries. Some of the problems that fall under this framework are:

- Design of hydrogen fuel cells (HFC);
- Problem of coupling between groundwater and surface water in order to predict how pollutions discharge into rivers;
- Technological applications involving filtration.

The motivation of this work comes from fluid dynamics in free air channels and porous gas diffusive layers of a HFC. HFCs are composed of a set of layered domains (see Figure 1.1). The oxygen of the cathode channel diffuses through the porous cathode GDL. The hydrogen flows into the anode channel and diffuses through the porous anode GDL. HFCs produce electricity by means of a chemical reaction between oxygen and hydrogen without combustion. The oxygen reduction reaction occurs in the cathode catalyst layer and the membrane. The only by-products of a HFC are H_2O and heat.

3D HFC fluid dynamics on each domain level is governed by a system of nonlinear PDEs such as the Navier-Stokes equation, the Darcy equation, the mass and heat conservation equations for each component of the fluid, such as oxygen, hydrogen, water vapour and nitrogen.

Our $2D$ model is a simplification of the 3D HFC model by considering steady state, dry, single component, isothermal fluid dynamics in the cathode channel and the GDL. Our model includes the steady state Stokes equation and the mass conservation equation in the cathode channel and the Darcy equation with mass conservation equation in the GDL. As coupling conditions on the interface between the channel and the porous GDL domain are imposed the Saffman's condition for the tangential velocity and the Darcy equation. The pressure and the normal velocity are supposed to be continuous on the interface. However some authors [6] admit discontinuity of the pressure on the interface.

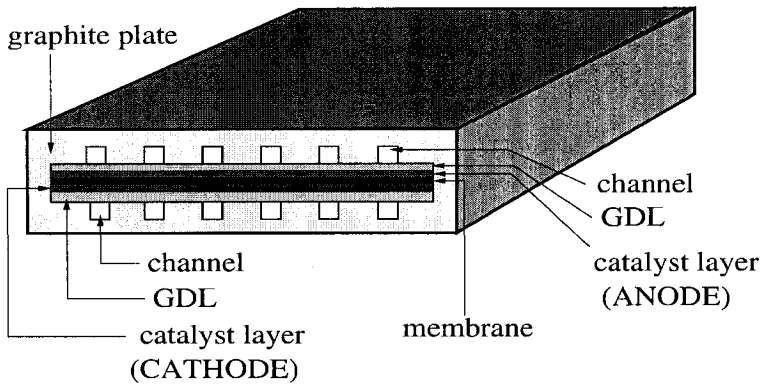

Figure 1.1: A stack of fuel cells.

There are two different approaches for finding an approximate solution of coupled multidomain and multiprocess problems. One of them is domain decomposition and decoupling of the solutions that leads to many separate problems which are supposed to be solved independently and coupled again. Our approach is based on finding of such an approximate solution which is valid for the whole domain without preliminary decomposition and decoupling. Our choice is motivated by the idea to solve precisely the interface coupling.

The problem admits implementation of the finite element method with a classical MINI finite element space for the velocity in the channel and a P1 finite element space for the pressure in the channel and the GDL. In the computational method is considered the equivalent system which is the Laplace equation for the pressure in the GDL, the Stokes equation and the mass conservation law equation in the channel. An approximate solution gives the velocity in the channel and the pressure in the channel and in the GDL. The velocity in the GDL can be found from the Darcy law equation that significantly reduces computations.

For the real data and a domain with large aspect ratio the resulting linear system with a sparse banded matrix is solved by the iterative Gauss-Seidel overlapping block method. This iterative method taking advantage of the block structure of the matrix gives accurate results, allows effective storage of the matrix and is almost twice faster then the direct Gaussian Elimination method. The iterative Gauss-Seidel overlapping block method also works fast and with the same precision for large matrices when the direct method is not efficient because of PC memory and CPU time consumption.

2

Mathematical model

Here we present the full 3D multicomponent HFC dry model and show how it can be reduced to the 2D single component model by concentrating only on the gas dynamics in the channel and the GDL. The gas dynamics in different coupled layers, in particular in the channel and the GDL, is very important for understanding the gas dynamics of HFCs.

2.1 The 3D multicomponent model

HFCs consist of the following components:

- **Cathode:**
  - Cathode channel;
  - Cathode gas diffusive layer;
  - Cathode catalyst layer: air region, carbon region, membrane region;
- **Membrane.**
- **Anode:**
  - Anode channel;
  - Anode gas diffusive layer;
  - Anode catalyst layer: air region, carbon region, membrane region;

The parameters $a_1, a_2, a_3, b_1, b_2 > 0$ prescribe the sizes of the HFC and the domains are defined as follows:

$$\begin{cases} \Omega_{GDL} = (0, 2a_1 + b_1) \times (0, a_2) \times (0, a_3), \\ \Omega_{CH} = (a_1, a_1 + b_1) \times (a_2, a_2 + b_2) \times (0, a_3), \\ \overline{\Omega} = \overline{\Omega}_{CH} \cup \overline{\Omega}_{GDL}. \end{cases} \tag{2.1.1}$$

The domain Ω_{GDL} represents the porous media (GDL) and Ω_{CH} represents the free air domain (channel).

On Figure 2.1 it is shown the interior design of a HFC and schematic behavior of the gas.

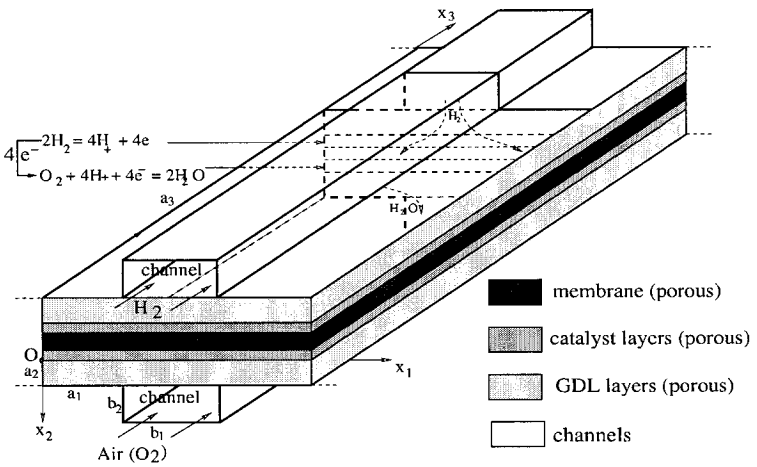

Figure 2.1: The interior design of the cathode, anode and membrane of a HFC.

Let us introduce the parameters of the 3D multicomponent model:

1. **Unknowns:**

   - c_O, c_v, c_N are the molar concentration of oxygen, vapour and nitrogen respectively which together represent a gas mixture that we simply call the gas; c_N can be found from the equation $c = c_O + c_v + c_N$;
   - T is the temperature of the gas;
   - P is the pressure of the gas;
   - $\mathbf{u} = (u_1, u_2, u_3)$ is the velocity of the gas.

2. **Constants:**

   - c is the total molar mass;
   - $\rho = M_O c_O + M_v c_v + M_N c_N$ is density of the gas which is considered incompressible;
   - M_O, M_v, M_N are molar masses of oxygen, vapour and nitrogen respectively;
   - D_O, D_v, D_N are diffusivity of oxygen, vapour and nitrogen, respectively;
   - c_T is specific heat of the gas;
   - k_C is thermal conductivity of carbon phase;
   - K is permeability;
   - S depends on the pore size and the shape of the GDL;

- μ is viscosity of the gas.

Restricting our interest to the cathode channel and the GDL, the 3D HFC dry model dynamics according to [3] is governed by the following equations:

The channel domain

$$\nabla \cdot (c_O \mathbf{u} - D_O \nabla \frac{c_O}{c}) = 0 \quad in\ \Omega_{CH}, \tag{2.1.2}$$

$$\nabla \cdot (c_v \mathbf{u} - D_v \nabla \frac{c_v}{c}) = 0 \quad in\ \Omega_{CH}, \tag{2.1.3}$$

$$\nabla \cdot (c_N \mathbf{u} - D_N \nabla \frac{c_N}{c}) = 0 \quad in\ \Omega_{CH}, \tag{2.1.4}$$

$$\nabla \cdot (c_T \rho T \mathbf{u} - k_C \nabla T) = 0 \quad in\ \Omega_{CH}, \tag{2.1.5}$$

$$\nabla \cdot (\rho \mathbf{u}) = 0 \quad in\ \Omega_{CH}, \tag{2.1.6}$$

$$-\mu \Delta \mathbf{u} + \rho(\mathbf{u} \cdot \nabla)\mathbf{u} + \nabla P = 0 \quad in\ \Omega_{CH}. \tag{2.1.7}$$

The GDL domain

$$\nabla \cdot (c_O \mathbf{u} - D_O \nabla \frac{c_O}{c}) = 0 \quad in\ \Omega_{GDL}, \tag{2.1.8}$$

$$\nabla \cdot (c_v \mathbf{u} - D_v \nabla \frac{c_v}{c}) = 0 \quad in\ \Omega_{GDL}, \tag{2.1.9}$$

$$\nabla \cdot (c_N \mathbf{u} - D_N \nabla \frac{c_N}{c}) = 0 \quad in\ \Omega_{GDL}, \tag{2.1.10}$$

$$\nabla \cdot (c_T \rho T \mathbf{u} - k_C \nabla T) = 0 \quad in\ \Omega_{GDL}, \tag{2.1.11}$$

$$\nabla \cdot (\rho \mathbf{u}) = 0 \quad in\ \Omega_{GDL}, \tag{2.1.12}$$

$$\mathbf{u} + \frac{K}{\mu} \nabla P = 0 \quad in\ \Omega_{GDL}. \tag{2.1.13}$$

Conditions on the interface between the channel and the GDL

The equations (2.1.2)-(2.1.13) in the channel and the GDL are equipped with boundary conditions. Most of them are straightforward and come from clear physical considerations. However, the boundary conditions on the interface between the channel and the GDL are particularly important and are object of different research (see [3]). For this reason we present these interface conditions here.

$$[c_O] = 0, \tag{2.1.14}$$

$$[c_O\ \mathbf{u} - D_O \nabla \frac{c_O}{c}] \cdot \mathbf{n} = 0, \tag{2.1.15}$$

$$[c_v] = 0, \tag{2.1.16}$$

$$[c_v\ \mathbf{u} - D_v \nabla \frac{c_v}{c}] \cdot \mathbf{n} = 0, \tag{2.1.17}$$

$$[c_N] = 0, \tag{2.1.18}$$

$$[c_N\ \mathbf{u} - D_N \nabla \frac{c_N}{c}] \cdot \mathbf{n} = 0, \tag{2.1.19}$$

$$[T] = 0, \tag{2.1.20}$$

$$[c_T\ \rho\ \mathbf{u} - \mathcal{K}\ \nabla T] \cdot \mathbf{n} = 0, \tag{2.1.21}$$

$$[\mathbf{u}] \cdot \mathbf{n} = 0, \tag{2.1.22}$$

$$[P] = 0, \tag{2.1.23}$$

$$(\frac{\partial \mathbf{u}}{\partial \mathbf{n}} - S\mathbf{u}) \cdot \boldsymbol{\tau} = 0, \tag{2.1.24}$$

where $\mathbf{n}$ and $\boldsymbol{\tau}$ are outward normal and tangent unit vectors to the boundaries of Ω, Ω_{CH} and Ω_{GDL}.

Suppose that (2.1.13) holds also on the interface and then from (2.1.22) follows

$$\mathbf{u} \cdot \mathbf{n}|_{channel\ side} + \frac{K}{\mu} \nabla P \cdot \mathbf{n}|_{GDL\ side} = 0. \tag{2.1.25}$$

2.2 The 2D one component model

Our model describes a steady-state 2D incompressible fluid flow in two rectangular domains Ω_0 (Channel) and Ω_1 (GDL) with the common boundary Σ (Interface) as it is shown on Figure 2.2. This model can be deduced from the 3D model when one considers a cross section of the cathode (or anode) of a HFC in the plane (x_2, x_3) (see Figure 2.1). We consider only one gas component with constant molar concentration, temperature and density in the channel and the GDL. Then the equations (2.1.2)-(2.1.13) are reduced only to (2.1.6)-(2.1.7) in the channel and to (2.1.12)-(2.1.13) in the GDL. The model that one obtains is as follows:

$$\begin{cases} \Omega_0 &= (0,l)\times(-H,0), \\ \Omega_1 &= (0,l)\times(0,h), \\ \Gamma &= (0,l)\times\{-H\}, \\ \Gamma_{in} &= \{0\}\times(-H,0), \\ \Gamma_{out} &= \{l\}\times(-H,0), \\ \Sigma &= (0,l)\times\{0\}, \\ M &= (0,l)\times\{h\}, \\ \Gamma_{iw} &= \{0\}\times(0,h), \\ \Gamma_{ow} &= \{l\}\times(0,h), \end{cases} \tag{2.2.1}$$

where constants $L, H, h > 0$ are the length of a HFC, the height of the channel and the height of the GDL, respectively. Let $\Omega = \Omega_0 \cup \Omega_1 \cup \Sigma$.

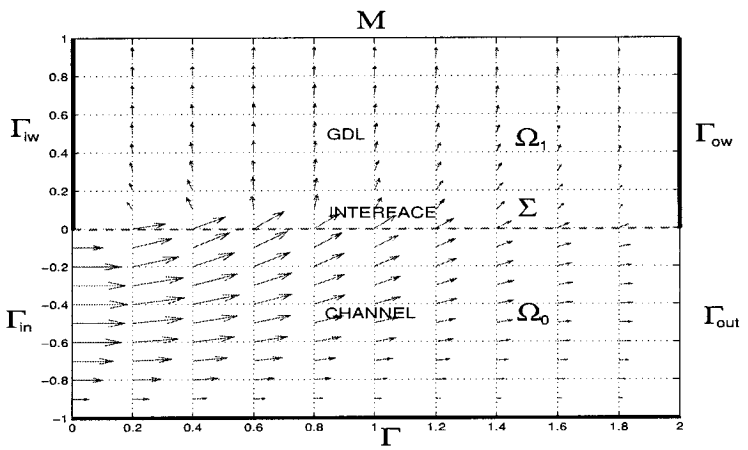

Figure 2.2: A fluid flow in a rectangular domain.

In both domains the fluid flow satisfies the mass conservation equation. In Ω_1 it satisfies

the Darcy equation:

$$\begin{cases} \nabla \cdot \mathbf{u} &= 0, \\ \mathbf{u} &= -\dfrac{K}{\mu}\nabla p, \end{cases} \quad in\ \Omega_1. \tag{2.2.2}$$

In Ω_0 it also satisfies the Stokes equation:

$$\begin{cases} \nabla \cdot \mathbf{u} &= 0, \\ -\mu\Delta\mathbf{u} + \nabla p &= 0, \end{cases} \quad in\ \Omega_0. \tag{2.2.3}$$

A classical solution of the problem is a vector function $\mathbf{u} = (u_1, u_2)$ and a function p such that $\mathbf{u} \in \boldsymbol{\mathcal{U}}$, $p \in \mathcal{P}$, where the velocity space $\boldsymbol{\mathcal{U}}$ and the pressure space $\mathcal{P}$ are defined as follows:

$$\begin{cases} \boldsymbol{\mathcal{U}} = \{\boldsymbol{u} \mid \mathbf{u}_{|\bar{\Omega}_0} \in (C^0(\bar{\Omega}_0) \cap C^1(\bar{\Omega}_0 \setminus \Gamma) \cap C^2(\Omega_0))^2, \\ \qquad\qquad \mathbf{u}_{|\bar{\Omega}_1} \in (C^0(\bar{\Omega}_1) \cap C^1(\Omega_1))^2,\ u_2 \in C^0(\bar{\Omega})\}, \\ \mathcal{P} = \{\, p \mid p \in C^0(\bar{\Omega}),\ p_{|\Omega_0} \in C^1(\Omega_0),\ p_{|\Omega_1} \in C^2(\Omega_1)\}. \end{cases} \tag{2.2.4}$$

We see that the tangential velocity u_1 may have discontinuity on the interface Σ.

In order to understand the behavior of the solution in the inlet and outlet/interface contact points we also consider the same problem (2.2.2)-(2.2.3) in a domain like in (2.2.1) but slightly modified: $\Omega_0 = (0 - \delta, L + \delta) \times (-H, 0)$, where $\delta > 0$ is some small constant and Ω_1 is the same (see Figure 2.3).

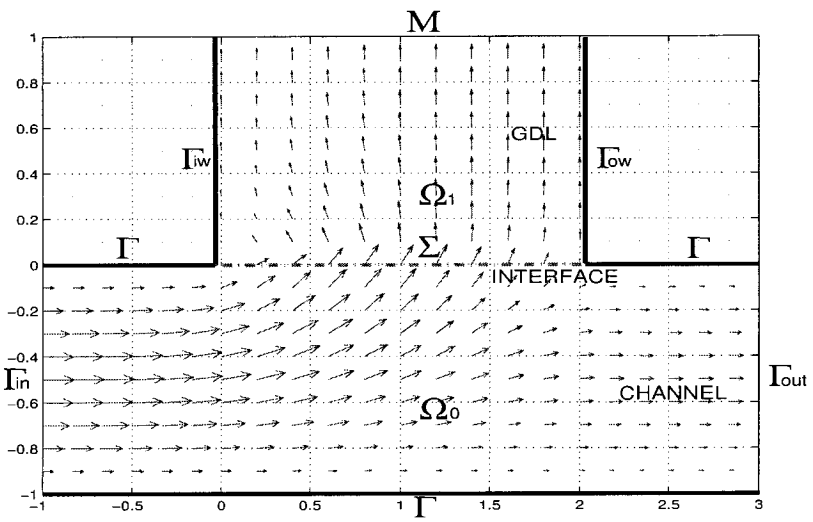

Figure 2.3: A fluid flow in a rectangular domain with modified Ω_0.

2.2.1 Boundary conditions

The set of equations (2.2.2)-(2.2.3) can be equipped with the following boundary conditions:

- The following are the basic boundary conditions where the pressure is prescribed on the inlet, outlet and membrane:

$$\begin{cases} \mathbf{u} = 0, & & on \ \Gamma, \\ u_2 = 0, & p = p_{in}, & on \ \Gamma_{in}, \\ u_2 = 0, & p = p_{out}, & on \ \Gamma_{out}, \\ u_2 = u_m, & (or\ p = p_m), & on \ M, \\ \partial_1 p = 0, & (or\ u_1 = 0), & on \ \Gamma_{iw} \cup \Gamma_{ow}. \end{cases} \tag{2.2.5}$$

- Alternatively boundary conditions can be imposed where the velocity u_1 is given on the inlet:

$$\begin{cases} \mathbf{u} = 0, & & on \ \Gamma, \\ u_1 = u_{in}, & u_2 = 0, & on \ \Gamma_{in}, \\ u_2 = 0, & p = p_{out}, & on \ \Gamma_{out}, \\ p = p_m, & & on \ M, \\ \partial_1 p = 0, & (or\ u_1 = 0), & on \ \Gamma_{iw} \cup \Gamma_{ow}. \end{cases} \tag{2.2.6}$$

  - K, μ are given constants;
  - p_{in}, p_{out}, p_m, u_{in}, u_m are given functions.

2.2.2 Interface conditions

Conditions on the interface Σ should be imposed in order to couple solutions in the channel and the GDL. On the interface we impose continuity of the normal velocity and the pressure, Darcy law and Saffman's condition (see [5] and [12]):

$$\begin{cases} u_2 \mid_{(\Omega_0 \ side)} = -\dfrac{K}{\mu} \partial_2 p \mid_{(\Omega_1 \ side)}, \\ \partial_2 u_1 = -S\, u_1, & on \ \Sigma, \\ [u_2] = 0, \\ [p] = 0, \end{cases} \tag{2.2.7}$$

where S is a given constant.

At this point we are not able to prove the theorem of existence and uniqueness of the solution of the problem (2.2.2)-(2.2.3) with boundary conditions (2.2.5) and interface conditions (2.2.7). However, if we replace (2.2.7) with the following interface conditions:

$$\begin{cases} u_2 \mid_{(\Omega_0 \ side)} = -\dfrac{K}{\mu}\, \partial_2 p \mid_{(\Omega_1 \ side)}, \\ u_1 = g(\mathbf{x}), \qquad on\ \Sigma, \\ [u_2] = 0, \\ [p] = 0, \end{cases} \tag{2.2.8}$$

where g is a given function such that $g(\mathbf{x})_{|\partial\Sigma} = 0$, then we can obtain existence and uniqueness result.

Remark 2.2.1 *The second equation in (2.2.8) can be considered as similar to the original Saffman's condition if the function $g(\mathbf{x})$ is close to porosity of the GDL. Indeed, since for the real HFCs the value of the coefficient S in (2.2.7) is very large then it makes sense to consider the limit case of the Saffman's condition in (2.2.7) when $S \to \infty$. So, we assume $S^{-1}\partial_2 u_1 \to 0$. In general, as a limit case we can take $u_1 = g(\mathbf{x})$ on Σ.*

Remark 2.2.2 *Some authors (see [6]) suppose the pressure to be discontinuous on the interface and consider the following condition:*

$$[p] = 2\ \mu\ \mathbf{n_1} \cdot \mathbf{D}(\mathbf{u}_{|GDL\ side}) \cdot\ \mathbf{n_1}, \tag{2.2.9}$$

where $\mathbf{D}(\mathbf{u}) = \frac{1}{2}(\frac{\partial u_i}{\partial x_j} + \frac{\partial u_j}{\partial x_i})$ is the deformation rate tensor and $\mathbf{n_1}$ is an outward normal vector to the interface from the porous domain side.

3

Existence and uniqueness

In this chapter we derive a weak formulation of the problem (2.2.2)-(2.2.3) and prove existence and uniqueness of the solution for the boundary conditions (2.2.5) when the normal velocity u_2 is prescribed on the membrane M and the conditions (2.2.8) are imposed on the interface.

3.1 Weak formulation

Following the classical approach to the general compliance problem, as it is shown in [4] M. DELFOUR, J.-P. ZOLÉSIO, pp.108, we use the characteristic functions $\mathbb{1}_{\Omega_0}$ and $\mathbb{1}_{\Omega_1}$ of the domains Ω_0 and Ω_1, respectively, in order to transform our problem (2.2.2)-(2.2.3) into the equivalent form:

$$\begin{cases} \mathbf{u} \in \boldsymbol{\mathcal{U}} \ , \ p \in \mathcal{P}, & \\ (-\mu \ \Delta \mathbf{u} + \nabla p) \ \mathbb{1}_{\Omega_0} + (\dfrac{\mu}{K} \mathbf{u} + \nabla p) \ \mathbb{1}_{\Omega_1} &= 0, \\ \nabla \cdot \mathbf{u} &= 0, \end{cases} \tag{3.1.1}$$

with boundary conditions:

$$\begin{cases} \mathbf{u} = 0, & on \quad \Gamma, \\ u_2 = 0, \ p = p_{in}, & on \quad \Gamma_{in}, \\ u_2 = 0, \ p = p_{out}, & on \quad \Gamma_{out}, \\ u_1 = 0, & on \quad \Gamma_{iw} \cup \Gamma_{ow}, \\ u_2 = u_m, & on \quad M. \end{cases} \tag{3.1.2}$$

where $u_m \in C^0(M)$, $p_{in} \in C^0(\Gamma_{in})$, $p_{out} \in C^0(\Gamma_{out})$.

On the interface Σ we impose the Darcy law and the reduced Saffman's condition:

$$\begin{cases} u_2 \mid_{(\Omega_0 \ side)} &= -\dfrac{K}{\mu}\, \partial_2 p \mid_{(\Omega_1 \ side)}, \\ u_1 &= g(x_1), \\ [u_2] &= 0, \\ [p] &= 0, \end{cases} \tag{3.1.3}$$

where $g(x_1) \in H_0^1(\Sigma)$.

Let us define the velocity functional set $\boldsymbol{\mathcal{U}}_{div}$, the pressure functional set $\mathcal{Q}$ which have boundary conditions and the Saffman's condition integrated and the velocity functional space $\boldsymbol{\mathcal{U}}^0_{div}$ as follows:

$$\begin{cases} \boldsymbol{\mathcal{U}}_{div} = \{\boldsymbol{\phi} = (\phi_1, \phi_2) \in \boldsymbol{\mathcal{U}} \mid & \nabla \cdot \boldsymbol{\phi} = 0, \\ & \phi_{1|\Gamma \cup \Gamma_{iw} \cup \Gamma_{ow}} = 0, \ \phi_{1|\Sigma} = g(x_1), \\ & \phi_{2|\Gamma \cup \Gamma_{in} \cup \Gamma_{out}} = 0, \ \phi_{2|M} = u_m \ \}, \\ \boldsymbol{\mathcal{U}}^0_{div} = \{\boldsymbol{\phi} = (\phi_1, \phi_2) \in \boldsymbol{\mathcal{U}} \mid & \nabla \cdot \boldsymbol{\phi} = 0, \\ & \phi_{1|\Gamma \cup \Gamma_{iw} \cup \Gamma_{ow} \cup \Sigma} = 0, \\ & \phi_{2|\Gamma \cup \Gamma_{in} \cup \Gamma_{out} \cup M} = 0\}, \\ \mathcal{Q} \quad = \{p \in \mathcal{P} \mid p_{|\Gamma_{in}} = p_{in}, & p_{|\Gamma_{out}} = p_{out} \ \}. \end{cases} \tag{3.1.4}$$

The problem (3.1.1)-(3.1.3) takes an equivalent form:

$$\begin{cases} \mathbf{u} \in \boldsymbol{\mathcal{U}}_{div} \ , \ p \in \mathcal{Q}, \\ (-\mu \Delta \mathbf{u} + \nabla p)\ \mathbb{1}_{\Omega_0} + (\dfrac{\mu}{K}\, \mathbf{u} + \nabla p)\ \mathbb{1}_{\Omega_1} \ = \ 0. \end{cases} \tag{3.1.5}$$

Let us consider the closures $\mathbf{U^0_{div}}$ and $\mathbf{U_{div}}$ of the subspace $\boldsymbol{\mathcal{U}}^0_{div}$ and subset $\boldsymbol{\mathcal{U}}_{div}$, respectively, in the Hilbert space $\{\boldsymbol{\phi} = (\phi_1, \phi_2) \in (L^2(\Omega))^2 \mid \boldsymbol{\phi}_{|\Omega_0} \in (H^1(\Omega_0))^2\}$ with the norm defined as follows:

$$||\cdot||^2 = ||\cdot||^2_{H^1(\Omega_0)} + ||\cdot||^2_{L^2(\Omega_1)}. \tag{3.1.6}$$

We need all these spaces and sets for defining a weak form of our problem.

Remark 3.1.1 *In Section 3.2 it will be shown that if $u_m \in L^1(M)$ then $\mathbf{U_{div}} \neq \emptyset$.*

Remark 3.1.2 *The functional space $\mathbf{U^0_{div}}$ inherits the norm $||\cdot||$ in (3.1.6) from the larger space $\{\boldsymbol{\phi} = (\phi_1, \phi_2) \in (L^2(\Omega))^2 \mid \boldsymbol{\phi}_{|\Omega_0} \in (H^1(\Omega_0))^2\}$. Applying the Poincaré inequality (see [8] Quarteroni, Valli, p.11.) in Ω_0 we obtain an equivalent norm as follows:*

$$||\boldsymbol{\phi}||^2_{\mathbf{U^0_{div}}} = ||\nabla \boldsymbol{\phi}||^2_{L^2(\Omega_0)} + ||\boldsymbol{\phi}||^2_{L^2(\Omega_1)}, \ \forall \boldsymbol{\phi} \in \mathbf{U^0_{div}}. \tag{3.1.7}$$

Multiplying both sides of the (3.1.5) by an arbitrary vector function $\boldsymbol{\phi} \in \boldsymbol{\mathcal{U}}^0_{div}$, integrating in Ω and applying Green's formula, we obtain the integral form of the problem which is equivalent to its differential form (3.1.5):

$$\left\{ \begin{array}{l} \textit{find } (\mathbf{u}, p) \in \boldsymbol{\mathcal{U}}_{div} \times \mathcal{Q}, \textit{ such that } \forall \boldsymbol{\phi} \in \boldsymbol{\mathcal{U}}^0_{div} \textit{ satisfies :} \\ \mu \int_{\Omega_0} \nabla \mathbf{u} \cdot \nabla \boldsymbol{\phi} - \mu \int_{\partial\Omega_0} \dfrac{\partial \mathbf{u}}{\partial \boldsymbol{\nu}_0} \cdot \boldsymbol{\phi} + \dfrac{\mu}{K} \int_{\Omega_1} \mathbf{u} \cdot \boldsymbol{\phi} - \int_{\Omega} p \, (\nabla \cdot \boldsymbol{\phi}) + \int_{\partial\Omega} p \, (\boldsymbol{\phi} \cdot \boldsymbol{\nu}) = 0, \end{array} \right. \tag{3.1.8}$$

where $\boldsymbol{\nu}_0$ and $\boldsymbol{\nu}$ are outward normal vectors to the boundaries $\partial\Omega_0$ and $\partial\Omega$ respectively. The equation (3.1.8) can be simplified by using the boundary conditions for the pressure and the definition of the space $\boldsymbol{\mathcal{U}}^0_{div}$. Indeed, we have:

$$\int_{\Omega} p \, (\nabla \cdot \boldsymbol{\phi}) \;=\; 0 \;, \quad \textit{since } \nabla \cdot \boldsymbol{\phi} = 0. \tag{3.1.9}$$

From the following facts:

$$\left\{ \begin{array}{lcl} \partial\Omega & = & (\Gamma_{in} \cup \Gamma_{out} \cup M) \cup (\Gamma_{iw} \cup \Gamma_{ow} \cup \Gamma), \\ \int_{\Gamma_{in} \cup \Gamma_{out} \cup M} p \, (\boldsymbol{\phi} \cdot \boldsymbol{\nu}) & = & - \int_{\Gamma_{in}} p_{in} \, \phi_1 + \int_{\Gamma_{out}} p_{out} \, \phi_1, \\ \int_{\Gamma_{iw} \cup \Gamma_{ow} \cup \Gamma} p \, (\boldsymbol{\phi} \cdot \boldsymbol{\nu}) & = & 0 \;, \quad \textit{since } \boldsymbol{\phi} \cdot \boldsymbol{\nu}_{|\Gamma_{iw} \cup \Gamma_{ow} \cup \Gamma} = 0, \end{array} \right. \tag{3.1.10}$$

we can deduce that

$$\int_{\partial\Omega} p \, (\boldsymbol{\phi} \cdot \boldsymbol{\nu}) \;=\; - \int_{\Gamma_{in}} p_{in} \, \phi_1 + \int_{\Gamma_{out}} p_{out} \, \phi_1. \tag{3.1.11}$$

Finally, from the following facts:

$$\left\{ \begin{array}{ll} \int_{\Gamma_{in}} \partial_2 u_2 \, \phi_1 & = 0, \text{ since } u_{2|\Gamma_{in}} = 0, \\ \int_{\Gamma_{in}} \partial_1 u_2 \, \phi_2 & = 0, \text{ since } \phi_{2|\Gamma_{in}} = 0, \\ \int_{\Gamma} \partial_2 \mathbf{u} \cdot \boldsymbol{\phi} & = 0, \text{ since } \boldsymbol{\phi}_{|\Gamma} = 0, \\ \int_{\Sigma} \partial_2 u_1 \, \phi_1 & = 0, \text{ since } \phi_{1|\Sigma} = 0, \\ \int_{\Sigma} \partial_1 u_1 \, \phi_2 & = \int_{\Sigma} g'(x_1) \, \phi_2, \text{ since } u_{1|\Sigma} = g(x_1), \\ \int_{\Gamma_{in}} \partial_1 \mathbf{u} \cdot \boldsymbol{\phi} & = \int_{\Gamma_{in}} (\partial_1 u_1 \, \phi_1 + \partial_1 u_2 \, \phi_2) = \int_{\Gamma_{in}} (-\partial_2 u_2 \, \phi_1 + \partial_1 u_2 \, \phi_2), \\ \int_{\Gamma_{out}} \partial_1 \mathbf{u} \cdot \boldsymbol{\phi} & = \int_{\Gamma_{out}} (\partial_1 u_1 \, \phi_1 + \partial_1 u_2 \, \phi_2) = \int_{\Gamma_{out}} (-\partial_2 u_2 \, \phi_1 + \partial_1 u_2 \, \phi_2), \\ \int_{\Sigma} \partial_2 \mathbf{u} \cdot \boldsymbol{\phi} & = \int_{\Sigma} (\partial_2 u_1 \, \phi_1 + \partial_2 u_2 \, \phi_2) = \int_{\Sigma} (\partial_2 u_1 \, \phi_1 - \partial_1 u_1 \, \phi_2). \end{array} \right. \tag{3.1.12}$$

we can deduce that:

$$\int_{\partial\Omega_0} \frac{\partial \mathbf{u}}{\partial \boldsymbol{\nu}_0} \cdot \boldsymbol{\phi} \;=\; - \int_{\Sigma} g'(x_1) \, \phi_2. \tag{3.1.13}$$

Remark 3.1.3 *The expression* $\partial_1 u_{1|\Gamma_{in}\cup\Gamma_{out}\cup\Sigma} = -\partial_2 u_2$ *that we use in (3.1.12) follows from the equation* $\nabla \cdot \mathbf{u} = 0$ *and the condition* $\mathbf{u}_{|\bar{\Omega}_0\setminus\Gamma} \in (C^1(\bar{\Omega}_0 \setminus \Gamma))^2$ *in the definition of the velocity space* $\boldsymbol{\mathcal{U}}$ *in (2.2.4).*

After substitution of the values of the integrals (3.1.9), (3.1.11) and (3.1.13) into the integral form (3.1.8) of the problem we have the final integral form of our problem, where the pressure unknown p is not involved:

$$\begin{cases} \textit{find } \mathbf{u} \in \boldsymbol{\mathcal{U}}_{div}, \textit{ such that } \forall \boldsymbol{\phi} \in \boldsymbol{\mathcal{U}}^0_{div} \textit{ satisfies :} \\ \mu \int_{\Omega_0} \nabla \mathbf{u} \cdot \nabla \boldsymbol{\phi} + \frac{\mu}{K} \int_{\Omega_1} \mathbf{u} \cdot \boldsymbol{\phi} = \int_{\Gamma_{in}} p_{in}\ \phi_1 - \int_{\Gamma_{out}} p_{out}\ \phi_1 - \int_{\Sigma} g'(x_1)\ \phi_2. \end{cases} \tag{3.1.14}$$

The left hand side of (3.1.14) is a bilinear form of $\mathbf{u}$, $\boldsymbol{\phi}$ and the right hand side is a linear functional of $\boldsymbol{\phi}$ which are both continuous in the norm $||\cdot||_{\mathbf{U^0_{div}}}$ of the space $\mathbf{U^0_{div}}$ (see (3.1.7)). Since $\boldsymbol{\mathcal{U}}^0_{div}$ is dense in $\mathbf{U^0_{div}}$ and $\boldsymbol{\mathcal{U}}_{div}$ is dense in $\mathbf{U_{div}}$ then the problem (3.1.14) can have a weaker form. This weaker form is called the weak formulation of the problem (3.1.5) and looks as follows:

$$\begin{cases} \textit{find } \mathbf{u} \in \boldsymbol{U}_{div}, \textit{ such that } \forall \boldsymbol{\phi} \in \boldsymbol{U}^0_{div} \textit{ satisfies :} \\ \mu \int_{\Omega_0} \nabla \mathbf{u} \cdot \nabla \boldsymbol{\phi} + \frac{\mu}{K} \int_{\Omega_1} \mathbf{u} \cdot \boldsymbol{\phi} = \int_{\Gamma_{in}} p_{in}\ \phi_1 - \int_{\Gamma_{out}} p_{out}\ \phi_1 - \int_{\Sigma} g'(x_1)\ \phi_2. \end{cases} \tag{3.1.15}$$

Remark 3.1.4 *The continuity of the left and right hand sides in (3.1.14) in the norm* $||\cdot||_{\mathbf{U^0_{div}}}$ *which is defined in (3.1.7) can be proved in the same way as we do it later in the proof of continuity of the bilinear form (3.2.5) and the functional (3.2.6).*

We simplified our problem by eliminating the pressure, but we cannot apply the Lax-Milgram Lemma directly to (3.1.15) yet, since the solution and the test functions do not belong to the same space. So, we need some transform of the unknown $\mathbf{u}$ such that the solution of the modified problem belongs to the space $\mathbf{U^0_{div}}$.

3.2 Transformation to the equivalent problem

Let us transform our problem (3.1.15) with the unknown $\mathbf{u} \in \mathbf{U}_{div}$ to the equivalent problem with the unknown $\mathbf{v} \in \mathbf{U^0_{div}}$, so that both the unknown $\mathbf{v}$ and the test functions $\boldsymbol{\phi}$ belong to the space $\mathbf{U^0_{div}}$. In order to do this we need to apply the following transform:

$$\mathbf{u} = \mathbf{v} + \mathbf{u_s} \quad \mathbf{v} \in \mathbf{U^0_{div}}, \qquad \mathbf{u}, \mathbf{u_s} \in \mathbf{U_{div}} \tag{3.2.1}$$

where the vector function $\mathbf{u_s} \in \mathbf{U_{div}}$ is some extension of the vector function $\mathbf{h} = (h_1, h_2)$ which is defined on the boundaries $\partial\Omega_0$ and $\partial\Omega_1$ as follows:

$$\begin{cases} \mathbf{h} = 0, & & & & on & \Gamma, \\ h_1 = \alpha\,\omega(x_2,-H), & h_2 = 0, & & & on & \Gamma_{in}, \\ h_1 = \beta\,\omega(x_2,-H), & h_2 = 0, & & & on & \Gamma_{out}, \\ h_1 = g(x_1), & h_2 = \gamma\,\omega(x_1,l), & & & on & \Sigma, \\ h_1 = 0, & & & & on & \Gamma_{iw} \cup \Gamma_{ow}, \\ h_2 = u_m, & & & & on & M, \end{cases} \tag{3.2.2}$$

where $\omega(x,y) = x^2(x-y)^2$, α, β, γ are some constants which will be defined below.
In [5] Ladyzhenskaya, Chapter 1, Problem 2.1, it was shown that if a domain D is simply connected then for any vector function $\mathbf{g}$ defined on ∂D such that $\int_{\partial D} \mathbf{g}\cdot\boldsymbol{\nu} = 0$, there exists a vector function $\mathbf{w}$ defined in D, such that $\mathbf{w} = \mathbf{g}$ on ∂D and $\nabla\cdot\mathbf{w} = 0$ in D. Applying this result to the vector function $\mathbf{h}$ defined in (3.2.2) we obtain a vector function $\mathbf{u_s}$ defined in the whole domain Ω such that $\mathbf{u_s} = \mathbf{h}$ on $\partial\Omega_0 \cup \partial\Omega_1$ and $\nabla\cdot\mathbf{u_s} = 0$ in $\Omega_0 \cup \Omega_1$.

The actual values for constants α, β, γ in (3.2.2) can be found from the compatibility conditions $\int_{\partial\Omega_0} \mathbf{h}\cdot\boldsymbol{\nu} = 0$ and $\int_{\partial\Omega_1} \mathbf{h}\cdot\boldsymbol{\nu} = 0$:

$$\begin{cases} \gamma = |\Sigma|^{-1}\int_M u_m, \\ \alpha = |\Gamma_{in}|^{-1}(\beta|\Gamma_{out}| + \gamma|\Sigma|), \end{cases} \tag{3.2.3}$$

where β is arbitrary and $|\Sigma| = \int_\Sigma \omega(x_1,l)$, $|\Gamma_{in}| = \int_{\Gamma_{in}} \omega(x_2,-H)$, $|\Gamma_{out}| = \int_{\Gamma_{out}} \omega(x_2,-H)$.

Remark 3.2.1 *We have just proved that* $\mathbf{U_{div}}$ *is not empty if* $u_m \in L^1(M)$.

After the transformation we have an equivalent problem:

$$\begin{cases} \textit{find } \mathbf{v} \in \mathbf{U^0_{div}}, \textit{ such that } \forall\boldsymbol{\phi} \in \mathbf{U^0_{div}} \textit{ satisfies :} \\ \mu\int_{\Omega_0} \nabla\mathbf{v}\cdot\nabla\boldsymbol{\phi} + \dfrac{\mu}{K}\int_{\Omega_1} \mathbf{v}\cdot\boldsymbol{\phi} = -\mu\int_{\Omega_0} \nabla\mathbf{u_s}\cdot\nabla\boldsymbol{\phi} - \dfrac{\mu}{K}\int_{\Omega_1} \mathbf{u_s}\cdot\boldsymbol{\phi} + \\ \qquad\qquad \int_{\Gamma_{in}} p_{in}\,\phi_1 - \int_{\Gamma_{out}} p_{out}\,\phi_1 - \int_\Sigma g'(x_1)\,\phi_2. \end{cases} \tag{3.2.4}$$

Let us define the bilinear form $a(\mathbf{v},\boldsymbol{\phi})$ and the functional $l(\boldsymbol{\phi})$ on $\mathbf{U_{div}}$, $\mathbf{U^0_{div}}$ follows:

$$a(\mathbf{v},\boldsymbol{\phi}) = \mu\int_{\Omega_0} \nabla\mathbf{v}\cdot\nabla\boldsymbol{\phi} + \frac{\mu}{K}\int_{\Omega_1} \mathbf{v}\cdot\boldsymbol{\phi}, \tag{3.2.5}$$

$$l(\boldsymbol{\phi}) = -\mu\int_{\Omega_0} \nabla\mathbf{u_s}\cdot\nabla\boldsymbol{\phi} - \frac{\mu}{K}\int_{\Omega_1} \mathbf{u_s}\cdot\boldsymbol{\phi} + \int_{\Gamma_{in}} p_{in}\cdot\phi_1 - \int_{\Gamma_{out}} p_{out}\,\phi_1 - \int_\Sigma g'(x_1)\,\phi_2. \tag{3.2.6}$$

V-ellipticity for $a(\mathbf{v}, \boldsymbol{\phi})$ follows from the definition of the norm (3.1.7):

$$a(\mathbf{v}, \mathbf{v}) = \mu \int_{\Omega_0} |\nabla \mathbf{v}|^2 + \frac{\mu}{K} \int_{\Omega_1} |\mathbf{v}|^2 \geq \bar{C} \, ||\mathbf{v}||^2_{U^0_{div}}. \tag{3.2.7}$$

Continuity of $a(\mathbf{v}, \boldsymbol{\phi})$ follows from the Hölder inequality:

$$\begin{aligned} |a(\mathbf{v}, \boldsymbol{\phi})| &\leq \mu \textstyle\int_{\Omega_0} |\nabla \mathbf{v}| \, |\nabla \boldsymbol{\phi}| + \frac{\mu}{K} \int_{\Omega_1} |\mathbf{v}| \, |\boldsymbol{\phi}| \\ &\leq \mu ||\nabla \mathbf{v}||_{L^2(\Omega)} \, ||\nabla \boldsymbol{\phi}||_{L^2(\Omega)} + \frac{\mu}{K} ||\mathbf{v}||_{L^2(\Omega)} \, ||\boldsymbol{\phi}||_{L^2(\Omega)} \\ &\leq \hat{C} \, ||\mathbf{v}||_{U^0_{div}} \, ||\boldsymbol{\phi}||_{U^0_{div}}. \end{aligned} \tag{3.2.8}$$

Continuity of $l(\boldsymbol{\phi})$ follows by applying the Hölder inequality:

$$\begin{aligned} |l(\boldsymbol{\phi})| &\leq \mu \textstyle\int_{\Omega_0} |\nabla \mathbf{u_s}| \, |\nabla \boldsymbol{\phi}| + \frac{\mu}{K} \int_{\Omega_1} |\mathbf{u_s}| \, |\boldsymbol{\phi}| + \int_{\Gamma_{in}} |p_{in}| \, |\phi_1| + \\ &\quad \textstyle\int_{\Gamma_{out}} |p_{out}| \, |\phi_1| + \int_{\Sigma} |g'(x_1)| \, |\phi_2| \\ &\leq ||\nabla \mathbf{u_s}||_{L^2(\Omega_0)} \, ||\nabla \boldsymbol{\phi}||_{L^2(\Omega_0)} + \\ &\quad \frac{\mu}{K} ||\mathbf{u_s}||_{L^2(\Omega_1)} \, ||\boldsymbol{\phi}||_{L^2(\Omega_1)} + ||p_{in}||_{L^2(\Gamma_{in})} \, ||\phi_1||_{L^2(\Gamma_{in})} + \\ &\quad ||p_{out}||_{L^2(\Gamma_{out})} \, ||\phi_1||_{L^2(\Gamma_{out})} + ||g'||_{L^2(\Sigma)} \, ||\phi_2||_{L^2(\Sigma)}. \end{aligned} \tag{3.2.9}$$

We can apply trace inequalities on $\Gamma_{in}, \Gamma_{out}, \Sigma$:

$$\begin{cases} ||\phi_1||_{L^2(\Gamma_{in})} \leq C_{\Gamma_{in}} ||\nabla \phi_1||_{L^2(\Omega_0)}, \\ ||\phi_1||_{L^2(\Gamma_{out})} \leq C_{\Gamma_{out}} ||\nabla \phi_1||_{L^2(\Omega_0)}, \\ ||\phi_2||_{L^2(\Sigma)} \leq C_{\Sigma} ||\nabla \phi_2||_{L^2(\Omega_0)}. \end{cases} \tag{3.2.10}$$

Substitute (3.2.10) into (3.2.9) and obtain:

$$\begin{aligned} |l(\boldsymbol{\phi})| &\leq ||\nabla \mathbf{u_s}||_{L^2(\Omega_0)} \, ||\nabla \boldsymbol{\phi}||_{L^2(\Omega_0)} + \frac{\mu}{K} ||\mathbf{u_s}||_{L^2(\Omega_1)} \, ||\boldsymbol{\phi}||_{L^2(\Omega_1)} + \\ &\quad C_{\Gamma_{in}} ||p_{in}||_{L^2(\Gamma_{in})} \, ||\nabla \phi_1||_{L^2(\Omega_0)} + C_{\Gamma_{out}} ||p_{out}||_{L^2(\Gamma_{out})} \, ||\nabla \phi_1||_{L^2(\Omega_0)} + \\ &\quad C_{\Sigma} ||g'||_{L^2(\Sigma)} \, ||\nabla \phi_2||_{L^2(\Omega_0)}. \end{aligned} \tag{3.2.11}$$

Finally from the definition of the norm $||\cdot||_{\mathbf{U^0_{div}}}$, it follows the continuity of $l(\boldsymbol{\phi})$:

$$|l(\boldsymbol{\phi})| \leq \hat{C} ||\boldsymbol{\phi}||_{\mathbf{U}^0{}_{div}}, \tag{3.2.12}$$

$$where\ \hat{C} \ = \ \sqrt{2}\ max(||\nabla \mathbf{u_s}||_{L^2(\Omega_0)} + C_{\Gamma_{in}}||p_{in}||_{L^2(\Gamma_{in})} +$$

$$C_{\Gamma_{out}}||p_{out}||_{L^2(\Gamma_{out})} + C_\Sigma||g'||_{L^2(\Sigma)}\ ;\ \frac{\mu}{K}||\mathbf{u_s}||_{L^2(\Omega_1)}).$$

Now existence and uniqueness of the solution $\mathbf{v}$ can be obtained by applying Lax-Milgram Lemma to the problem:

$$Find\ \mathbf{v} \in \mathbf{U}^0_{div}\ ,\ such\ that\ a(\mathbf{v}, \boldsymbol{\phi}) = l(\boldsymbol{\phi}), \forall \boldsymbol{\phi} \in \mathbf{U}^0_{div}. \tag{3.2.13}$$

So we have proved that our problem (3.1.14) has the unique solution $\mathbf{u} = \mathbf{v} + \mathbf{u_s}$, where $\mathbf{v}$ is the unique solution of the problem (3.2.13).

Remark 3.2.2 *We can reduce our requirements for the functions u_m, p_{in}, p_{out} as follows: $u_m \in L^1(M)$, $p_{in} \in L^2(\Gamma_{in})$, $p_{out} \in L^2(\Gamma_{out})$.*

Remark 3.2.3 *The pressure solution was excluded from the consideration by the choice of the functional space $\mathbf{U}^0_{div}$ and we did not prove its existence.*

Remark 3.2.4 *If we use interface conditions (2.2.7) with the regular Saffman's condition instead of the reduced one that we used in our prove, then we obtain the following bilinear form:*

$$a(\mathbf{u}, \boldsymbol{\phi}) = \mu \int_{\Omega_0} \nabla \mathbf{u} \cdot \nabla \boldsymbol{\phi} + \frac{\mu}{K} \int_{\Omega_1} \mathbf{u} \cdot \boldsymbol{\phi} - \int_\Sigma (S\ u_1\ \phi_1 + \partial_1 u_1\ \phi_2). \tag{3.2.14}$$

In order to use the the Lax-Milgram lemma in the proof of existence we need V-ellipticity of this bilinear form. Unfortunately we did not obtain this result.

4

Computational method

The weak form (3.1.14) of the problem that is obtained in Chapter 3 is not convenient for numerical implementation since it involves the divergence free space $\mathbf{U}^0_{div}$ in (3.1.4), which is expensive to be constructed. In order to avoid this difficulty we use a mixed weak form of the problem such that in Ω_0 our solution is $(\mathbf{u}, p)$, but in Ω_1 it is only p. The velocities in Ω_1 are completely determined by the Darcy equation. Therefore, by excluding unknown velocities in Ω_1 we significantly reduce overall computations.

4.1 Weak formulation of the problem

Applying the divergence operator to the Darcy equation in the domain Ω_1 we obtain the Laplace equation for the pressure and eliminate the velocity. Now we use only the Stokes equation and the mass conservation equation in Ω_0 and the Laplace equation for the pressure in Ω_1. Later we can easily restore the velocity in Ω_1 by using the Darcy equation. Like in the existence proof, let us combine equations (2.2.2)-(2.2.3) into the system which is equivalent to the original one in the whole domain $\Omega = \Omega_0 \cup \Omega_1 \cup \Sigma$:

$$\begin{cases} -(\nabla \cdot \mathbf{u})\ \mathbb{1}_{\Omega_0} - \Delta p\ \mathbb{1}_{\Omega_1} &= 0, \\ (-\mu\Delta\mathbf{u} + \nabla p)\ \mathbb{1}_{\Omega_0} &= 0, \end{cases} \tag{4.1.1}$$

with boundary conditions (2.2.5) and interface conditions (2.2.7) for the case when p_{in}, p_{out}, p_m, S are given constants. The velocity space here includes restrictions on $\bar{\Omega}_0$ of vector functions belonging to $\boldsymbol{\mathcal{U}}$ (see (2.2.4)). The pressure space $\mathcal{P}$ here is the same space as it is in (2.2.4). Using boundary conditions (2.2.5) we construct functional sets and spaces with boundary conditions integrated and their closures, in larger Hilbert

spaces, which are necessary for the weak formulation of the problem (4.1.1):

$$\begin{cases} \boldsymbol{\mathcal{V}}_0 &= \{\boldsymbol{\phi} = (\phi_1, \phi_2) \mid \exists \boldsymbol{u} \in \boldsymbol{\mathcal{U}},\ \boldsymbol{\phi} = \boldsymbol{u}_{|\bar{\Omega}_0},\ \boldsymbol{\phi}_{|\Gamma} = 0,\ \phi_{2|\Gamma_{in} \cup \Gamma_{out}} = 0\}, \\ \mathcal{Q} &= \{q \in \mathcal{P} \mid q_{|\Gamma_{in}} = p_{in},\ q_{|\Gamma_{out}} = p_{out},\ q_{|\Gamma_M} = p_m\}, \\ \mathcal{Q}_0 &= \{q \in \mathcal{P} \mid q_{|\Gamma_{in} \cup \Gamma_{out} \cup M} = 0\}, \\ \mathbf{V}_0 &= \overline{\boldsymbol{\mathcal{V}}_0}^{\|\cdot\|_{(H^1(\Omega_0))^2}}, \\ Q &= \overline{\mathcal{Q}}^{\|\cdot\|_{H^1(\Omega_0)} + \|\cdot\|_{H^1(\Omega_1)}}, \\ Q_0 &= \overline{\mathcal{Q}_0}^{\|\cdot\|_{H^1(\Omega_0)} + \|\cdot\|_{H^1(\Omega_1)}}. \end{cases} \tag{4.1.2}$$

Following the standard procedure for obtaining weak formulations, let us multiply both sides of each equation in (4.1.1) by appropriate test functions from $\boldsymbol{\mathcal{V}}_0$ and $\mathcal{Q}_0$. We multiply the first equation by an arbitrary function $\psi \in \mathcal{Q}_0$. We multiply the second equation which is in a vector form, having two components for the velocity $\mathbf{u} = \binom{u_1}{u_2}$, by vector functions in the form $\binom{\phi_1}{0}, \binom{0}{\phi_2} \in \boldsymbol{\mathcal{V}}_0$. Finally, applying the Green's formula to the divergence term and the Laplace operator term we obtain an integral form which is equivalent to the problem (4.1.1):

find $(\mathbf{u}, p) \in \boldsymbol{\mathcal{V}}_0 \times \mathcal{Q}$ *such that* $\forall \boldsymbol{\phi} = \binom{\phi_1}{\phi_1} \in \boldsymbol{\mathcal{V}}_0, \forall \psi \in \mathcal{Q}_0$ *the following equations are satisfied:*

$$\begin{cases} \int_{\Omega_0} \mathbf{u} \cdot \nabla \psi - \int_{\partial\Omega_0} (\mathbf{u} \cdot \boldsymbol{\nu}_0)\ \psi + \int_{\Omega_1} \nabla p \cdot \nabla \psi - \int_{\partial\Omega_1} \dfrac{\partial p}{\partial \boldsymbol{\nu}_1}\ \psi &= 0, \\ \mu \int_{\Omega_0} \nabla u_1 \cdot \nabla \phi_1 - \mu \int_{\partial\Omega_0} \dfrac{\partial u_1}{\partial \boldsymbol{\nu}_0}\ \phi_1 + \int_{\Omega_0} \partial_1 p\ \phi_1 &= 0, \\ \mu \int_{\Omega_0} \nabla u_2 \cdot \nabla \phi_2 - \mu \int_{\partial\Omega_0} \dfrac{\partial u_2}{\partial \boldsymbol{\nu}_0}\ \phi_2 + \int_{\Omega_0} \partial_2 p\ \phi_2 &= 0. \end{cases} \tag{4.1.3}$$

In order to apply interface conditions let us separate the integrals over the interface Σ from the other integrals in (4.1.3):

$$\begin{cases} \int_{\Omega_1} \nabla p \cdot \nabla \psi + \int_{\Omega_0} \mathbf{u} \cdot \nabla \psi - \int_{\partial\Omega_0 \setminus \Sigma} (\mathbf{u} \cdot \boldsymbol{\nu}_0)\ \psi - \int_{\partial\Omega_1 \setminus \Sigma} \dfrac{\partial p}{\partial \boldsymbol{\nu}_1}\ \psi - \\ \qquad\qquad \int_{\Sigma} (\mathbf{u} \cdot \boldsymbol{\nu}_0)\ \psi - \int_{\Sigma} \dfrac{\partial p}{\partial \boldsymbol{\nu}_1}\ \psi &= 0, \\ \int_{\Omega_0} \partial_1 p\ \phi_1 + \mu \int_{\Omega_0} \nabla u_1 \cdot \nabla \phi_1 - \mu \int_{\partial\Omega_0 \setminus \Sigma} \dfrac{\partial u_1}{\partial \boldsymbol{\nu}_0}\ \phi_1 - \mu \int_{\Sigma} \dfrac{\partial u_1}{\partial \boldsymbol{\nu}_0}\ \phi_1 &= 0, \\ \int_{\Omega_0} \partial_2 p\ \phi_2 + \mu \int_{\Omega_0} \nabla u_2 \cdot \nabla \phi_2 - \mu \int_{\partial\Omega_0 \setminus \Sigma} \dfrac{\partial u_2}{\partial \boldsymbol{\nu}_0}\ \phi_2 - \mu \int_{\Sigma} \dfrac{\partial u_2}{\partial \boldsymbol{\nu}_0}\ \phi_2 &= 0, \end{cases} \tag{4.1.4}$$

where $\boldsymbol{\nu}_0$ and $\boldsymbol{\nu}_1$ are outward normal vectors to the boundaries $\partial\Omega_0$ and $\partial\Omega_1$ respectively.

Using the interface conditions (2.2.7) and the mass conservation equation in Ω, which gives $\partial_1 u_1 = -\partial_2 u_2$, we can modify all terms in (4.1.4) involving normal derivatives on Σ as follows:

$$\begin{cases} \int_\Sigma \dfrac{\partial p}{\partial \boldsymbol{\nu}_1}\,\psi &= \dfrac{\mu}{K}\int_\Sigma u_2\,\psi \qquad \text{in the first equation,} \\ \int_\Sigma \dfrac{\partial u_1}{\partial \boldsymbol{\nu}_0}\,\phi_1 &= -S\int_\Sigma u_1\,\phi_1 \qquad \text{in the second equation,} \\ \int_\Sigma \dfrac{\partial u_2}{\partial \boldsymbol{\nu}_0}\,\phi_2 &= -\int_\Sigma \partial_1 u_1\,\phi_2 \qquad \text{in the third equation.} \end{cases} \tag{4.1.5}$$

In order to apply the boundary conditions (2.2.5) we consider all the integrals on the boundaries $\partial\Omega_0 \setminus \Sigma$ and $\partial\Omega_1 \setminus \Sigma$ in (4.1.4):

$$\begin{cases} \int_{\partial\Omega_1\setminus\Sigma} \dfrac{\partial p}{\partial \boldsymbol{\nu}_1}\,\psi &= -\int_{\Gamma_{iw}} \partial_1 p\,\psi + \int_{\Gamma_{ow}} \partial_1 p\,\psi + \int_M \partial_2 p\,\psi, \\ \int_{\partial\Omega_0\setminus\Sigma} (\mathbf{u}\cdot\boldsymbol{\nu}_0)\,\psi &= -\int_{\Gamma_{in}} u_1\,\psi + \int_{\Gamma_{out}} u_1\,\psi - \int_\Gamma u_2\,\psi, \\ \mu\int_{\partial\Omega_0\setminus\Sigma} \dfrac{\partial u_1}{\partial \boldsymbol{\nu}_0}\,\phi_1 &= -\mu\int_{\Gamma_{in}} \partial_1 u_1\,\phi_1 + \mu\int_{\Gamma_{out}} \partial_1 u_1\,\phi_1 - \mu\int_\Gamma \partial_2 u_1\,\phi_1, \\ \mu\int_{\partial\Omega_0\setminus\Sigma} \dfrac{\partial u_2}{\partial \boldsymbol{\nu}_0}\,\phi_2 &= -\mu\int_{\Gamma_{in}} \partial_1 u_2\,\phi_2 + \mu\int_{\Gamma_{out}} \partial_1 u_2\,\phi_2 - \mu\int_\Gamma \partial_2 u_2\,\phi_2. \end{cases} \tag{4.1.6}$$

Some of the terms in (4.1.6) will be zero and the others can be modified:

$$\begin{cases} \int_{\Gamma_{in}} u_1\,\psi &= \int_{\Gamma_{out}} u_1\,\psi = 0, & \textit{since} \quad \psi_{|\Gamma_{in}\cup\Gamma_{out}} = 0, \\ \int_{\Gamma_{in}} \partial_1 u_1\,\phi_1 &= -\int_{\Gamma_{in}} \partial_2 u_2\,\phi_1 = 0, & \textit{since} \quad u_{2|\Gamma_{in}} = 0, \\ \int_{\Gamma_{in}} \partial_1 u_2\,\phi_2 &= \int_{\Gamma_{out}} \partial_1 u_2\,\phi_2 = 0, & \textit{since} \quad \phi_{2|\Gamma_{in}\cup\Gamma_{out}} = 0, \\ \int_{\Gamma_{out}} \partial_1 u_1\,\phi_1 &= -\int_{\Gamma_{out}} \partial_2 u_2\,\phi_1 = 0, & \textit{since} \quad u_{2|\Gamma_{out}} = 0, \\ \int_{\Gamma_{iw}} \partial_1 p\,\psi &= \int_{\Gamma_{ow}} \partial_1 p\,\psi = 0, & \textit{since} \quad \partial_1 p_{|\Gamma_{iw}\cup\Gamma_{ow}} = 0, \\ \int_\Gamma \partial_2 u_1\,\phi_1 &= 0, & \textit{since} \quad \phi_{1|_\Gamma} = 0, \\ \int_\Gamma u_2\,\psi &= 0, & \textit{since} \quad u_{2|_\Gamma} = 0, \\ \int_\Gamma \partial_2 u_2\,\phi_2 &= 0, & \textit{since} \quad \phi_{2|\Gamma} = 0, \\ \int_M \partial_2 p\,\psi &= 0, & \textit{since} \quad \psi_{|_M} = 0. \end{cases} \tag{4.1.7}$$

Let us substitute (4.1.6) and (4.1.7) into (4.1.4) and since $\mathcal{V}_0$, $\mathcal{Q}$, $\mathcal{Q}_0$ are dense in $\boldsymbol{V}_0$, Q, Q_0, respectively we obtain the final weak form of the problem (4.1.1):

find $(\mathbf{u}, p) \in \mathbf{V}_0 \times Q$ *such that* $\forall(\binom{\phi_1}{\phi_2}, \psi) \in \mathbf{V}_0 \times Q_0$ *the* following equations are satisfied:

$$\begin{cases} \int_{\Omega_1} \nabla p \cdot \nabla \psi + \int_{\Omega_0} \mathbf{u} \cdot \nabla \psi - (1 + \frac{\mu}{K}) \int_\Sigma u_2 \, \psi &= 0, \\ \int_{\Omega_0} \partial_1 p \, \phi_1 + \mu \int_{\Omega_0} \nabla u_1 \cdot \nabla \phi_1 + \mu S \int_\Sigma u_1 \, \phi_1 &= 0, \\ \int_{\Omega_0} \partial_2 p \, \phi_2 + \mu \int_{\Omega_0} \nabla u_2 \cdot \nabla \phi_2 + \mu \int_\Sigma \partial_1 u_1 \, \phi_2 &= 0. \end{cases} \tag{4.1.8}$$

Remark 4.1.1 *Since* $\mathcal{V}_0$ *is dense in* $\mathbf{V}_0$, $\mathcal{Q}$ *is dense in* Q *and* $\mathcal{Q}_0$ *is dense in* Q_0 *and the left hand sides in (4.1.8) are sums of continuous bilinear forms, then the equations in (4.1.8) make sense for* $(\mathbf{u}, p) \in \boldsymbol{V}_0 \times Q$, $\forall \boldsymbol{\phi} = \binom{\phi_1}{\phi_1} \in \mathbf{V}_0$ *and* $\forall \psi \in Q_0$. $\mathbf{V}_0$ *is the space of the velocity and velocity test functions.* Q_0 *is the space of the pressure test functions.*

From this point we assume existence and uniqueness of the solution (**u**,p) of the problem in a weak form (4.1.8).

4.2 Finite elements

For computations in Ω_0 we have chosen the MINI element (see [1]): a triangle with three nodes on vertices and one node in the center as shown on Figure 4.1.

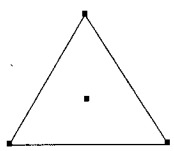

Figure 4.1: The standard MINI element

Basis functions which correspond to vertex nodes are linear and those which correspond to center nodes are cubics. For example, if ϕ_1, ϕ_2, ϕ_3 are basis piecewise linear functions which correspond to vertex nodes of some triangle, then the basis function which corresponds to the center node is the function $27\ \phi_1\ \phi_2\ \phi_3$. For computations in Ω_1 the P_1 element was chosen: triangle with three nodes on vertices.

It was proved in [1] D.Arnold, F.Brezzi, M.Fortin, that the MINI element as a velocity-pressure finite element gives a stable approximation for the Stokes problem when the pressure is linear and the velocities contain cubic functions in its approximations.

In our case we have two coupled domains and the finite element space is complicated by the boundary and interface conditions. This stability result is not valid in our case. Up to this moment we can say that only numerical experiments show that our method is stable.

4.3 Finite element approximation

Let us introduce velocity and pressure finite element spaces V_h and Q_h:

$$\mathcal{X}_h = \{v_h \in C^0(\bar{\Omega}) : v_{h|_K} \in P_K^1, \forall \mathrm{K} \in \mathcal{T}_h\}, \tag{4.3.1}$$

$$\mathcal{X}_{h,b} = \{v_h \in C^0(\bar{\Omega}_0) : v_{h|_K} \in P_K^1 \cup \{v_1\ v_2\ v_3\}, \forall \mathrm{K} \in \mathcal{T}_h\}, \tag{4.3.2}$$

$$\mathbf{V_h} = \mathbf{V}_0 \cap (\mathcal{X}_{h,b})^2, \tag{4.3.3}$$

$$Q_h = Q \cap \mathcal{X}_h, \tag{4.3.4}$$

where $\mathcal{T}_h$ is an appropriate triangulation of the domain Ω and P_K^1 is the space of polynomials of the first order in K; $v_j \in P_K^1$ are the basis functions of P_K^1.

Definition 4.3.1 *If $A \subseteq \bar{\Omega}$ then the notation $[A]$ means the set of all the nodes that belong to A.*

Let ψ_j and ϕ_j be basis functions of the finite dimensional spaces $\mathcal{X}_h$ and $\mathcal{X}_{h,b}$ respectively. We look for an approximate solution of the problem (4.1.8) in the form:

$$p_h = \sum_{j \in [\bar{\Omega} \setminus (\Gamma_{in} \cup \Gamma_{out} \cup M)]} p_j\ \psi_j + \sum_{j \in [\Gamma_{in} \cup \Gamma_{out} \cup M]} \bar{p}_j\ \psi_j = \hat{p}_h + \bar{p}_h \tag{4.3.5}$$

$$u_{1,h} = \sum_{j \in [\bar{\Omega} \setminus \Gamma]} u_{1,j}\ \phi_j + \sum_{j \in [\Gamma]} \bar{u}_{1,j}\ \phi_j = \hat{u}_{1,h} + \bar{u}_{1,h} \tag{4.3.6}$$

$$u_{2,h} = \sum_{j \in [\bar{\Omega} \setminus (\Gamma_{in} \cup \Gamma_{out} \cup \Gamma)]} u_{2,j}\ \phi_j + \sum_{j \in [\Gamma_{in} \cup \Gamma_{out} \cup \Gamma]} \bar{u}_{2,j}\ \phi_j = \hat{u}_{2,h} + \bar{u}_{2,h} \tag{4.3.7}$$

- $p_j, u_{1,j}, u_{2,j}$ are unknown values of the solution in the node j;
- $\bar{p}_j, \bar{u}_{1,j}, \bar{u}_{2,j}$ are given boundary values of the solution in the node j;
- $p_h \in \mathcal{X}_h$ and $u_{1,h},\ u_{2,h} \in \mathcal{X}_{h,b}$;
- $\hat{p}_h \in Q_h$ and $\begin{pmatrix} \hat{u}_{1,h} \\ \hat{u}_{2,h} \end{pmatrix} \in \mathbf{V_h}$;
- in our case $\bar{u}_{1,h} = 0$ and $\bar{u}_{2,h} = 0$.

Remark 4.3.2 *We write here ϕ_i instead of $\phi_{1,i}$ and $\phi_{2,i}$ because velocities u_1, u_2 belong to the same space finite element space $\mathcal{X}_{h,b}$.*

Since $\mathcal{X}_h \subset \mathcal{X}_{h,b}$ then we can write $u_{1,h}, u_{2,h}$ in (4.3.5)-(4.3.7) using linear basis functions ψ_j corresponding to vertex nodes and cubic basis functions φ_j corresponding to center nodes:

$$\begin{cases} p_h &= \sum_{j\in v[\bar{\Omega}]} p_j\ \psi_j, \\ u_{1,h} &= \sum_{j\in v[\bar{\Omega}_0]} u_{1,j}\ \psi_j + \sum_{j\in c[\bar{\Omega}_0]} u_{1,j}\ \varphi_j, \\ u_{2,h} &= \sum_{j\in v[\bar{\Omega}_0]} u_{2,j}\ \psi_j + \sum_{j\in c[\bar{\Omega}_0]} u_{2,j}\ \varphi_j, \\ p_j &= \bar{p}_j\ , for\ j \in [\Gamma_{in} \cup \Gamma_{out} \cup M], \\ u_{1,j} &= 0\ , for\ j \in [\Gamma], \\ u_{2,j} &= 0\ , for\ j \in [\Gamma_{in} \cup \Gamma_{out} \cup \Gamma], \end{cases} \tag{4.3.8}$$

where $v[A]$ and $c[A]$ are collections of nodes corresponding to the vertices and centers of the triangles contained in the set $A \subset \bar{\Omega}$, respectively.

4.4 Discrete variational problem

Let us write equations (4.1.8) distinguishing the cases $i \in [\Sigma]$, $i \in [\bar{\Omega}_1 \backslash \Sigma]$, $i \in [\bar{\Omega}_0 \backslash \Sigma]$. Inside each equation we separate unknowns in the order: p, u_1, u_2. This order and structure of equations will help us to understand the structure of the matrix which we use later in our iterative method.

$i \in [\Sigma]$:

$$\begin{cases} \left(\int_{\Omega_1} \nabla p \cdot \nabla \psi_i\right) + \left(\int_{\Omega_0} u_1\ \partial_1 \psi_i\right) + \\ \qquad\qquad \left(\int_{\Omega_0} u_2\ \partial_2 \psi_i - (1 + \frac{\mu}{K}) \int_{\Sigma} u_2\ \psi_i\right) &= 0, \\ \left(\int_{\Omega_0} \partial_1 p\ \phi_i\right) + \left(\mu \int_{\Omega_0} \nabla u_1 \cdot \nabla \phi_i + \mu S \int_{\Sigma} u_1\ \phi_i\right) &= 0, \\ \left(\int_{\Omega_0} \partial_2 p\ \phi_i\right) + \left(\mu \int_{\Sigma} \partial_1 u_1\ \phi_i\right) + \left(\mu \int_{\Omega_0} \nabla u_2 \cdot \nabla \phi_i\right) &= 0. \end{cases} \tag{4.4.1}$$

$i \in [\bar{\Omega}_1 \setminus \Sigma]$:

$$\left\{ \left(\int_{\Omega_1} \nabla p \cdot \nabla \psi_i\right) = 0. \right. \tag{4.4.2}$$

$i \in [\bar{\Omega}_0 \setminus \Sigma]$:

$$\begin{cases} \left(\int_{\Omega_0} u_1\ \partial_1\psi_i\right) & + & \left(\int_{\Omega_0} u_2\ \partial_2\psi_i\right) & = & 0, \\ \left(\int_{\Omega_0} \partial_1 p\ \phi_i\right) & + & \left(\mu \int_{\Omega_0} \nabla u_1 \cdot \nabla\phi_i\right) & = & 0, \\ \left(\int_{\Omega_0} \partial_2 p\ \phi_i\right) & + & \left(\mu \int_{\Omega_0} \nabla u_2 \cdot \nabla\phi_i\right) & = & 0. \end{cases} \tag{4.4.3}$$

We obtain a linear system by substituting the representation (4.3.8) of an approximate solution into (4.4.1)-(4.4.3). Also we should remember that the equations (4.4.1) involve only linear test functions, but equations (4.4.2) and (4.4.3) involve both linear and cubic test functions.

$i \in [\Sigma]$:

$$\begin{cases} \sum_{j\in v[\bar{\Omega}\setminus\bar{\Omega}_0]} p_j\ b_{ij} + \\ \sum_{j\in v[\bar{\Omega}_0]}\left(p_j\ b_{ij} + u_{1,j}\ c_{ij} + u_{2,j}\ (d_{ij} + \alpha e_{ij})\right) & + \sum_{j\in c[\bar{\Omega}_0]}\left(u_{1,j}\ \bar{c}_{ij} + u_{2,j}\ \bar{d}_{ij}\right) & = 0, \\ \sum_{j\in v[\bar{\Omega}_0]}\left(p_j\ c^t_{ij} + u_{1,j}\ (\mu a_{ij} + \mu S e_{ij}) + u_{2,j}\ 0\right) & + \sum_{j\in c[\bar{\Omega}_0]}\left(u_{1,j}\ \mu\bar{a}_{ij} + u_{2,j}\ 0\right) & = 0, \\ \sum_{j\in v[\bar{\Omega}_0]}\left(p_j\ d^t_{ij} + u_{1,j}\ \mu g_{ij} + u_{2,j}\ \mu a_{ij}\right) & + \sum_{j\in c[\bar{\Omega}_0]}\left(u_{1,j}\ 0 + u_{2,j}\ \mu\bar{a}_{ij}\right) & = 0. \end{cases} \tag{4.4.4}$$

$i \in v[\bar{\Omega}_1 \setminus \Sigma]$:

$$\left\{ \sum_{j\in v[\bar{\Omega}\setminus\bar{\Omega}_0]} p_j\ b_{ij} + \sum_{j\in v[\bar{\Omega}_0]}\left(p_j\ 0 + u_{1,j}\ 0 + u_{2,j}\ 0\right) + \sum_{j\in c[\bar{\Omega}_0]}\left(u_{1,j}\ 0 + u_{2,j}\ 0\right) = 0. \right. \tag{4.4.5}$$

$i \in v[\bar{\Omega}_0 \setminus \Sigma]$:

$$\begin{cases} \sum_{j\in v[\bar{\Omega}_0]}\left(p_j\ 0 + u_{1,j}\ c_{ij} + u_{2,j}\ d_{ij}\right) & + & \sum_{j\in c[\bar{\Omega}_0]}\left(u_{1,j}\ \bar{c}_{ij} + u_{2,j}\ \bar{d}_{ij}\right) & = 0, \\ \sum_{j\in v[\bar{\Omega}_0]}\left(p_j\ c^t_{ij} + u_{1,j}\ \mu a_{ij} + u_{2,j}\ 0\right) & + & \sum_{j\in c[\bar{\Omega}_0]}\left(u_{1,j}\ \mu\bar{a}_{ij} + u_{2,j}\ 0\right) & = 0, \\ \sum_{j\in v[\bar{\Omega}_0]}\left(p_j\ d^t_{ij} + u_{1,j}\ 0 + u_{2,j}\ \mu a_{ij}\right) & + & \sum_{j\in c[\bar{\Omega}_0]}\left(u_{1,j}\ 0 + u_{2,j}\ \mu\bar{a}_{ij}\right) & = 0. \end{cases} \tag{4.4.6}$$

$i \in c[\bar{\Omega}_0 \setminus \Sigma]$:

$$\begin{cases} \sum_{j\in v[\bar{\Omega}_0]}\left(p_j\ \bar{c}^t_{ij} + u_{1,j}\ \mu\bar{a}^t_{ij} + u_{2,j}\ 0\right) + \sum_{j\in c[\bar{\Omega}_0]}\left(u_{1,j}\ \mu\hat{a}_{ij} + u_{2,j}\ 0\right) = 0, \\ \sum_{j\in v[\bar{\Omega}_0]}\left(p_j\ \bar{d}^t_{ij} + u_{1,j}\ 0 + u_{2,j}\ \mu\bar{a}^t_{ij}\right) + \sum_{j\in c[\bar{\Omega}_0]}\left(u_{1,j}\ 0 + u_{2,j}\ \mu\hat{a}_{ij}\right) = 0, \end{cases} \tag{4.4.7}$$

where the coefficients of the linear system are as follows:

$$
\begin{cases}
\alpha = -(1+\dfrac{\mu}{K}), \\
b_{ij} = \int_{\Omega_1} \nabla\psi_j \cdot \nabla\psi_i, \\
e_{ij} = \int_{\Sigma} \psi_j \ \psi_i, \\
g_{ij} = \int_{\Sigma} \partial_1\psi_j \ \psi_i, \\
c_{ij} = \int_{\Omega_0} \psi_j \ \partial_1\psi_i \ , \qquad c^t_{ij} = \int_{\Omega_0} \partial_1\psi_j \ \psi_i, \\
\bar{c}_{ij} = \int_{\Omega_0} \varphi_j \ \partial_1\psi_i \ , \qquad \bar{c}^t_{ij} = \int_{\Omega_0} \partial_1\psi_j \ \varphi_i, \\
d_{ij} = \int_{\Omega_0} \psi_j \ \partial_2\psi_i \ , \qquad d^t_{ij} = \int_{\Omega_0} \partial_2\psi_j \ \psi_i, \\
\bar{d}_{ij} = \int_{\Omega_0} \varphi_j \ \partial_2\psi_i \ , \qquad \bar{d}^t_{ij} = \int_{\Omega_0} \partial_2\psi_j \ \varphi_i, \\
a_{ij} = \int_{\Omega_0} \nabla\psi_j \cdot \nabla\psi_i \ , \quad \bar{a}^t_{ij} = \int_{\Omega_0} \nabla\psi_j \cdot \nabla\varphi_i, \\
\bar{a}_{ij} = \int_{\Omega_0} \nabla\varphi_j \cdot \nabla\psi_i \ , \quad \hat{a}_{ij} = \int_{\Omega_0} \nabla\varphi_j \cdot \nabla\varphi_i.
\end{cases}
\tag{4.4.8}
$$

In order to complete our matrix linear system we need to add equations for the boundary conditions:

$$
\begin{cases}
p_j &= \bar{p}_j \ , for \ j \in [\Gamma_{in} \cup \Gamma_{out} \cup M] \\
u_{1,j} &= 0 \ , for \ j \in [\Gamma] \\
u_{2,j} &= 0 \ , for \ j \in [\Gamma_{in} \cup \Gamma_{out} \cup \Gamma]
\end{cases}
\tag{4.4.9}
$$

Now, let us define a super vector of unknowns $\mathbf{U} = \left(\mathbf{U_j}\right)_{j\in[\bar{\Omega}]}$

- for $j \in v[\bar{\Omega}_0]$:

$$
\mathbf{U_j} = \begin{pmatrix} p_j \\ u_{1,j} \\ u_{2,j} \end{pmatrix}
\tag{4.4.10}
$$

- for $j \in c[\bar{\Omega}_0]$:

$$
\mathbf{U_j} = \begin{pmatrix} u_{1,j} \\ u_{2,j} \end{pmatrix}
\tag{4.4.11}
$$

- for $j \in v[\bar{\Omega}_1 \setminus \Sigma]$:

$$\mathbf{U_j} = (\ p_j\ ) \tag{4.4.12}$$

In the same way we define the super vector $\mathbf{b} = \left(\mathbf{b_j}\right)_{j \in [\bar{\Omega}]}$ containing the right hand side of the linear system (4.4.4)-(4.4.7) and boundary conditions (4.4.9). So, our linear system has its final form:

$$\boldsymbol{A} \cdot \boldsymbol{U} = \boldsymbol{b} \tag{4.4.13}$$

4.5 Structure of the matrix

The matrix of the linear system (4.4.4)-(4.4.7) can be represented as $\bar{\mathbf{A}} = (\bar{\mathbf{A}}_{ij})_{i,j \in [\bar{\Omega}]}$, where each of the elements A_{ij} is sub-matrix of dimension 1x1, 1x2, 1x3, 2x1,3x1, 2x2, 2x3, 3x2, 3x3 with the coefficients which were defined in (4.4.8)

Let us write all possible kinds of sub-matrices for different i and j:

- for $i, j \in [\Sigma]$:

$$\bar{\mathbf{A}}_{ij} = \begin{pmatrix} b_{ij} & c_{ij} & d_{ij} + \alpha\ e_{ij} \\ c_{ij}^t & \mu a_{ij} + \mu S\ e_{ij} & 0 \\ d_{ij}^t & \mu g_{ij} & \mu a_{ij} \end{pmatrix} \tag{4.5.1}$$

- for $i, j \in v[\bar{\Omega}_0 \setminus \Sigma]$:

$$\bar{\mathbf{A}}_{ij} = \begin{pmatrix} 0 & c_{ij} & d_{ij} \\ c_{ij}^t & \mu a_{ij} & 0 \\ d_{ij}^t & 0 & \mu a_{ij} \end{pmatrix} \tag{4.5.2}$$

- for $i \in v[\bar{\Omega}_0 \setminus \Sigma]$, $j \in c[\bar{\Omega}_0 \setminus \Sigma]$:

$$\bar{\mathbf{A}}_{ij} = \begin{pmatrix} \bar{c}_{ij} & \bar{d}_{ij} \\ \mu \bar{a}_{ij} & 0 \\ 0 & \mu \bar{a}_{ij} \end{pmatrix} \tag{4.5.3}$$

- for $i \in c[\bar{\Omega}_0 \setminus \Sigma]$, $j \in v[\bar{\Omega}_0 \setminus \Sigma]$:

$$\bar{\mathbf{A}}_{ij} = \begin{pmatrix} \bar{c}_{ij}^t & \mu \bar{a}_{ij}^t & 0 \\ \bar{d}_{ij}^t & 0 & \mu \bar{a}_{ij}^t \end{pmatrix} \tag{4.5.4}$$

- for $i, j \in c[\bar{\Omega}_0 \setminus \Sigma]$:

$$\mathbf{A}_{ij} = \begin{pmatrix} \mu\hat{a}_{ij} & 0 \\ 0 & \mu\hat{a}_{ij} \end{pmatrix} \tag{4.5.5}$$

- for $i, j \in v[\bar{\Omega}_1 \setminus \Sigma]$:

$$\mathbf{A}_{ij} = \begin{pmatrix} b_{ij} \end{pmatrix} \tag{4.5.6}$$

- for $i \in v[\bar{\Omega}_1 \setminus \Sigma], j \in v[\bar{\Omega}_0]$:

$$\mathbf{A}_{ij} = \begin{pmatrix} b_{ij} & 0 & 0 \end{pmatrix} \tag{4.5.7}$$

- for $i \in v[\bar{\Omega}_1 \setminus \Sigma], j \in c[\bar{\Omega}_0]$:

$$\mathbf{A}_{ij} = \begin{pmatrix} 0 & 0 \end{pmatrix} \tag{4.5.8}$$

- for $i \in v[\bar{\Omega}_0], j \in v[\bar{\Omega}_1 \setminus \Sigma]$:

$$\mathbf{A}_{ij} = \begin{pmatrix} b_{ij} \\ 0 \\ 0 \end{pmatrix} \tag{4.5.9}$$

- for $i \in c[\bar{\Omega}_0], j \in v[\bar{\Omega}_1 \setminus \Sigma]$:

$$\mathbf{A}_{ij} = \begin{pmatrix} 0 \\ 0 \end{pmatrix} \tag{4.5.10}$$

Remark 4.5.1 *A matrix of the resulting linear system (4.4.4)-(4.4.7) is sparse banded but it is just one way to assemble the matrix. If in the weak form (4.1.8) we consider each equation on the whole domain independently of the others then we obtain a linear system as follows:*

$$\begin{pmatrix} \mathbf{B} & \mathbf{C}^t & \mathbf{D}^t + \alpha\,\mathbf{E} \\ \mathbf{C} & \mu(\mathbf{M} + S\,\mathbf{E}) & 0 \\ \mathbf{D} & \mu\,\mathbf{G} & \mu\mathbf{M} \end{pmatrix} \begin{pmatrix} \mathbf{p} \\ \mathbf{u_1} \\ \mathbf{u_2} \end{pmatrix} = \begin{pmatrix} \mathbf{p_0} \\ \mathbf{0} \\ \mathbf{0} \end{pmatrix}, \tag{4.5.11}$$

where the constants μ and S are the same as in (2.2.3) and (2.2.7); the constant α is defined in (4.4.8); the vector $\mathbf{p_0}$ contains the boundary conditions imposed on the pressure in (4.4.9); the submatrices $\mathbf{M}, \mathbf{B}, \mathbf{C}, \mathbf{D}, \mathbf{E}, \mathbf{G}$ are defined as follows:

$$\begin{cases} \mathbf{M} &= (\int_{\Omega_0} \nabla\phi_j \cdot \nabla\phi_i), \\ \mathbf{B} &= (\int_{\Omega_1} \nabla\psi_j \cdot \nabla\psi_i), \\ \mathbf{C} &= (\int_{\Omega_0} \partial_1\psi_j \ \phi_i), \\ \mathbf{D} &= (\int_{\Omega_0} \partial_2\psi_j \ \phi_i), \\ \mathbf{E} &= (\int_{\Sigma} \psi_j \ \psi_i), \\ \mathbf{G} &= (\int_{\Sigma} \partial_1\psi_j \ \psi_i). \end{cases} \tag{4.5.12}$$

The system (4.5.11) can be written in the following form:

$$\begin{pmatrix} \mathcal{B} & \mathcal{C}_\alpha^t \\ \mathcal{C} & \mathcal{M} \end{pmatrix} \begin{pmatrix} \mathbf{p} \\ \mathbf{u} \end{pmatrix} = \begin{pmatrix} \mathbf{p_0} \\ \mathbf{0} \end{pmatrix}, \tag{4.5.13}$$

where

$$\begin{cases} \mathcal{B} &= \mathbf{B}, \\ \mathcal{M} &= \begin{pmatrix} \mu(\mathbf{M} + S\ \mathbf{E}) & 0 \\ \mu\ \mathbf{G} & \mu\mathbf{M} \end{pmatrix}, \\ \mathcal{C} &= \begin{pmatrix} \mathbf{C} \\ \mathbf{D} \end{pmatrix}, \\ \mathcal{C}_\alpha^t &= (\mathbf{C}^t \quad \mathbf{D}^t + \alpha\ \mathbf{E}). \end{cases} \tag{4.5.14}$$

The matrices $\mathbf{M}$ and $\mathbf{B}$ are invertible since they are positive definite and symmetric. We can express the pressure trough the velocity and obtain the following linear system:

$$\begin{cases} \mathbf{p} &= \mathcal{B}^{-1}\ \mathbf{p_0} - \mathcal{B}^{-1}\ \mathcal{C}_\alpha^t\ \mathbf{u}, \\ (\ \mathcal{C}\ \mathcal{B}^{-1}\ \mathcal{C}_\alpha^t - \mathcal{M}\ )\mathbf{u} &= \mathcal{C}_\alpha^t\ \mathcal{B}^{-1}\ \mathbf{p_0}. \end{cases} \tag{4.5.15}$$

If the matrix $(\ \mathcal{C}\ \mathcal{B}^{-1}\ \mathcal{C}_\alpha^t - \mathcal{M}\ )$ is invertible then the linear system (4.5.11) has a unique solution.

4.6 Restoration of the velocities in the GDL

The finite element approximation (4.3.8) which we obtained is a restriction of the approximation (4.3.5)-(4.3.7) that we look for. The only thing left is to find the values of $u_{1,j}$ and $u_{2,j}$ for $j \in [\bar{\Omega} \setminus \bar{\Omega}_0]$.

Let us take a weak form of the Darcy equation $\mathbf{u} = -\dfrac{K}{\mu} \nabla p$ in the domain Ω_1:

$$\begin{cases} \int_{\Omega_1} u_1 \, \psi = -\dfrac{K}{\mu} \int_{\Omega_1} \partial_1 p \, \psi, \\ \int_{\Omega_1} u_2 \, \psi = -\dfrac{K}{\mu} \int_{\Omega_1} \partial_2 p \, \psi, \end{cases} \qquad \forall \psi \in Q. \tag{4.6.1}$$

If we substitute the approximation (4.3.5)-(4.3.7) into the weak form (4.6.1) we obtain two independent liner systems:

$$\sum_{j \in [\bar{\Omega} \setminus \bar{\Omega}_0]} u_{1,j} \, m_{ij} = \sum_{j \in [\bar{\Omega} \setminus \bar{\Omega}_0]} \bar{p}_j \, r_{ij}, \tag{4.6.2}$$

$$\sum_{j \in [\bar{\Omega} \setminus \bar{\Omega}_0]} u_{2,j} \, m_{ij} = \sum_{j \in [\bar{\Omega} \setminus \bar{\Omega}_0]} \bar{p}_j \, s_{ij}, \tag{4.6.3}$$

where $i \in [\bar{\Omega} \setminus \bar{\Omega}_0]$, $\bar{p}_j$ are already known $\forall j \in [\bar{\Omega}]$ and m_{ij}, r_{ij}, s_{ij} are defined by:

$$\begin{cases} m_{ij} = \int_{\Omega_1} \psi_j \, \psi_i, \\ r_{ij} = -\dfrac{K}{\mu} \int_{\Omega_1} \partial_1 \psi_j \, \psi_i, \\ s_{ij} = -\dfrac{K}{\mu} \int_{\Omega_1} \partial_2 \psi_j \, \psi_i, \end{cases} \qquad \forall i, j \in [\bar{\Omega} \setminus \bar{\Omega}_0]. \tag{4.6.4}$$

Let us extend the linear systems (4.6.2)-(4.6.3) and define coefficients m_{ij} for $i, j \in [\bar{\Omega}_0]$ and right hand sides $b_{1,i}$ $b_{2,i}$ for $i \in [\bar{\Omega}]$:

$$\begin{cases} m_{ii} = 1, & i \in [\bar{\Omega}_0], \\ m_{ij} = 0, & i \neq j \in [\bar{\Omega}_0], \\ b_{1,i} = \bar{u}_{1,i}, & i \in [\bar{\Omega}_0], \\ b_{2,i} = \bar{u}_{2,i}, & i \in [\bar{\Omega}_0], \\ b_{1,i} = \sum_{j \in [\bar{\Omega} \setminus \bar{\Omega}_0]} \bar{p}_j \, r_{ij}, & i \in [\bar{\Omega} \setminus \bar{\Omega}_0], \\ b_{2,i} = \sum_{j \in [\bar{\Omega} \setminus \bar{\Omega}_0]} \bar{p}_j \, s_{ij}, & i \in [\bar{\Omega} \setminus \bar{\Omega}_0]. \end{cases} \tag{4.6.5}$$

We obtain two linear systems which can easily be solved since matrix $M = (m_{ij})$ is symmetric positive definite and therefore invertible:

$$\begin{cases} M \cdot \mathbf{u_1} &= \mathbf{b_1}, \\ M \cdot \mathbf{u_2} &= \mathbf{b_2}. \end{cases} \tag{4.6.6}$$

Remark 4.6.1 *We can restore velocities u_1, u_2 without extending the linear systems (4.6.2)-(4.6.3). In order to do this we define some bijective map $\sigma : \{1, ..., L\} \to [\bar{\Omega} \setminus \bar{\Omega}_0]$, where L is the number of elements in $[\bar{\Omega} \setminus \bar{\Omega}_0]$. The map σ transforms the linear systems (4.6.2)-(4.6.3) as follows:*

$$\sum_{j=1}^{L} u_{1,\sigma(j)}\ m_{\sigma(i)\sigma(j)} = \sum_{j=1}^{L} \bar{p}_{\sigma(j)}\ r_{\sigma(i)\sigma(j)}, \tag{4.6.7}$$

$$\sum_{j=1}^{L} u_{2,\sigma(j)}\ m_{\sigma(i)\sigma(j)} = \sum_{j=1}^{L} \bar{p}_{\sigma(j)}\ s_{\sigma(i)\sigma(j)}, \tag{4.6.8}$$

where $i = 1, ..., L$. Solving systems (4.6.7)-(4.6.8) we obtain velocities $u_{1,j}$ and $u_{2,j}$ for $j \in [\bar{\Omega} \setminus \bar{\Omega}_0]$.

4.7 Precision criterion

A criterion of how precise is our numerical solution is related to satisfaction of the mass conservation equation in the domain Ω_0 and the whole domain $\Omega = \Omega_0 \cup \Sigma \cup \Omega_1$. Integrating the equation $\nabla \cdot \mathbf{u} = 0$ over domains Ω_0 and Ω we obtain integral conditions (4.7.1) that can be considered as a precision criterion that we call the mass conservation precision criterion.

$$\begin{cases} \int_{\partial\Omega_0} \mathbf{u} \cdot \boldsymbol{\nu}_0 &= -\int_{\Gamma_{in}} u_1 + \int_{\Gamma_{out}} u_1 + \int_{\Sigma} u_2 &= 0, \\ \int_{\partial\Omega} \mathbf{u} \cdot \boldsymbol{\nu} &= -\int_{\Gamma_{in}} u_1 + \int_{\Gamma_{out}} u_1 + \int_{M} u_2 &= 0. \end{cases} \tag{4.7.1}$$

After obtaining the numerical solution we can compute values of integrals in (4.7.1) and decide how precisely our solution satisfies the mass conservation equation. In order to do this we substitute the approximation (4.3.5)-(4.3.7) of u_1, u_2 into (4.7.1) and obtain the mass conservation precision criterion in a discrete form:

$$E_{\Omega_0} := \int_{\partial\Omega_0} \mathbf{u_h} \cdot \boldsymbol{\nu}_0 = -\sum_{j\in[\Gamma_{in}]} u_{1,j} \int_{\Gamma_{in}} \psi_j + \sum_{j\in[\Gamma_{out}]} u_{1,j} \int_{\Gamma_{out}} \psi_j + \sum_{j\in[\Sigma]} u_{2,j} \int_{\Sigma} \psi_j, \tag{4.7.2}$$

$$E_{\Omega} := \int_{\partial\Omega} \mathbf{u_h} \cdot \boldsymbol{\nu} = -\sum_{j\in[\Gamma_{in}]} u_{1,j} \int_{\Gamma_{in}} \psi_j + \sum_{j\in[\Gamma_{out}]} u_{1,j} \int_{\Gamma_{out}} \psi_j + \sum_{j\in[M]} u_{2,j} \int_{M} \psi_j, \tag{4.7.3}$$

where coefficients $u_{1,j}, u_{2,j}$ are already known. Values E_{Ω_0} and E_{Ω} represent error on the mass conservation in domains Ω_0 and Ω.

The maximum norm of the residual is used as a precision criterion of the iterative method for solving the resulting linear system. The precision criterion of the iterative method and the mass conservation precision criterion are connected to each other. The mass conservation precision criterion can be considered as a measure of precision of the numerical solution globally on the whole domain. The iterative method precision criterion contains a local form of the mass conservation precision criterion on each finite element.

4.8 Iterative Gauss-Seidel overlapping block method

Here we present the iterative Gauss-Seidel overlapping block method (see [9]) for solving the linear system (4.4.13). This iterative method efficiently uses block diagonal structure of the matrix and gives results with the same precision and much faster than the direct Gaussian Elimination method. It works for large matrices when the direct method does not work because of PC memory shortage. This approach is applied to the 3D Hydrogen Fuel Cell Problem, see [7] A.Novruzi, K.Promislow, B.Wetton.

In our implementation of the iterative Gauss-Seidel overlapping block method we use the "separated" and the "direct" numbering of nodes. In the "separated" one we number nodes first in the channel and next in the GDL as it is shown on the first picture on Figure 4.2. In the "direct" numbering we start from the left bottom corner of the channel and keep numbering nodes in the vertical direction up to the membrane in the GDL, as it is shown on the second picture on Figure 4.2. Nodes numbering

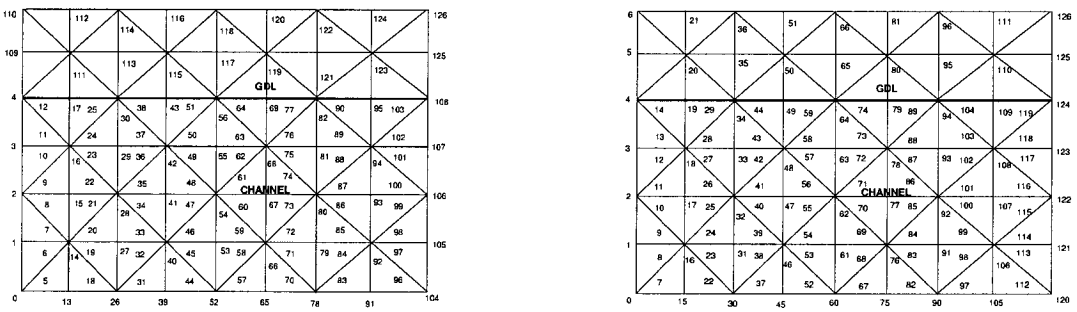

Figure 4.2: The "separated" numbering and the "direct" numbering of nodes.

determines an overlapping blocks structure of the domain. Matrices which are obtained from the meshes with the "separated" and the "direct" numbering of nodes also have an overlapping blocks structure.

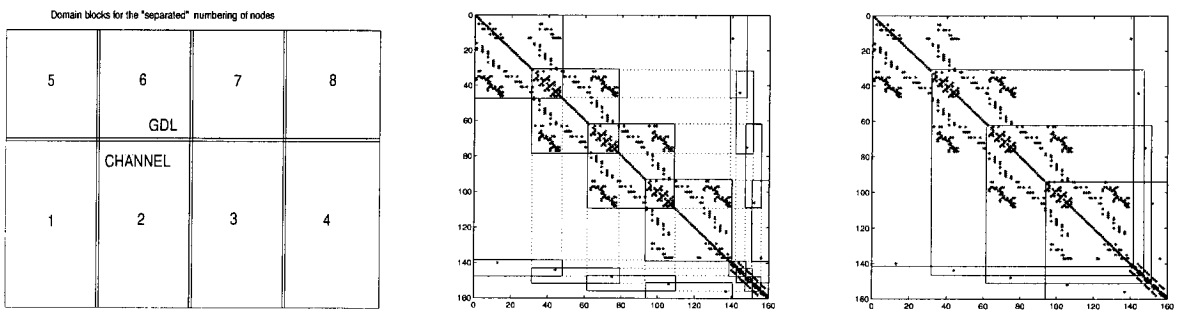

Figure 4.3: An overlapping blocks structure of the mesh with the "separated" numbering of nodes and matrices obtained from this mesh.

A matrix obtained from the mesh with the "separated" numbering of nodes is shown on the second picture on Figure 4.3. It has overlapping diagonal blocks with different

sizes and some overlapping non-diagonal blocks. There exist a correspondence between domain blocks on the first picture and matrix blocks on the second picture on Figure 4.3. Larger diagonal matrix blocks correspond to the domain blocks located in the channel. Smaller diagonal matrix blocks correspond to the domain blocks located in the GDL. Non-diagonal matrix blocks correspond to some nodes that belong to triangles which are located in the GDL and have common nodes with the interface. Elements of the non-diagonal matrix blocks contain information about coupling that is preferable to have in diagonal matrix blocks. In order to avoid non-diagonal matrix blocks we can consider larger diagonal matrix blocks (see the third picture on Figure 4.3). In this case diagonal matrix blocks almost coincide with the whole matrix and have very large overlapping area, that gives no reason to apply the iterative overlapping block method. So, the "separated" numbering of nodes is not adequate for solving the resulting linear system by the iterative Gauss-Seidel overlapping block method. In order to avoid these difficulties we need a mesh with the "direct" numbering of nodes.

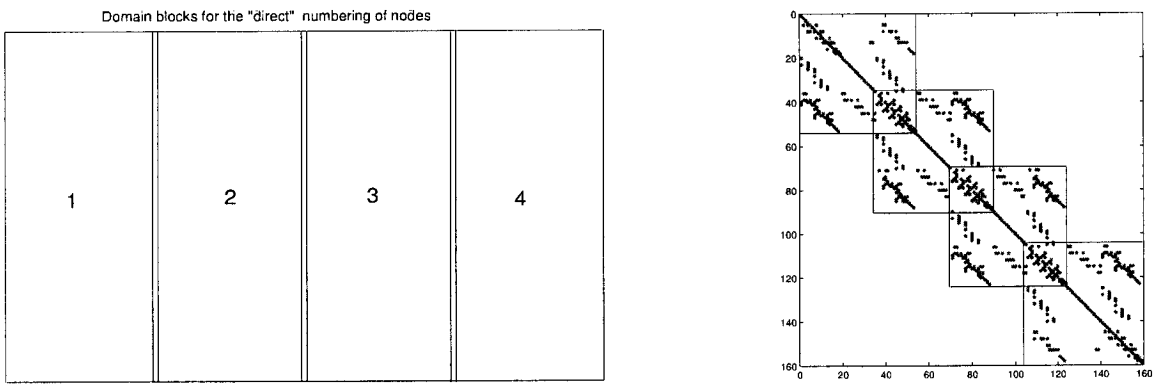

Figure 4.4: Block structure of the mesh with the "direct" numbering of nodes and a matrix obtained from this mesh. (The case of elementary domain blocks.)

A domain with the "direct" numbering of nodes has the natural division into vertical strips with the same number of nodes in each of them (see the second picture on Figure 4.2). Each vertical strip has common nodes (overlapping) with its neighbor strips. Those nodes belong to the right or left vertical sides of the strip. These vertical strips we call *elementary* domain blocks. The number of elementary domain blocks is the number of divisions N_{Ω_0,x_1} of the coupled domain along the axis x_1. As it is seen on the second picture on Figure 4.4, the "direct" numbering gives a resulting matrix with overlapping diagonal matrix blocks, each of them with the same size. Each elementary domain block corresponds to a diagonal matrix block in the resulting matrix. These diagonal matrix blocks are called *elementary* diagonal matrix blocks. So, the natural domain block structure generated by the "direct" numbering gives a possibility to apply the iterative Gauss-Seidel overlapping block method for solving the resulting linear system.

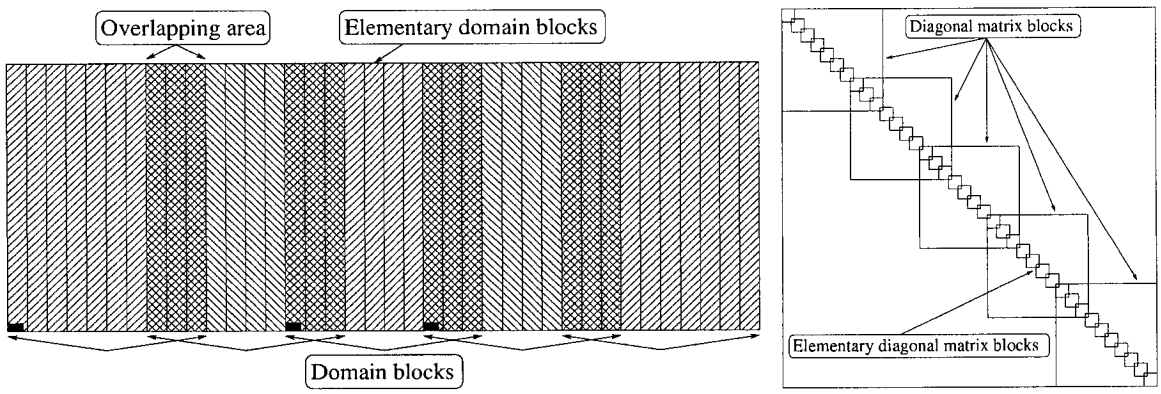

Figure 4.5: Domain blocks of the mesh with the "direct" numbering of nodes and a matrix obtained from this mesh.

Definition 4.8.1 *A connected domain block (see Figure 4.5) composed of k elementary domain blocks is called a domain block of an order k. A collection of domain blocks of an order k which covers the coupled domain is called a covering of an order k.*

The number $N_n(k)$ of nodes in a domain block of an order k is defined as follows:

$$\begin{cases} n_v & = & N_{\Omega_0,x_2} + N_{\Omega_1,x_2} + 1, & (\text{ is the number of vertex nodes along } x_2 \text{ axis }), \\ n_c & = & 2\, N_{\Omega_0,x_2}, & (\text{ is the number of center nodes along } x_2 \text{ axis }), \\ N_n(k) & = & n_v\ (k+1) + n_c\ k, & \forall k = 1...N_{\Omega_0,x_1}. \end{cases} \tag{4.8.1}$$

As it is seen on Figure 4.5, each domain block has some displacement relatively to a previous domain block. Displacement is the number of those nodes of the previous domain block which do not belong to the current domain block.

Here we consider coverings of the coupled domain by domain blocks with equal displacements. For any fixed k the displacement d is not unique and defined as follows:

$$d = l\ (n_v + n_c),\ \text{for } l = 1...k \text{ such that } \frac{N_{nodes,\Omega} - N_n(k)}{l\ (n_v + n_c)} \in \mathbb{N}. \tag{4.8.2}$$

As soon as we have chosen the displacement d we can define uniquely the covering of the order k. The number $N_b(k,d)$ of domain blocks in the covering is given by:

$$N_b(k,d) \ = \ 1 + \frac{N_{nodes,\Omega} - N_n(k)}{d}. \tag{4.8.3}$$

The covering of an order $k = 1$ consists of elementary domain blocks and their number is $N_b(1,d) = N_{\Omega_0,x_1}$. In this case each block, except the first and the last ones, is overlapped with neighbor domain blocks from the right and from the left along sides containing only vertex nodes. The only displacement for this covering is $d = n_v + n_c$ nodes. In the case when $k = N_{\Omega_0,x_1}$ we have the least possible number of domain blocks,

that is just one domain block which coincides with the whole domain Ω. In order to create some covering of the domain with domain blocks which are different from the above cases we need to fix the order k for the covering and choose one of the possible displacements from (4.8.2) and then compute the number of domain blocks by (4.8.3).

In order to construct a correspondence between domain blocks and matrix blocks we choose some covering of an order k, some displacement d satisfying (4.8.2) and define the set $\mathcal{B}(k,m)$ containing the nodes belonging to a m_{th} domain block as follows:

$$\mathcal{B}(k,m) \;=\; \{m\ d, ..., m\ d + N_n(k) - 1\}, \text{where } 0 \le m \le N_b(k,d) - 1. \qquad (4.8.4)$$

Now we can construct matrix blocks $\boldsymbol{B}_{n,m}$ of the resulting matrix, the block right hand side vector $\boldsymbol{R}_n$ and the block vector of unknowns $\boldsymbol{V}_n$ as follows:

$$\begin{cases} \boldsymbol{B}^{i,j}_{n,m} = \boldsymbol{A}_{i,j}, & where \quad (i,j) \in \mathcal{B}(k,n) \times \mathcal{B}(k,m), \\ \boldsymbol{V}^{i}_{n} = \boldsymbol{U}_{i}, & where \quad i \in \mathcal{B}(k,n), \\ \boldsymbol{R}^{i}_{n} = \boldsymbol{b}_{i}, & where \quad i \in \mathcal{B}(k,n), \end{cases} \qquad (4.8.5)$$

where $0 \le n, m \le N_b(k,d) - 1$ and $\boldsymbol{A}$, $\boldsymbol{U}$, $\boldsymbol{b}$ are defined in (4.4.10)-(4.4.12) and (4.4.13).

The next step in our construction is to make matrix blocks, lying in the same block row n, be "non-overlapping" in the following way:

$$\begin{cases} \boldsymbol{B}^{i,j}_{n,m} = 0, \quad \forall (i,j) \in \mathcal{B}(k,n) \times (\mathcal{B}(k,m-1) \cap \mathcal{B}(k,m)), \\ where\ 0 \le n < m \le N_b(k,d) - 1, \end{cases} \qquad (4.8.6)$$

$$\begin{cases} \boldsymbol{B}^{i,j}_{n,m} = 0, \quad \forall (i,j) \in \mathcal{B}(k,n) \times (\mathcal{B}(k,m) \cap \mathcal{B}(k,m+1)), \\ where\ 0 \le m < n \le N_b(k,d) - 1, \end{cases} \qquad (4.8.7)$$

Remark 4.8.2 *This modification of matrix blocks is made to avoid repetition in the iterative Gauss-Seidel scheme(see (4.8.8)).*

Now we can apply the iterative Gauss-Seidel overlapping block method to the block linear system $\boldsymbol{BV} = \boldsymbol{R}$ obtained in (4.8.5). The general scheme for the iterative method is:

$$\boldsymbol{B}_{n,n}\boldsymbol{V}^{(l)}_{n} = \boldsymbol{R}_n - \sum_{m<n} \boldsymbol{B}_{n,m}\boldsymbol{V}^{(l)}_{m} - \sum_{m>n} \boldsymbol{B}_{n,m}\boldsymbol{V}^{(l-1)}_{m}, \ for\ 0 \le n,m \le N_b(k,d) - 1. \qquad (4.8.8)$$

We can significantly reduce overall computations by choosing the displacement d such that $d > \dfrac{N_n(k)}{2}$. In this case blocks $\boldsymbol{B}_{n,m}$ contain only zero elements for $\forall m, n$ such that $m < n - 1$ and $m > n + 1$. It means that in each n-th row of the block matrix $\boldsymbol{B}$ we have three non-zero matrix blocks $\boldsymbol{B}_{n-1,n}$, $\boldsymbol{B}_{n,n}$ and $\boldsymbol{B}_{n,n+1}$ for $0 < n < N_b(k,d) - 1$ and just two non-zero blocks for $n = 0$ and $n = N_b(k,d) - 1$ (see Figure 4.6).

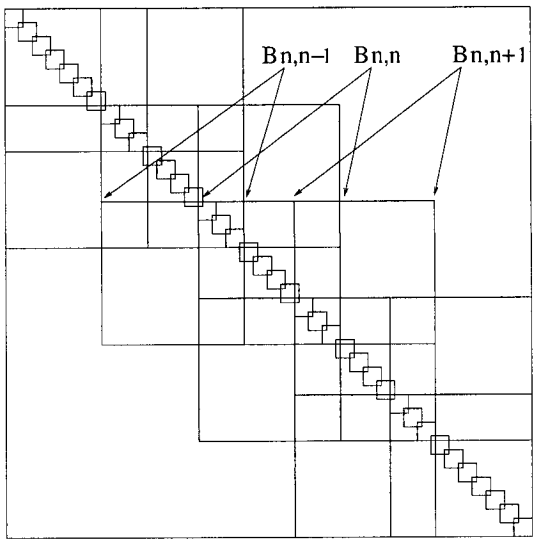

Figure 4.6: A resulting matrix with no more then three non-zero matrix blocks in each row.

Taking in account this observation we have modification of the iterative scheme (4.8.8) in the form:

$$\begin{cases} \boldsymbol{B}_{n,n}\boldsymbol{V}_n^{(l)} = \boldsymbol{R}_n - \boldsymbol{B}_{n,n+1}\boldsymbol{V}_{n+1}^{(l-1)}, & for \quad n = 0, \\ \boldsymbol{B}_{n,n}\boldsymbol{V}_n^{(l)} = \boldsymbol{R}_n - \boldsymbol{B}_{n,n-1}\boldsymbol{V}_{n-1}^{(l)} - \boldsymbol{B}_{n,n+1}\boldsymbol{V}_{n+1}^{(l-1)}, & for \quad 0 < n < N_b(k,d) - 1, \\ \boldsymbol{B}_{n,n}\boldsymbol{V}_n^{(l)} = \boldsymbol{R}_n - \boldsymbol{B}_{n,n-1}\boldsymbol{V}_{n-1}^{(l-1)}, & for \quad n = N_b(k,d) - 1. \end{cases} \tag{4.8.9}$$

For the initial approximation $\boldsymbol{V}^{(0)}$ we have many choices. The simplest is $\boldsymbol{V}_n^{(0)} = 0$. We also can take the Poiseuille solution computed in the channel and extended it to the GDL or a multigrid approximation. The multigrid approximation can be obtained by assembling the resulting linear system on a coarse mesh, then solving it by the direct Gaussian Elimination method and then projecting the solution to a fine mesh. In the first iteration $l = 1$ we apply LUP decomposition for diagonal blocks $\boldsymbol{B}_{n,n}$ and backstep substitution for solving the linear systems in (4.8.8). We store obtained LUP decompositions of the diagonal blocks $\boldsymbol{B}_{n,n}$ and pivot vectors. For solving linear systems (4.8.8) on other iterations we apply only the backstep substitution method. In all our numerical experiments overlapping diagonal blocks $\boldsymbol{B}_{n,n}$ for $0 \leq n \leq N_b(k,d) - 1$ are non-singular. Iterative schemes (4.8.8) and (4.8.9) converge and give precision of the same order as the direct method. Our computations in Section 5.6.5 show that the iterative scheme (4.8.9) gives results faster than the direct method and with the same precision.

Now we present the algorithm for the LUP decomposition with scaling which is very important for precision and convergence of the iterative schemes (4.8.8) and (4.8.9).

The LUP decomposition algorithm with scaling

(001) $N \leftarrow size(M[N][N])$
(002) $idx[N] \leftarrow 0$
(003) $scale[N] \leftarrow 0$
(004) $jPivot \leftarrow 0$
(005) $scaleMax \leftarrow 0$
(006) $ratiomax \leftarrow 0$
(007) $ratio \leftarrow 0$
(008) **for** $i \leftarrow 0$ **to** $N-1$
(009) $\quad idx[i] \leftarrow i$
(010) $\quad scaleMax \leftarrow 0$
(011) $\quad$ **for** $j \leftarrow 0$ **to** $N-1$
(012) $\quad\quad$ **if**$(scaleMax \leq ABS(M[i][j])$
(013) $\quad\quad\quad scaleMax \leftarrow ABS(M[i][j])$
(014) $\quad scale[i] \leftarrow scaleMax$
(015) **for** $k \leftarrow 0$ **to** $N-1$
(016) $\quad ratiomax \leftarrow 0$
(017) $\quad jPivot \leftarrow k$
(018) $\quad$ **for** $i \leftarrow k$ **to** $N-1$
(019) $\quad\quad ratio \leftarrow \dfrac{ABS(M[i][k])}{scale[idx[i]]}$
(020) $\quad\quad$ **if** $ratio > ratiomax$
(021) $\quad\quad\quad ratiomax \leftarrow ratio$
(022) $\quad\quad\quad jPivot \leftarrow i$
(023) $\quad$ **if** $ratiomax = 0$
(024) $\quad\quad$ The matrix is singular!
(025) $\quad\quad STOP$
(026) $\quad$ **if** $k \neq jPivot$
(027) $\quad\quad idx[jPivot] \leftrightarrow idx[k]$
(028) $\quad\quad$ **for** $i \leftarrow 0$ **to** $N-1$
(029) $\quad\quad\quad M[k][i] \leftrightarrow M[jPivot][i]$
(030) $\quad$ **for** $i \leftarrow k+1$ **to** $N-1$
(031) $\quad\quad M[i][k] \leftarrow \dfrac{M[i][k]}{M[k][k]}$
(032) $\quad\quad$ **for** $j \leftarrow k+1$ **to** $N-1$
(033) $\quad\quad\quad M[i][j] \leftarrow M[i][j] - M[i][k]M[k][j]$
(034) RETURN $M[N][N], idx[N]$

5

Numerical results

5.1 Choice of the mesh

In numerical computations we experimented with two different mesh patterns: the "center oriented" mesh with diagonals of rectangles which are oriented to the center of the domain and the "symmetric" mesh, as it is seen on the Figure 5.1. The choice was made in favor of "symmetric" mesh because the numerical solution for the Poiseuille flow in the channel obtained on the "symmetric" mesh gives the normal velocity u_2 of order 10^{-14}, but the "center oriented mesh" gives the normal velocity u_2 of order 10^{-3} (see the results in Section 5.6).

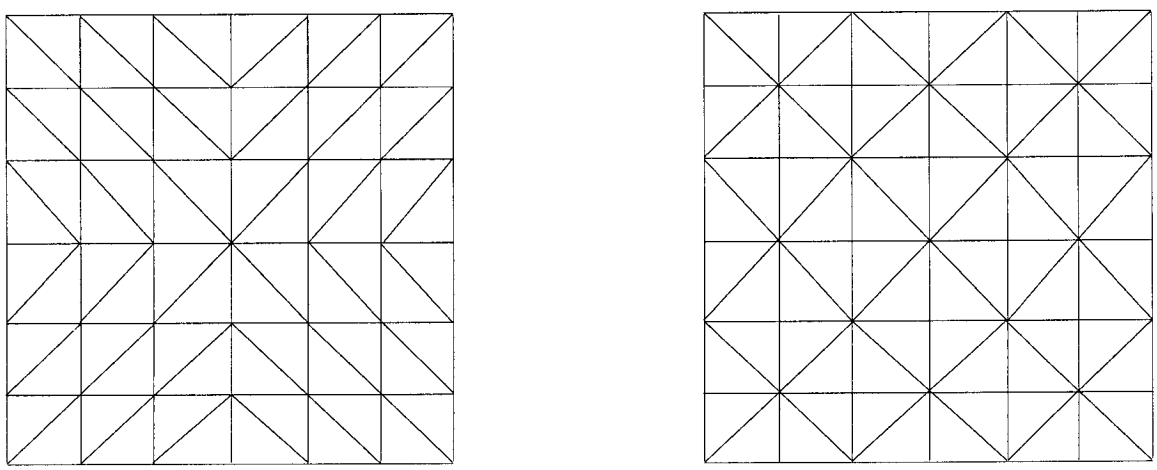

Figure 5.1: The "center oriented" mesh and the "symmetric" mesh.

5.2 Parameters for numerical results

Parameters that will be used in numerical results for the model and real domains are presented in Table 5.1.

Parameters	Description
l, h, H	dimensions of the domain, (page 7)
μ	viscosity coefficient, (page 8)
K	Darcy Law coefficient, (page 8)
S	Safman's condition coefficient, (page 9)
α, β	balancing coefficients, (page 49)
p_{in}	pressure given on Γ_{in}, (page 9)
p_{out}	pressure given on Γ_{out}, (page 9)
p_m	pressure given on M, (page 9)
N_{Ω_0,x_1}	the number of divisions along axis x_1 of Ω_0
N_{Ω_0,x_2}	the number of divisions along axis x_2 of Ω_0
N_{Ω_1,x_2}	the number of divisions along axis x_2 of Ω_1
N_{ext,x_1}	the number of divisions along axis x_1 of extensions of Ω_0
L_{ext}	the length of each extension of Ω_0
ϵ_1	the power of mesh adaptation along x_1, (page 51)
ϵ_2	the power of mesh adaptation along x_2 or along x_1 in the opposite direction, (page 51)
$N_{\triangle,\Omega}$	the total number of triangles
$N_{nodes,\Omega}$	the number of nodes in Ω
Dim_{Matrix}	the dimension of the matrix
N_{blocks}	the number of domain blocks, (page 34)
$N_{block,nodes}$	the number of nodes in a domain block, (page 34)
$N_{displ,nodes}$	the displacement, (page 34)
$N_{iterations}$	the number of iterations of the iterative method, (page 36)
$Time_{GS}$	time to solve the linear system with the iterative Gauss-Seidel overlapped block method
$Time_{GE}$	time to solve the linear system with direct Gauss Elimination method
Res_{GS}	the residual obtained by the iterative Gauss-Seidel overlapped block method
Res_{GE}	the residual obtained by the direct Gauss Elimination method
$u_{1\Gamma_{in}}$	total flux on Γ_{in}
$u_{1\Gamma_{out}}$	total flux on Γ_{out}
$u_{2\Sigma}$	total flux on Σ
u_{2M}	total flux on M

Table 5.1: Parameters of numerical results.

5.3 Solution for a model domain

Here we consider a model domain with aspect ratio 1. The reason of these computations is to show the precision of the method for non-singular data, the fluid flow in the whole domain and behavior of the solution in the boundary-interface contact points.

5.3.1 Solution for the model domain with constant pressure on the membrane

In Table 5.2 are presented numerical results for the model problem for the case when the domain Ω_0 has no extensions (I)-(IV) (see Figure 2.2) and for the domain Ω_0 with extensions (V)-(VI) (see Figure 2.3). For our computations here we take the sizes (2.2.1) of the domain as follows: $H = 1$, $h = 1$, $l = 2$.

	Domains with no extensions				**Domains with extensions**	
Parameters	**(I)**	**(II)**	**(III)**	**(IV)**	**(V)**	**(VI)**
μ, K, S	1	1	1	1	1	1
p_{in}	100	100	100	100	100	100
p_{out}	0	0	0	0	0	0
p_m	10	10	10	10	10	10
N_{Ω_0,x_1}	10	20	30	40	14	40
N_{Ω_0,x_2}	10	20	30	28	14	24
N_{Ω_1,x_2}	10	10	20	20	14	18
N_{ext,x_1}	-	-	-	-	2	2
L_{ext}	-	-	-	-	0.5	0.2
$N_{nodes,\Omega}$	431	1451	3381	4249	999	4267
$N_{\triangle,\Omega}$	400	1200	3000	3840	896	3744
Dim_{Matrix}	873	3133	7103	8867	2073	9021
$u_{1\Gamma_{in}}$	12.9060	14.3568	15.0027	15.2281	7.1628	10.5796
$u_{1\Gamma_{out}}$	3.0608	3.4571	3.6387	3.7068	1.2059	1.9983
$u_{2\Sigma}$	9.8846	10.9526	11.4072	11.5634	5.9683	8.5945
u_{2M}	9.8772	10.9545	11.4100	11.5811	5.9049	8.5976
$\int_{\partial\Omega_0} \mathbf{u_h} \cdot \boldsymbol{\nu}_0$	0.0394	0.0529	0.0432	0.0420	0.0114	0.0132
$\int_{\partial\Omega} \mathbf{u_h} \cdot \boldsymbol{\nu}$	0.0320	0.0548	0.0460	0.0598	-0.0518	0.0163
$\frac{\int_{\partial\Omega_0} \mathbf{u_h} \cdot \boldsymbol{\nu}_0}{u_{2M}}$	0.0039	0.0047	0.0037	0.0036	0.0018	0.0015
$\frac{\int_{\partial\Omega} \mathbf{u_h} \cdot \boldsymbol{\nu}}{u_{2M}}$	0.0032	0.0050	0.0040	0.0050	-0.0086	0.0018

Table 5.2: Numerical results for the model domain. Condition numbers of all resulting matrices are of order 10^{+04}.

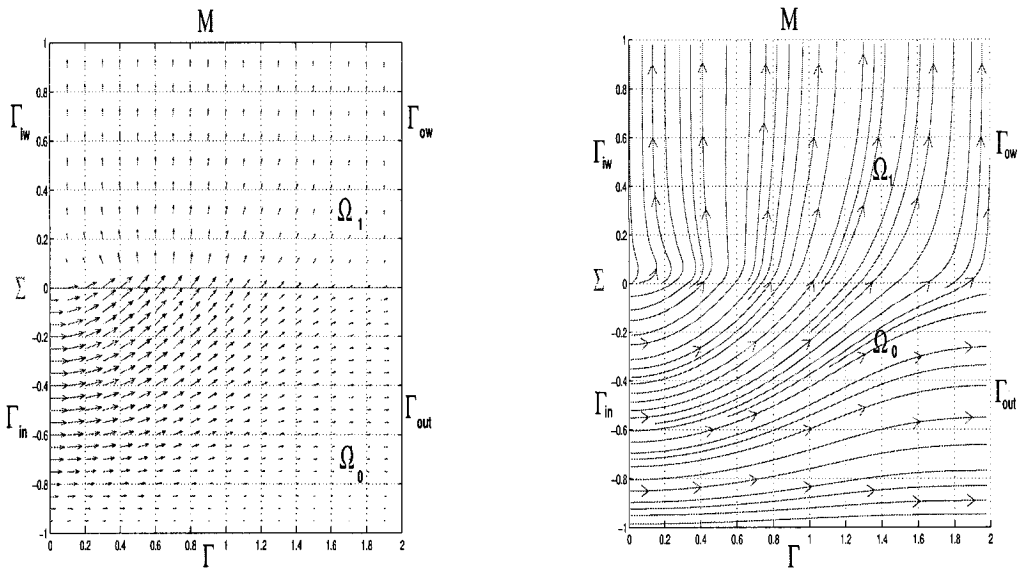

Figure 5.2: Vector field and stream lines of the fluid flow for the model problem for the domain with no extensions. The domain division is $N_{\Omega_0,x_1} = 20$, $N_{\Omega_0,x_2} = 20$, $N_{\Omega_1,x_2} = 10$.

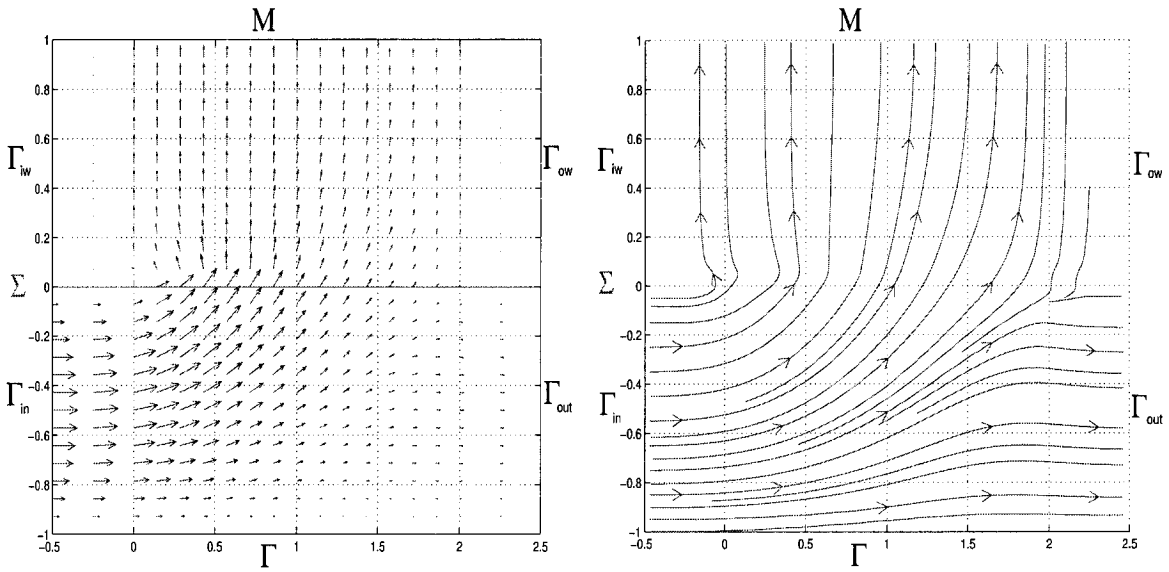

Figure 5.3: Vector field and stream lines of the fluid flow for the model problem for the domain with extensions. The domain division is $N_{\Omega_0,x_1} = 14$, $N_{\Omega_0,x_2} = 14$, $N_{\Omega_1,x_2} = 14$. The extensions division is $N_{ext,x_1} = 2$ and length is $L_{ext} = 0.5$.

The numerical results presented in Table 5.2 are made in order to understand behavior of the solution in the whole domain and in the inlet-interface and the outlet-interface contact points. For this purpose we make computations for the domain with no extensions and for the domain with extensions. The numerical results show that the problem with no extensions on Figure 5.2 can be considered as the limit case of the problem with extensions on Figure 5.3. For the domain with extensions the boundary where $u_1 = 0$ includes points $\partial\Sigma$. Therefore, in our numerical method instead of prescribing $u_2 = 0$ and p we impose $\mathbf{u} = \mathbf{0}$ in the points $\partial\Sigma$.

On Figure 7.1 (see page 73) we can see singularities of the pressure in the boundary-interface contact points. On Figure 7.4 (see page 75) we can see that extensions reduce the singularities of the pressure in the boundary-interface contact points.

In general, singularities of a solution in the boundary-interface contact points are expected due to incompatibilities of boundary and interface conditions in these points (see [5] and [7]).

5.3.2 Solution for the model domain with non-constant pressure on the membrane

In the Table 5.3 we present numerical results for the model problem when the pressure p_m is given on the membrane and depends on the variable x_1. In the numerical results (I)-(II) on the interface Σ we impose conditions (2.2.8) with the homogeneous reduced Saffman's condition $u_1 = 0$.

Parameters	Domains with no extensions			
	(I)	(II)	(III)	(IV)
H	1	1	1	1
h	1	1	1	1
l	2	2	2	2
μ	1	1	1	1
K	1	1	1	1
S	$u_1 = 0$	$u_1 = 0$	1	1
p_{in}	100	100	100	100
p_{out}	0	0	0	0
p_m	$20(1 - cos(\pi\frac{x_1}{l}))$	$30(1 - cos(\pi\frac{x_1}{l}))$	$30(1 - cos(\pi\frac{x_1}{l}))$	$30(1 + cos(\pi\frac{x_1}{l}))$
N_{Ω_0,x_1}	10	20	20	30
N_{Ω_0,x_2}	10	10	10	10
N_{Ω_1,x_2}	10	8	8	8
$N_{\triangle,\Omega}$	400	720	720	1080
$N_{nodes,\Omega}$	431	799	799	1189
Dim_{Matrix}	873	1661	1661	2471
$u_{1\Gamma_{in}}$	8.824	8.088	11.490	10.840
$u_{1\Gamma_{out}}$	3.004	4.173	6.300	5.566
$u_{2\Sigma}$	5.739	3.921	5.240	5.327
u_{2M}	5.730	3.928	5.280	5.385
$\int_{\partial\Omega_0} \mathbf{u_h} \cdot \boldsymbol{\nu}_0$	0.080	0.00605	0.0506	0.0540
$\int_{\partial\Omega} \mathbf{u_h} \cdot \boldsymbol{\nu}$	0.089	0.01304	0.0906	0.1123
$\frac{\int_{\partial\Omega_0} \mathbf{u_h} \cdot \boldsymbol{\nu}_0}{u_{2M}}$	0.014	0.00154	0.00965	0.0101
$\frac{\int_{\partial\Omega} \mathbf{u_h} \cdot \boldsymbol{\nu}}{u_{2M}}$	0.015	0.00332	0.01715	0.0208

Table 5.3: Numerical results for the model domain with the non-constant pressure on the membrane M. Condition numbers of all resulting matrices are of order 10^{+04}.

In Remark 2.2.1 we mentioned that the regular and reduced Saffman's conditions can be considered as "similar" if the function $g(\mathbf{x})$ in (2.2.8) is close to porosity of the GDL. In the results (II) on Figure 5.4 on the interface is imposed reduced Saffman's condition with $g(\mathbf{x}) = 0$. The shape of the flow is very similar to the one of the result (III) on Figure 5.5 with the regular Saffman's conditions and constant $S = 1$. The only difference can be seen on pictures of the vector field where for the fluid flow with the reduced Saffman's condition the tangential component of the velocity is zero on the interface.

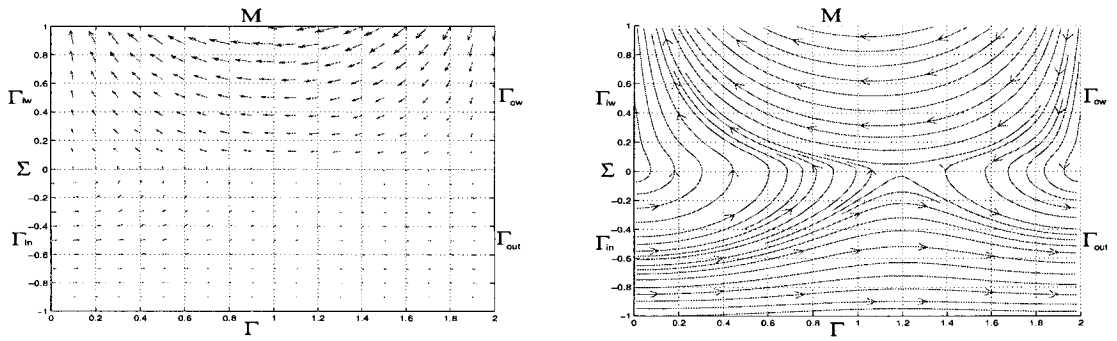

Figure 5.4: The vector field and stream lines of the fluid flow for the model domain with no extensions and non-constant pressure prescribed on M. The domain division is $N_{\Omega_0,x_1} = 20$, $N_{\Omega_0,x_2} = 10$, $N_{\Omega_1,x_2} = 8$. The homogeneous reduced Saffman's condition $u_1 = 0$ is imposed on the interface and the pressure $p_m = 30(1 - cos(\pi \frac{x_1}{l}))$ is prescribed on the membrane M. (II)

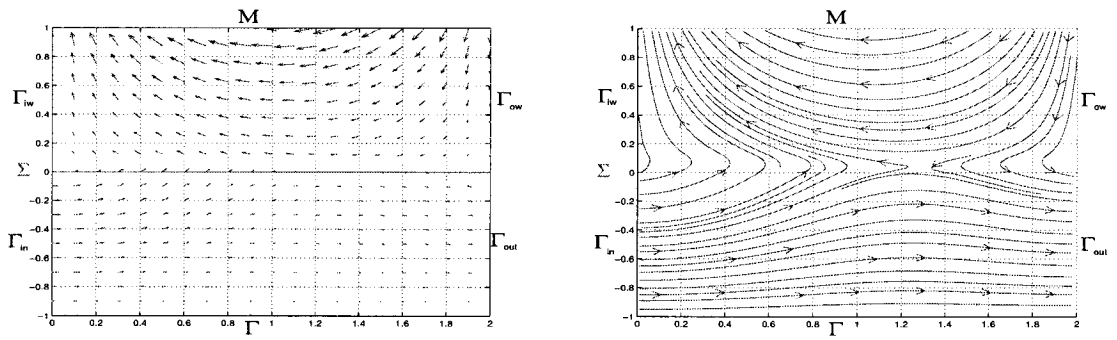

Figure 5.5: The vector field and stream lines of the fluid flow for the model domain with no extensions and non-constant pressure prescribed on M. The domain division is $N_{\Omega_0,x_1} = 20$, $N_{\Omega_0,x_2} = 10$, $N_{\Omega_1,x_2} = 8$. The regular Saffman's condition on the interface ($S = 1$). The pressure $p_m = 30(1 - cos(\pi \frac{x_1}{l}))$ is prescribed on the membrane M. (III)

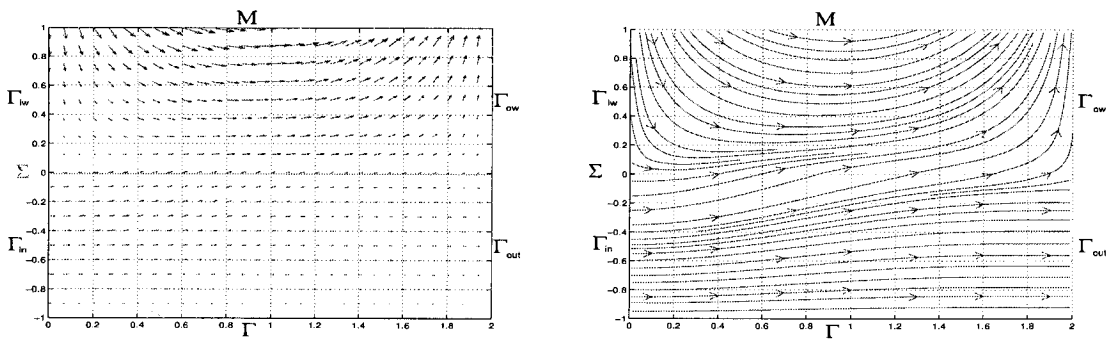

Figure 5.6: The vector field and stream lines of the fluid flow for the model domain with no extensions and non-constant pressure prescribed on M. The domain division is $N_{\Omega_0,x_1} = 30$, $N_{\Omega_0,x_2} = 10$, $N_{\Omega_1,x_2} = 8$. The regular Saffman's condition on the interface ($S = 1$). The pressure $p_m = 30(1 + cos(\pi \frac{x_1}{l}))$ is prescribed on the membrane M. (IV)

5.3.3 Solution for the model domain with no flow on the membrane

In the Table 5.4 we present numerical results for the model problem when the membrane M is closed, so that the boundary condition $p_{|M} = p_m$ is replaced by $\partial_2 p_{|M} = 0$.

Parameters	Domains with no extensions (I)	(II)	Domains with extensions (III)
H	1	1	1
h	3	1	1
l	3	2	2
μ	0.1	1	1
K	1	1	1
S	1	1	1
p_{in}	100	100	100
p_{out}	0	0	0
p_m	$\partial_2 p_{\|M} = 0$	$\partial_2 p_{\|M} = 0$	$\partial_2 p_{\|M} = 0$
N_{Ω_0,x_1}	14	14	14
N_{Ω_0,x_2}	14	14	14
N_{Ω_1,x_2}	14	14	14
N_{ext,x_1}	-	-	2
L_{ext}	-	-	0.5
$N_{\triangle,\Omega}$	784	784	896
$N_{nodes,\Omega}$	827	827	999
Dim_{Matrix}	1669	1669	2073
$u_{1\Gamma_{in}}$	73.256	8.465	4.181
$u_{1\Gamma_{out}}$	73.256	8.465	4.181
$u_{2\Sigma}$	$-5.22 \cdot 10^{-12}$	$2.55 \cdot 10^{-12}$	$2.04 \cdot 10^{-12}$
u_{2M}	$-7.35 \cdot 10^{-13}$	$1.26 \cdot 10^{-13}$	$2.00 \cdot 10^{-13}$
$\int_{\partial\Omega_0} \mathbf{u_h} \cdot \boldsymbol{\nu}_0$	$-2.74 \cdot 10^{-14}$	$9.34 \cdot 10^{-15}$	$2.515 \cdot 10^{-15}$
$\int_{\partial\Omega} \mathbf{u_h} \cdot \boldsymbol{\nu}$	$4.46 \cdot 10^{-12}$	$-2.41 \cdot 10^{-12}$	$-1.84 \cdot 10^{-12}$
$\frac{\int_{\partial\Omega_0} \mathbf{u_h} \cdot \boldsymbol{\nu}_0}{u_{2M}}$	0.037	0.036	0.012
$\frac{\int_{\partial\Omega} \mathbf{u_h} \cdot \boldsymbol{\nu}}{u_{2M}}$	-6.06	-19.12	-9.1

Table 5.4: Numerical results for the model domain with no flow on the membrane M. Condition numbers of all resulting matrices are of order 10^{+04}.

The numerical results presented in Table 5.4 are made in order to understand behavior of the solution in the whole domain and in the boundary-interface contact points, when the condition $\partial_2 p_{|M} = 0$ is imposed on the membrane. The numerical results show that the problem with no extensions can be considered as the limit case of the problem with extensions, the same way when the pressure is constant on the membrane. On Figure 7.11 (see page 79) we can see singularities of the pressure in the boundary-interface contact points for the result (II). On Figure 7.17 (see page 82) we can see that extensions reduce the singularities of the pressure in the boundary-interface contact points for the result (III). The mass conservation precision criterion is very well satisfied. The values of $\frac{\int_{\partial\Omega} \mathbf{u_h} \cdot \boldsymbol{\nu}}{u_{2M}}$ reflect the relative loss of precision. The result (I) shows the behavior of the fluid for different than in (II) parameters.

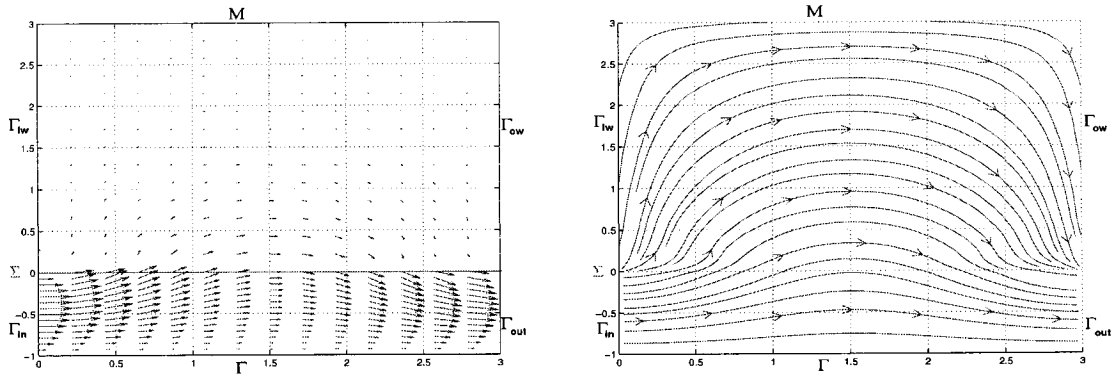

Figure 5.7: The vector field and stream lines of the fluid flow for the model domain with no extensions and closed boundary M. Domain division is $N_{\Omega_0,x_1} = 14$, $N_{\Omega_0,x_2} = 14$, $N_{\Omega_1,x_2} = 14$. Viscosity $\mu = 0.1$, the domain sizes are $l = 3$, $h = 3$, $H = 1$. (I)

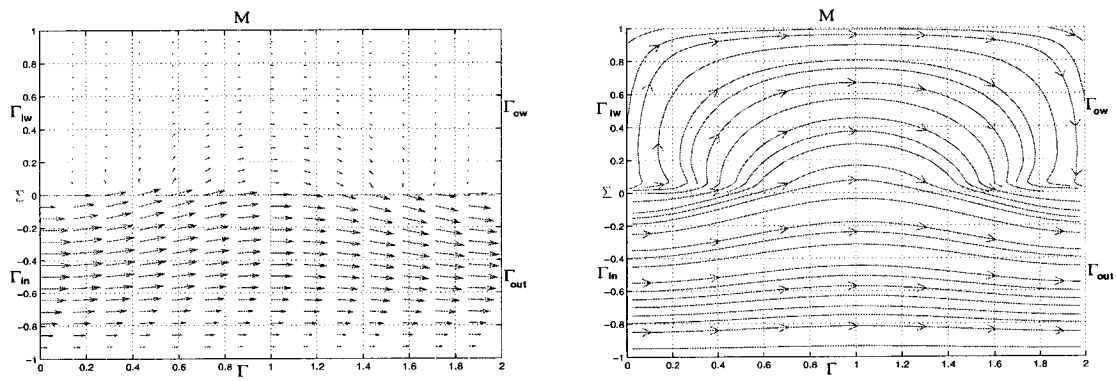

Figure 5.8: The vector field and stream lines of the fluid flow for the model domain with no extensions and closed boundary M. Domain division is $N_{\Omega_0,x_1} = 14$, $N_{\Omega_0,x_2} = 14$, $N_{\Omega_1,x_2} = 14$. (II)

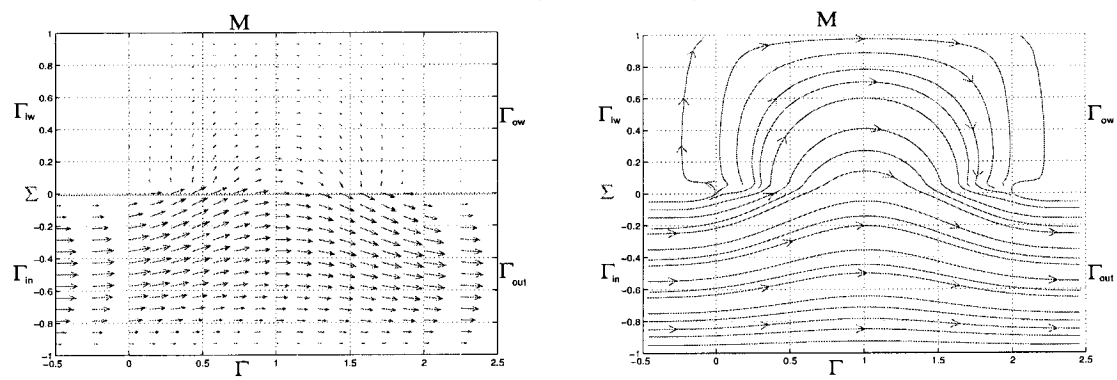

Figure 5.9: The vector field and stream lines of the fluid flow for the model domain with extensions and closed boundary M. Domain division is $N_{\Omega_0,x_1} = 14$, $N_{\Omega_0,x_2} = 14$, $N_{\Omega_1,x_2} = 14$. Extension division is $N_{ext,x_1} = 2$ and length is $L_{ext} = 0.5$. (III)

5.4 Solution for a real domain

Here we consider the domain which represents a cross section of a real 3D hydrogen fuel cell. So, that the domain sizes, viscosity μ, the Darcy coefficient K, the Saffman's coefficient S, boundary and interface conditions are the same as real hydrogen fuel cells have. It means that the pressure on the inlet is very large, the domain is very thin and relatively long. For these parameters it is very difficult to solve the the resulting linear system since whether it is a direct or some iterative method they will accumulate round-off errors which can affect the numerical solution. But the round-off errors are not the only problem that appears in computations. Another problem comes from the aspect ratio of the domain. If the mesh was chosen uniform for the whole domain then accurate results usually can't be obtained. It means that we need a finer mesh in those parts of the domain where the solution changes rapidly and a coarser mesh in those parts where the solution changes slowly. In order to remove these difficulties we need some transformation of the problem that makes it less singular and some transformation of the mesh to make it adjustable to the problem.

5.4.1 Scaling

In order to consider domains with large aspect ratio we need to apply to our original problem (4.1.1) the following standard scaling process.
Suppose that our original problem is:

$$\begin{cases} -(\hat{\alpha}\,\hat{\nabla}\cdot\hat{\mathbf{u}})\,\mathbb{1}_{\hat{\Omega}_0} - \hat{\beta}\,\hat{\Delta}\hat{p}\,\mathbb{1}_{\hat{\Omega}_1} &= 0, \\ (-\hat{\mu}\hat{\Delta}\hat{\mathbf{u}} + \hat{\nabla}\hat{p})\,\mathbb{1}_{\hat{\Omega}_0} &= 0, \end{cases} \quad in\ \hat{\Omega} = \hat{\Omega}_0 \cup \hat{\Omega}_1 \cup \hat{\Sigma}. \tag{5.4.1}$$

Remark 5.4.1 *Here we introduce some coefficients $\hat{\alpha}$ and $\hat{\beta}$ which are used for balancing of the resulting matrix. They are not arbitrary but satisfy some scaling condition. These coefficients affect only the first equation in (4.4.1).*

To (5.4.1) we associate the following boundary conditions:

$$\begin{cases} \hat{\mathbf{u}} &= 0\,, & on & \hat{\Gamma}, \\ \hat{u}_2 &= 0\,, & on & \hat{\Gamma}_{in} \cup \hat{\Gamma}_{out}, \\ \hat{p} &= \hat{p}_{in}\,, & on & \hat{\Gamma}_{in}, \\ \hat{p} &= \hat{p}_{out}\,, & on & \hat{\Gamma}_{out}, \\ \hat{p} &= \hat{p}_m\,, & on & \hat{M}, \\ \hat{\partial}_\nu \hat{p} &= 0\,, & on & \hat{\Gamma}_{iw} \cup \hat{\Gamma}_{ow}. \end{cases} \tag{5.4.2}$$

and interface conditions:

$$\begin{cases} \hat{\partial}_2 \hat{u}_1 &= -\hat{S}\ \hat{u}_1, \\ \hat{u}_2 &= -\dfrac{\hat{K}}{\hat{\mu}}\ \hat{\partial}_2 \hat{p}, \end{cases} \quad on\ \hat{\Sigma}. \tag{5.4.3}$$

The geometrical parameters of the domains $\hat{\Omega}_0$ and $\hat{\Omega}_1$ are as follows:

$$\begin{cases} \hat{\Omega}_0 &= (0, \hat{l}) \times (-\hat{H}, 0), \\ \hat{\Omega}_1 &= (0, \hat{l}) \times (0, \hat{h}), \\ \hat{\Gamma} &= (0, \hat{l}) \times \{-\hat{H}\}, \\ \hat{\Gamma}_{in} &= \{0\} \times (-\hat{H}, 0), \\ \hat{\Gamma}_{out} &= \{\hat{l}\} \times (-\hat{H}, 0), \\ \hat{\Sigma} &= (0, \hat{l}) \times \{0\}, \\ \hat{\Gamma}_{iw} &= \{0\} \times (0, \hat{h}), \\ \hat{\Gamma}_{ow} &= \{\hat{l}\} \times (0, \hat{h}), \\ \hat{M} &= (0, \hat{l}) \times \{\hat{h}\}. \end{cases} \tag{5.4.4}$$

We apply to the original problem (5.4.1) the following "similarity" transform: (where L_0, U_0, P_0 are some constants)

$$\begin{cases} \hat{\mathbf{x}} &= L_0\ \mathbf{x}, \\ \hat{\mathbf{u}}(\hat{\mathbf{x}}) &= U_0\ \mathbf{u}(\frac{\hat{\mathbf{x}}}{L_0}), \qquad where\ \ \hat{\mathbf{x}} \in \hat{\Omega} = \hat{\Omega}_0 \cup \hat{\Omega}_1 \cup \hat{\Sigma}, \\ \hat{p}(\hat{\mathbf{x}}) &= P_0\ p(\frac{\hat{\mathbf{x}}}{L_0}). \end{cases} \tag{5.4.5}$$

Under the transform (5.4.5) differential operators $\hat{\Delta}, \hat{\nabla}$ and domains change to the new form:

$$\begin{cases} \hat{\Delta}\hat{\mathbf{u}} &= \frac{U_0}{L_0^2}\ \Delta \mathbf{u}, \\ \hat{\nabla} \cdot \hat{\mathbf{u}} &= \frac{U_0}{L_0}\ \nabla \cdot \mathbf{u}, \\ \hat{\nabla}\hat{p} &= \frac{P_0}{L_0}\ \nabla p, \\ \hat{\Delta}\hat{p} &= \frac{P_0}{L_0^2}\ \Delta p, \\ \hat{\Omega}_0 &= L_0\ \Omega_0, \\ \hat{\Omega}_1 &= L_0\ \Omega_1. \end{cases} \tag{5.4.6}$$

Substituting (5.4.5)-(5.4.6) into (5.4.1)-(5.4.4) we obtain a new scaled problem :

$$\begin{cases} -(\alpha\ \nabla\cdot\mathbf{u})\ 1_{\Omega_0} - \beta\ \Delta p\ 1_{\Omega_1} &= 0 \\ (-\mu\Delta\mathbf{u} + \nabla p)\ 1_{\Omega_0} &= 0 \end{cases} \quad in\ \Omega = \Omega_0 \cup \Omega_1 \cup \Sigma, \tag{5.4.7}$$

with new boundary conditions:

$$\begin{cases} \mathbf{u} &= 0\ , & on & \Gamma, \\ u_2 &= 0\ , & on & \Gamma_{in} \cup \Gamma_{out}, \\ p &= p_{in}\ , & on & \Gamma_{in}, \\ p &= p_{out}\ , & on & \Gamma_{out}, \\ p &= p_m\ , & on & M, \\ \partial_\nu p &= 0\ , & on & \Gamma_{iw} \cup \Gamma_{ow}, \end{cases} \tag{5.4.8}$$

with new interface conditions:

$$\begin{cases} \partial_2 u_1 &= -S\ u_1, \\ \hat{u}_2 &= -\dfrac{K}{\mu}\ \partial_2 p, \end{cases} \quad , on\ \Sigma \tag{5.4.9}$$

and new constants and boundary values:

$$\begin{cases} \frac{\alpha}{\beta} &= \frac{\hat{\alpha}}{\hat{\beta}}\ \frac{P_0}{L_0}, \\ \mu &= \frac{\hat{\mu}\ U_0}{L_0\ P_0}, \\ K &= \frac{\hat{K}}{L_0^2}, \\ S &= \hat{S}\ L_0, \\ p_{|\Gamma_{in}} &= \frac{\hat{p}_{in}}{P_0}, \\ p_{|\Gamma_{out}} &= \frac{\hat{p}_{out}}{P_0}, \\ p_{|M} &= \frac{\hat{p}_m}{P_0}, \\ l &= \frac{\hat{l}}{L_0}, \\ h &= \frac{\hat{h}}{L_0}, \\ H &= \frac{\hat{H}}{L_0}. \end{cases} \tag{5.4.10}$$

Since the scaling constants L_0, P_0, U_0 are arbitrary then we choose them so that the scaled problem would not contain in boundary and interface conditions too small or too big numbers. We choose the following scaling constants:

$$\begin{cases} L_0 = \hat{h}, \\ P_0 = \hat{p}_{in}, \\ U_0 = \frac{1}{\hat{H}} \int_{-\hat{H}}^{0} (\hat{u}_{1,Poiseuille}) dx_2, \end{cases} \tag{5.4.11}$$

where U_0 is the average value of the velocity $\hat{u}_{1,Poiseuille}$ solution of the Stokes problem for the case of the Poiseuille flow in the domain $\hat{\Omega}_0$ with the original boundary conditions (5.4.2) for the pressure, that has the exact form:

$$\hat{u}_{1,Poiseuille} = \frac{\hat{p}_{out} - \hat{p}_{in}}{2\ \hat{l}\ \hat{\mu}} (\hat{x}_2 + \hat{H})\ \hat{x}_2. \tag{5.4.12}$$

Parameters of the domain, boundary and interface conditions for the original and scaled problems are shown in Table 5.5:

Parameters	**Original values**	**Scaled values**	**Description**
h	10^{-4}	1	Height of Ω_1 (GDL)
H	10^{-3}	10	Height of the Ω_0 (Channel)
l	1	10^{+4}	The length of the domain
μ	10^{-6}	$8.333 \cdot 10^{-4}$	viscosity coefficient
K	10^{-12}	10^{-4}	Darcy Law coefficient k
S	10^{+5}	10	Safman's condition coefficient
p_{in}	2000	1	pressure given on Γ_{in}
p_{out}	0	0	pressure given on Γ_{out}
p_m	1	$5 \cdot 10^{-4}$	pressure given on M

Table 5.5: Parameters for the original and scaled problems.

The scaling constants are $L_0 = 10^{-4}$, $U_0 = \frac{500}{3}$, $P_0 = 2000$. The coefficients α and β are chosen such that the matrix becomes less ill-conditioned. The only requirement they should satisfy is the aspect ratio condition in (5.4.10).

5.4.2 Mesh generation

From computations we observed that the solution changes faster closer to the inlet Γ_{in} and closer to the outlet Γ_{out}. The further we are from Γ_{in} and Γ_{out} the coarser mesh we need because the solution changes slowly. In order to refine the mesh in these particular areas we generate a uniform mesh and then pull it to the areas where we need more nodes for approximation. For this purpose we have chosen adaptation of the mesh close to the boundary Γ_{in}, namely to the origin of coordinates, by using the following transform from the old independent variables $\mathbf{x} = \binom{x_1}{x_2}$ to the new ones $\mathbf{y} = \binom{y_1}{y_2}$ with the power of adaptation $\epsilon = \binom{\epsilon_1}{\epsilon_2}, \epsilon_i \geq 0$:

$$\begin{cases} y_i = x_i \; exp\{\epsilon_i \; (|\dfrac{x_i}{L_i}| - 1)\}, & for \; i = 1, 2 \\ x_{i,min} \leq 0 \leq x_{i,max}, \end{cases} \tag{5.4.13}$$

where:

$$L_i = \begin{cases} x_{i,max} \;\; , & if \;\; x_i \geq 0 \\ x_{i,min} \;\; , & if \;\; x_i \leq 0 \end{cases} , for \; i = 1, 2 \tag{5.4.14}$$

As it is seen on the first picture on Figure 5.10 this transformation moves all nodes uniformly closer to the point $(0, 0)$, leaving all the boundary nodes on their original places.

If we want to move nodes closer to the inlet and outlet, i.e. closer to vertical lines $x_1 = 0$ and $x_1 = l$, simultaneously only along the axis x_1, we need the following transform:

$$\begin{cases} y_1 = x_1 \; exp\{\epsilon_1 \; (\dfrac{x_1}{a} - 1)\}, & for \; 0 \leq x_1 \leq a, \\ y_1 = l + (x_1 - l) \; exp\{\epsilon_2 \; (\dfrac{a - x_1}{l - a})\}, & for \; a \leq x_1 \leq l, \\ y_2 = x_2, \end{cases} \tag{5.4.15}$$

where a is an arbitrary number satisfying $0 \leq a \leq l$ and l is the length of the domain. If we need to move nodes closer to some point or vertical line inside the domain the formulas (5.4.15) must be modified. As it is seen on the second picture on Figure 5.10 this transformation moves all nodes uniformly closer to the boundaries $\bar{\Gamma}_{in} \cup \bar{\Gamma}_{iw}$ and $\bar{\Gamma}_{out} \cup \bar{\Gamma}_{ow}$, leaving all the nodes lying on some chosen vertical line and crossing the whole domain somewhere in the middle, on their original places.

We recognize that this way of mesh adaptation is not an ultimate solution of the problem of refining the mesh in particular parts of the domain. The way we make the mesh adaptation may increase aspect ratio of triangles that can make the matrix more ill-conditioned then it was before adaptation.

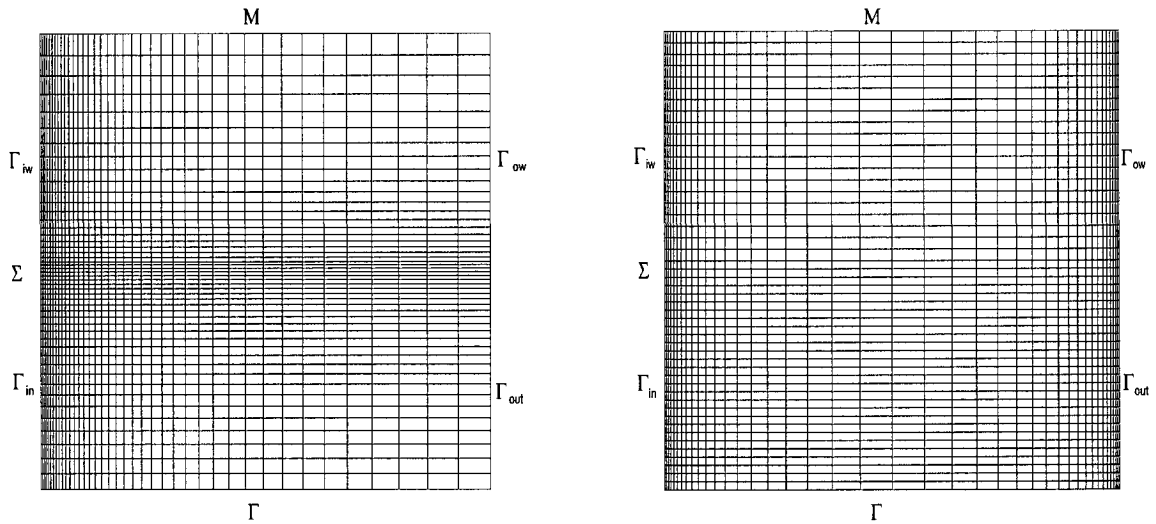

Figure 5.10: Two types of mesh adaptation.

5.4.3 Numerical results when the pressure is constant on the membrane

In Table 5.6 are presented numerical results for the real domain for the both cases when the domain Ω_0 has extensions or does not. For all the numerical results sizes of the domains Ω_0 and Ω_1, parameters μ, K, S, p_{in}, p_{out}, p_m have their original values defined in Table 5.5. The powers of mesh adaptation are $\epsilon_1 = 7$ and $\epsilon_2 = 0$. The values of the balancing coefficients are shown for the scaled problem. As it is seen in Table 5.6, for α and β satisfying the given aspect ratio our computations give the same result.

Parameters	Domains with no extensions				Domains with extensions		
	(I)	(II)	(III)	(IV)	(V)	(VI)	(VII)
α	10^{-04}	$8.333 \cdot 10^{-06}$	10^{-04}	1	$8.333 \cdot 10^{-06}$	$8.333 \cdot 10^{-06}$	1
β	12	1	12	$12 \cdot 10^{+04}$	1	1	$12 \cdot 10^{+04}$
N_{Ω_0,x_1}	62	62	76	76	74	80	80
N_{Ω_0,x_2}	20	20	16	16	10	10	14
N_{Ω_1,x_2}	8	8	6	6	6	6	6
N_{ext,x_1}	-	-	-	-	2	2	2
L_{ext}	-	-	-	-	0.5	0.2	0.2
$N_{\Delta,\Omega}$	3472	3472	3344	3344	2448	2640	3312
$N_{nodes,\Omega}$	4307	4307	4203	4203	2879	3101	4113
Dim_{Matrix}	9433	9433	9253	9253	6177	6651	9015
$u_{1\Gamma_{in}}$	1.8541	1.8541	1.8534	1.8534	1.84504	1.84476	1.8482
$u_{1\Gamma_{out}}$	-0.001129	-0.001129	-0.00137	-0.00137	0.00313	0.00563	0.00196
$u_{2\Sigma}$	1.8427	1.8427	1.8433	1.8433	1.84700	1.84824	1.8491
u_{2M}	1.8399	1.8399	1.8391	1.8391	1.83650	1.83804	1.8430
$\int_{\partial\Omega_0} \mathbf{u_h} \cdot \boldsymbol{\nu}_0$	-0.0125	-0.0125	-0.01153	-0.01153	0.00509	0.00912	0.00285
$\int_{\partial\Omega} \mathbf{u_h} \cdot \boldsymbol{\nu}$	-0.0153	-0.0153	-0.01569	-0.01569	-0.005401	-0.00108	-0.00322
$\frac{\int_{\partial\Omega_0} \mathbf{u_h} \cdot \boldsymbol{\nu}_0}{u_{2M}}$	-0.0068	-0.0067	-0.0062	-0.0062	0.0027	0.0049	0.0015
$\frac{\int_{\partial\Omega} \mathbf{u_h} \cdot \boldsymbol{\nu}}{u_{2M}}$	-0.0083	-0.0082	-0.0085	-0.0085	-0.0029	-0.00058	-0.0017

Table 5.6: Numerical results for the real flow. Condition numbers of all the resulting matrices are of order 10^{+13}.

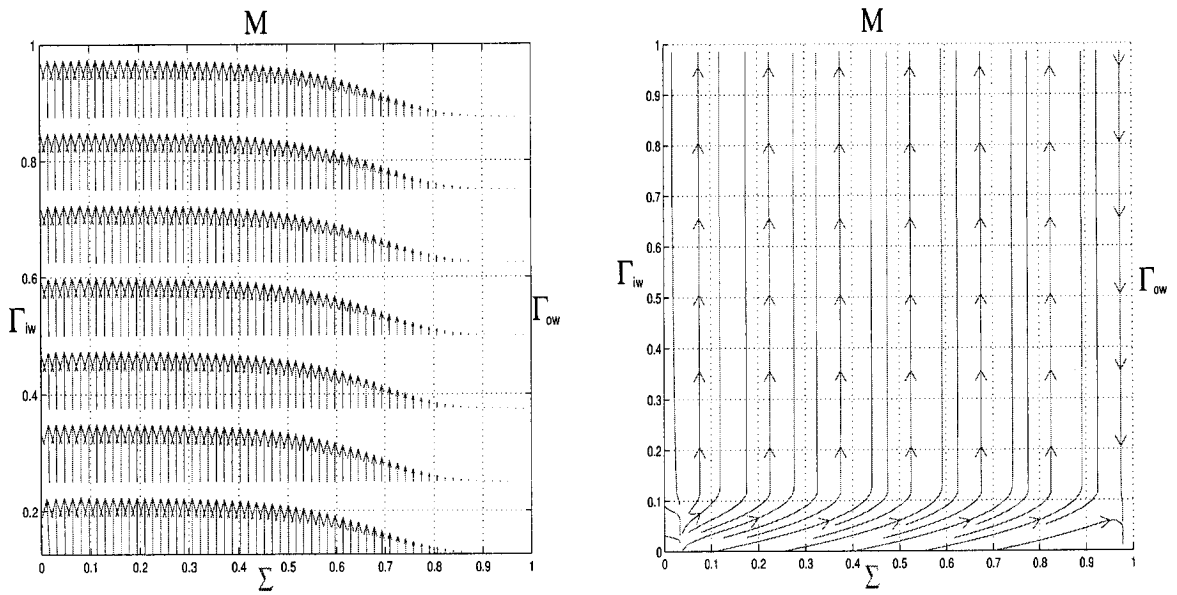

Figure 5.11: Th vector field and stream lines of the fluid flow in Ω_1 (GDL) for the real domain. The domain division is $N_{\Omega_0,x_1} = 62$, $N_{\Omega_0,x_2} = 20$, $N_{\Omega_1,x_2} = 8$.

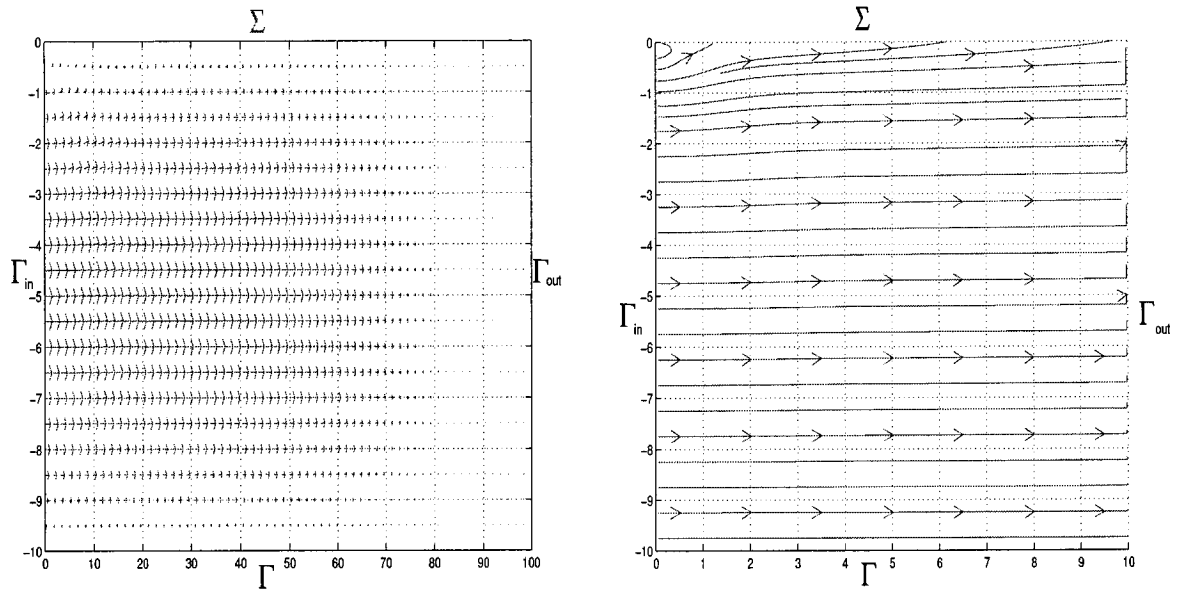

Figure 5.12: The vector field and stream lines of the fluid flow in Ω_0 (Channel) for the real domain. The domain division is $N_{\Omega_0,x_1} = 62$, $N_{\Omega_0,x_2} = 20$, $N_{\Omega_1,x_2} = 8$.

5.4.4 Numerical results when the pressure is non-constant on the membrane

In Table 5.7 we present numerical results for the real domain Ω_0 with no extensions when the pressure p_m on the membrane is given and depends on the variable x_1.

Parameters	The regular Saffman's conditions (I)	The regular Saffman's conditions (II)	The reduced Saffman's conditions (III)
p_m	$300(1+cos(\pi\frac{x_1}{l}))$	$300(1-cos(\pi\frac{x_1}{l}))$	$300(1-cos(\pi\frac{x_1}{l}))$
N_{Ω_0,x_1} N_{Ω_0,x_2} N_{Ω_1,x_2}	80 10 8	80 10 8	80 10 8
$N_{\triangle,\Omega}$ $N_{nodes,\Omega}$ Dim_{Matrix}	2880 3139 6521	2880 3139 6521	2880 3139 6521
$u_{1\Gamma_{in}}$ $u_{1\Gamma_{out}}$ $u_{2\Sigma}$ u_{2M}	1.32249 0.02188 1.29351 1.28512	1.83657 0.54488 1.29427 1.28612	1.81275 0.53621 1.27531 1.26706
$\int_{\partial\Omega_0}\mathbf{u_h}\cdot\nu_0$ $\int_{\partial\Omega}\mathbf{u_h}\cdot\nu$	-0.0070 -0.0154	0.00257 -0.0055	-0.0012 -0.0094
$\frac{\int_{\partial\Omega_0}\mathbf{u_h}\cdot\nu_0}{u_{2M}}$ $\frac{\int_{\partial\Omega}\mathbf{u_h}\cdot\nu}{u_{2M}}$	0.0054 0.0120	0.00199 0.00432	0.00096 0.00748

Table 5.7: Numerical results for the real domain when the pressure is given on the membrane and depends on the variable x_1. Condition numbers of all the resulting matrices are of order 10^{+13}.

For all the results presented in Table 5.7, sizes of the domains Ω_0 and Ω_1, parameters μ, K, S, p_{in}, p_{out}, have their values defined in Table 5.5. Balancing parameters $\alpha = 1$, $\beta = 12\cdot 10^{+04}$. In the numerical experiment (III) on the interface Σ we impose conditions (2.2.8) with the homogeneous reduced Saffman's condition $u_{1|\Sigma} = 0$. The powers of mesh adaptation $\epsilon_1 = 7$ and $\epsilon_2 = 6$ are applied along the x_1 axis in opposite horizontal directions, as it is shown in the adaptation method (5.4.15).

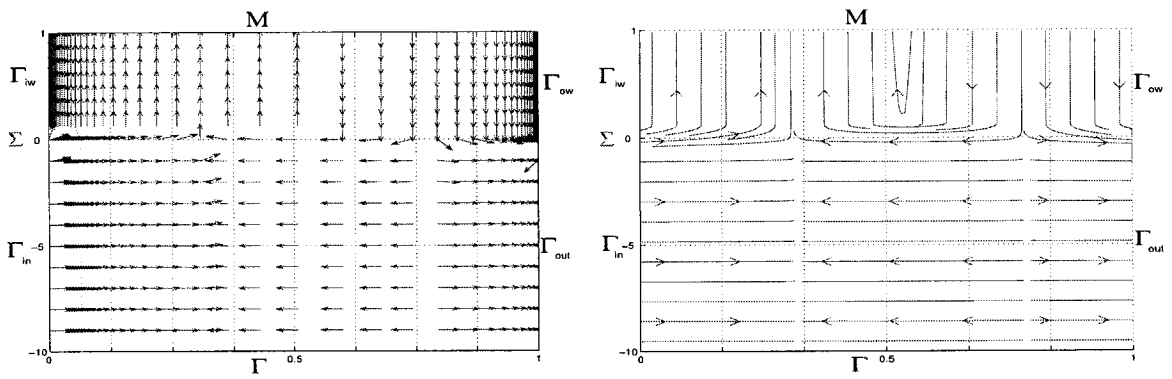

Figure 5.13: The vector field and stream lines of the fluid flow in the whole real domain. The domain division is $N_{\Omega_0,x_1} = 80$, $N_{\Omega_0,x_2} = 10$, $N_{\Omega_1,x_2} = 8$. The pressure $p_m = 300(1 - cos(\pi \frac{x_1}{l}))$ is prescribed on the membrane M.

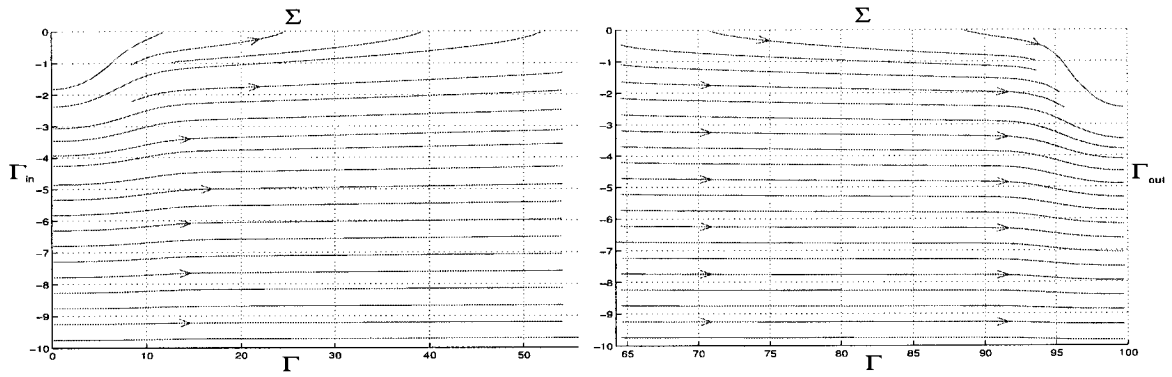

Figure 5.14: Stream lines of the fluid flow in Ω_0 (Channel) for the real domain with zoom close to Γ_{in} and Γ_{out}. The domain division is $N_{\Omega_0,x_1} = 80$, $N_{\Omega_0,x_2} = 10$, $N_{\Omega_1,x_2} = 8$. The pressure $p_m = 300(1 - cos(\pi \frac{x_1}{l}))$ is prescribed on the membrane M.

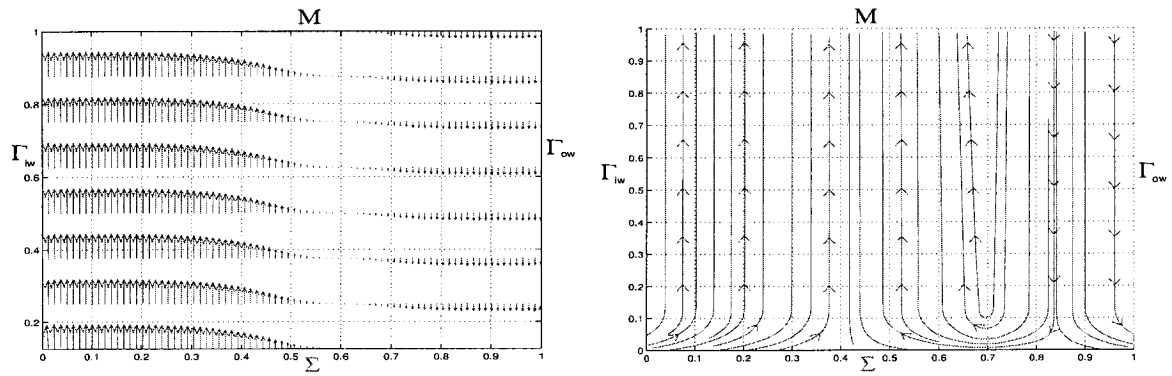

Figure 5.15: The vector field and stream lines of the fluid flow in Ω_1 (GDL) for the real domain. The domain division is $N_{\Omega_0,x_1} = 80$, $N_{\Omega_0,x_2} = 10$, $N_{\Omega_1,x_2} = 8$. The pressure $p_m = 300(1 - cos(\pi \frac{x_1}{l}))$ is prescribed on the membrane M.

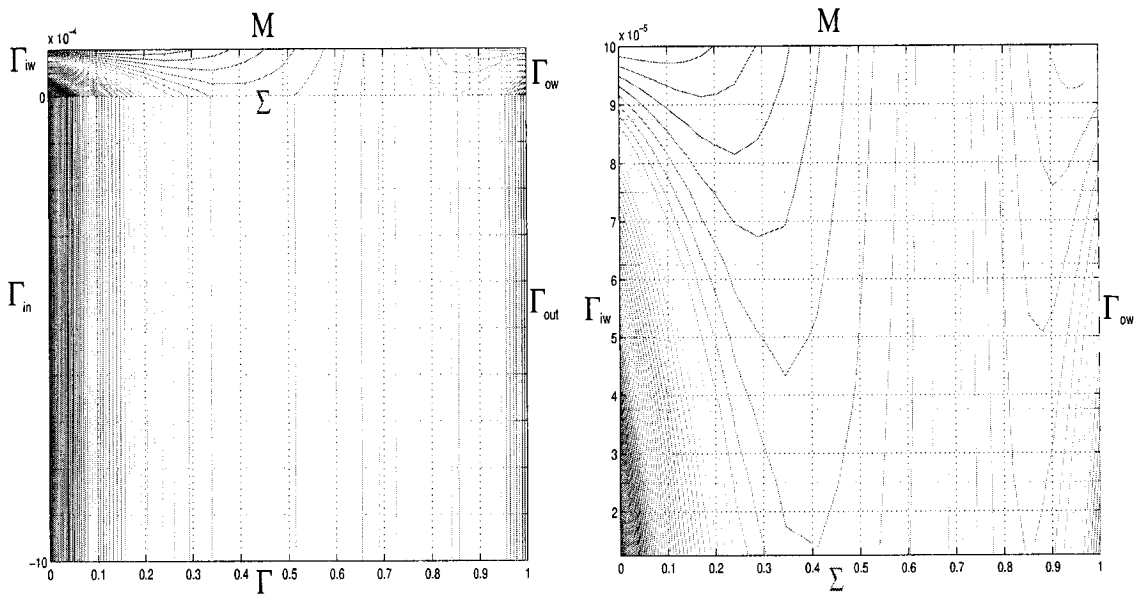

Figure 5.16: The pressure isolines of the fluid flow for the real domain in the whole domain Ω and in Ω_1 (GDL). The domain division is $N_{\Omega_0,x_1} = 80$, $N_{\Omega_0,x_2} = 10$, $N_{\Omega_1,x_2} = 8$. The pressure $p_m = 300(1 - cos(\pi \frac{x_1}{l}))$ is prescribed on the membrane M.

5.4.5 Comparison of performance of the iterative Gauss-Seidel overlapping block method and the direct Gaussian Elimination method

We present a comparison of numerical results obtained by the iterative Gauss-Seidel overlapping block method and the direct Gaussian Elimination method. For all the results, sizes of the domains Ω_0 and Ω_1, parameters μ, K, S, p_{in}, p_{out}, p_m have the values defined in Table 5.5 (see page 50). The powers of mesh adaptation are $\epsilon_1 = 7$, $\epsilon_2 = 0$. The balancing parameters are $\alpha = 1$, $\beta = 12 \cdot 10^{+04}$.

Parameters	(I)	(II)	(III)	(IV)	(V)	(VI)	(VII)	(VIII)	(IX)
N_{Ω_0,x_1}	24	30	40	50	60	76	62	80	90
N_{Ω_0,x_2}	8	10	12	14	14	16	20	16	16
N_{Ω_1,x_2}	8	10	10	10	10	6	8	10	8
$N_{nodes,\Omega}$	809	1251	1903	2675	3205	4203	4307	4747	5155
$N_{\triangle,\Omega}$	768	1200	1760	2400	2880	3344	3472	4160	4320
Dim_{Matrix}	1643	2533	3929	5605	6715	9253	9433	10061	11129
N_{blocks}	2	2	3	4	3	4	4	4	4
$N_{block,nodes}$	512	759	775	926	1297	1398	1409	1384	1735
$N_{displ,nodes}$	297	492	564	583	954	935	966	1121	1140
Overlapping	42 %	35 %	27 %	37 %	27 %	33 %	32 %	19 %	34 %
$\mathbf{N_{iterations}}$	18	27	31	41	33	33	59	58	18
Memory $\frac{GS}{GE}$	89 %	81 %	55 %	52 %	53 %	47 %	46 %	36 %	47 %
$\mathbf{Time_{GS}}$	00:00:52	00:02:51	00:06:19	00:16:53	00:21:05	00:39:25	01:04:26	01:28:52	02:25:05
$\mathbf{Time_{GE}}$	00:00:48	00:02:54	00:10:30	00:31:20	00:53:30	02:21:30	02:30:14	-	-
$\mathbf{Res_{GS}}$	8.49e-08	1.06e-07	1.29e-07	2.14e-07	3.22e-07	1.97e-07	9.38e-08	1.35e-07	1.31e-07
$\mathbf{Res_{GE}}$	6.02e-08	1.43e-07	1.07e-07	1.64e-07	7.83e-08	7.96e-08	9.49e-08	-	-
$u_{1\Gamma_{in}}$	1.928	1.888	1.86797	1.859	1.857	1.853	1.854	1.854	1.851
$u_{1\Gamma_{out}}$	-0.0001	-0.0003	-0.0006	-0.0008	-0.001	-0.001	-0.001	-0.001	-0.001
$u_{2\Sigma}$	1.824	1.832	1.837	1.840	1.841	1.843	1.842	1.843	1.843
u_{2M}	1.805	1.819	1.828	1.834	1.837	1.839	1.839	1.839	1.839
$\int_{\partial\Omega_0} \mathbf{u_h} \cdot \nu_0$	-0.103	-0.057	-0.031	-0.020	-0.016	-0.0115	-0.0125	-0.0120	-0.0092
$\int_{\partial\Omega} \mathbf{u_h} \cdot \nu$	-0.122	-0.069	-0.039	-0.026	-0.022	-0.0156	-0.0153	-0.0160	-0.0133
$\frac{\int_{\partial\Omega_0} \mathbf{u_h} \cdot \nu_0}{u_{2M}}$	-0.057	-0.031	-0.017	-0.011	-0.009	-0.0062	-0.0068	-0.0065	-0.0050
$\frac{\int_{\partial\Omega} \mathbf{u_h} \cdot \nu}{u_{2M}}$	-0.068	-0.038	-0.021	-0.014	-0.012	-0.0085	-0.0082	-0.0087	-0.0077

Table 5.8: Comparison of the iterative Gauss-Seidel overlapping block method with the Gaussian Elimination method. Numerical results for the real domain with no extensions.

The results in Table 5.8 show that by refining the mesh we can better satisfy the precision criterion (4.7.2)-(4.7.3) (see page 31).

On Figures 5.17 and 5.18 we present comparison of performance of the iterative Gauss-Seidel overlapping block method and the direct Gaussian Elimination method. The graphs show growth of the computation time and relative PC memory consumption for each method, depending on the number of nodes.

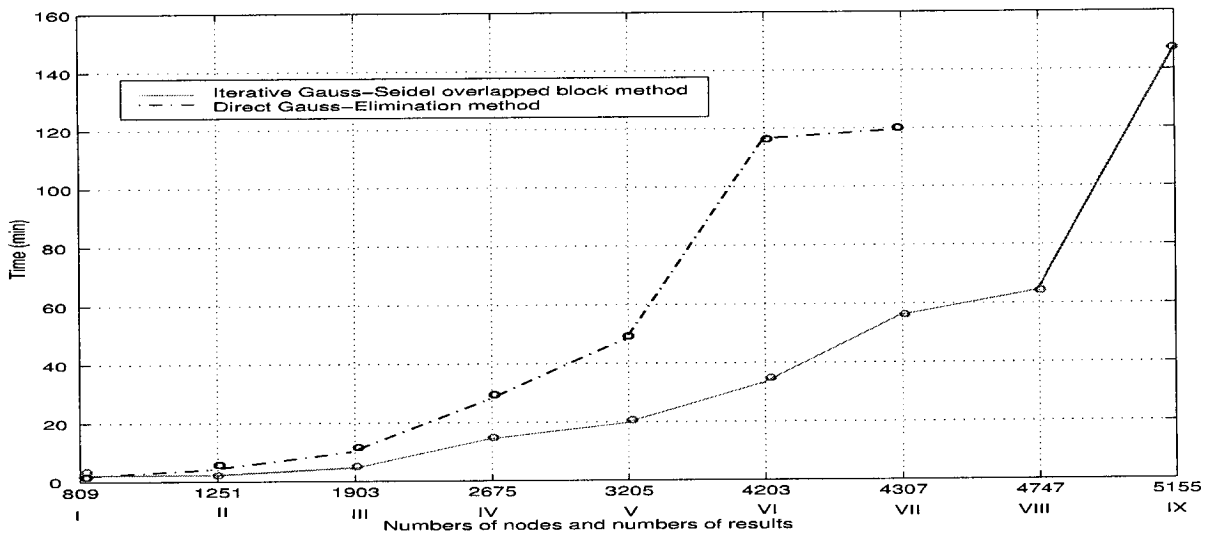

Figure 5.17: Comparison of performance of the iterative Gauss-Seidel overlapping block method and the direct Gaussian Elimination method.

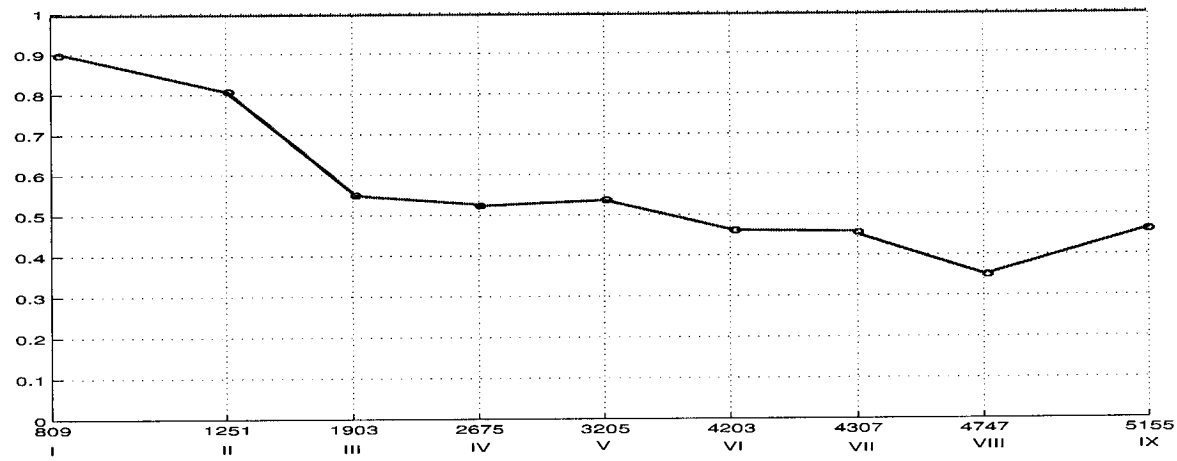

Figure 5.18: PC memory consumption of the iterative Gauss-Seidel overlapping block method relatively to the direct Gaussian Elimination method.

The comparison of these two methods shows obvious superiority of the iterative Gauss-Seidel overlapping block method over the direct one. The iterative method not only provides possibility to compute faster, but also gives results for the finer mesh when the direct method does not work because of computer memory shortage. We also applied GMRES iterative method (see [10]), with no preconditioner, to the problems with the same parameters. Krylov subspace dimension was 300. GMRES did not converge and we did not obtain any result.

Graphs of the maximum norm of the residual and convergence ratios

On Figures 5.19 - 5.23 we present graphs (other graphs see on the page 91) of the maximum norm of the residual R_n at the n-th iteration step of the Gauss-Seidel overlapping block method, the residual convergence ratio $\frac{R_{n+1}}{R_n}$ and the Cauchy convergence ratio $\frac{\|\mathbf{X_{n+1}}-\mathbf{X_n}\|}{\|\mathbf{X_n}-\mathbf{X_{n-1}}\|}$, where $\mathbf{X_n}$ is a solution obtained at the n-th iteration step (see page 36). In order to understand how the the size of domain blocks and the displacement influence convergence we provide some results for the same mesh but with the size of domain blocks and the displacement different from the ones chosen in the results presented in Table 5.8. The graphs show that the number of blocks and percentage of overlapping make significant influence on convergence ratios. The area on Figures 5.19 - 5.23 where the graphs of convergence ratios start oscillating around 1 determines the limit of the iterative scheme for the given number of nodes in a domain block and the displacement. All iterations beyond this limit do not decrease the residual.

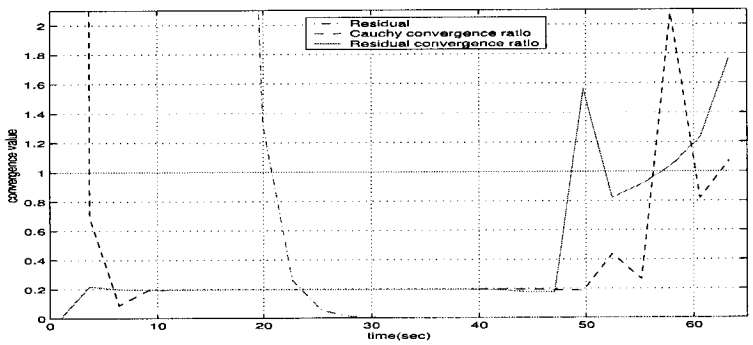

Figure 5.19: Graphs of the residual and convergence ratios for the domain division 24-8-8, $N_{blocks} = 2$, $N_{block,nodes} = 512$, $N_{displ,nodes} = 297$, Overlapping = 42 %, $N_{iterations} = 18$, $Time_{GS} = 00:00:52$, $Res_{GS} = 8.49 \cdot 10^{-08}$ (the result (I) in Table 5.8).

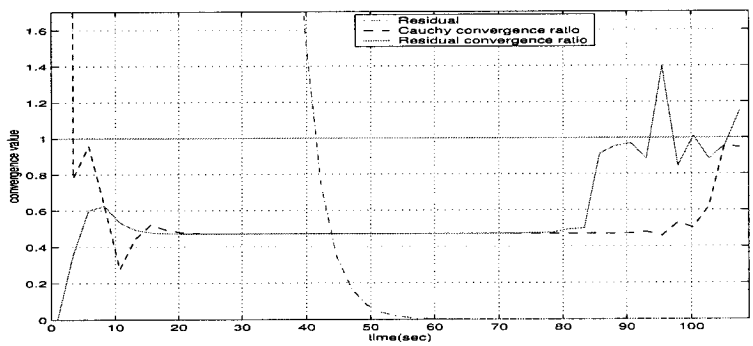

Figure 5.20: Graphs of the residual and convergence ratios for the domain division 24-8-8, $N_{blocks} = 5$, $N_{block,nodes} = 281$, $N_{displ,nodes} = 132$, Overlapping = 53 %, $N_{iterations} = 39$, $Time_{GS} = 00:01:35$, $Res_{GS} = 1.75 \cdot 10^{-06}$.

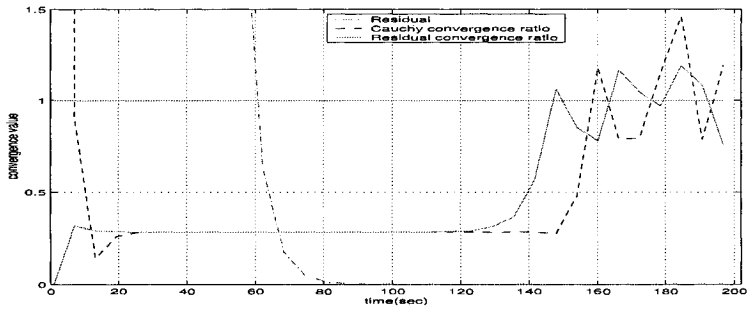

Figure 5.21: Graphs of the residual and convergence ratios for the domain division 30-10-10, $N_{blocks} = 2$, $N_{block,nodes} = 759$, $N_{displ,nodes} = 492$, Overlapping = 35 %, $N_{iterations} = 27$, $Time_{GS} = 00:02:51$, $Res_{GS} = 1.06 \cdot 10^{-07}$ (the result (II) in Table 5.8).

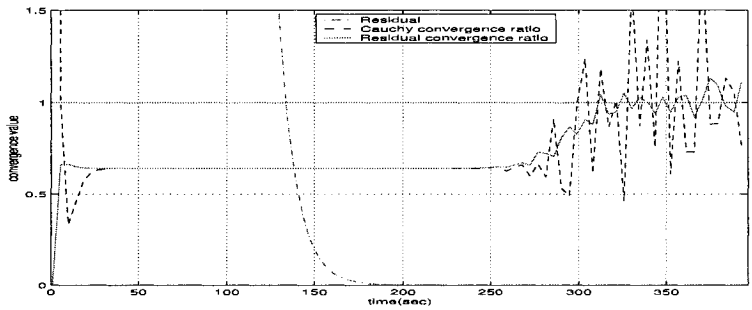

Figure 5.22: Graphs of the residual and convergence ratios for the domain division 30-10-10, $N_{blocks} = 2$, $N_{block,nodes} = 677$, $N_{displ,nodes} = 574$, Overlapping = 15 %, $N_{iterations} = 83$, $Time_{GS} = 00:06:11$, $Res_{GS} = 1.82 \cdot 10^{-07}$.

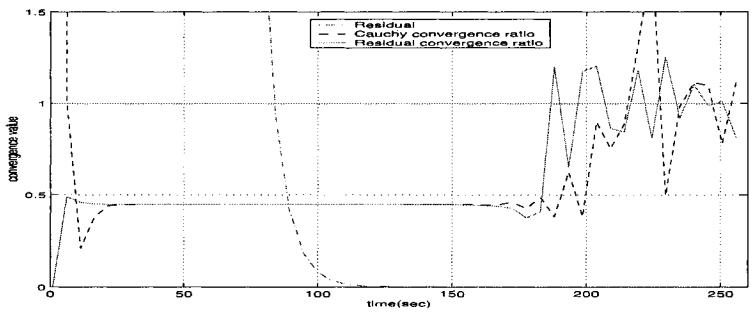

Figure 5.23: Graphs of the residual and convergence ratios for the domain division 30-10-10, $N_{blocks} = 2$, $N_{block,nodes} = 718$, $N_{displ,nodes} = 533$, Overlapping = 26 %, $N_{iterations} = 44$, $Time_{GS} = 00:03:52$, $Res_{GS} = 1.2 \cdot 10^{-07}$.

5.5 Numerical algorithm

Here we describe a numerical algorithm which represents the main steps that we use in our c++ code. Some steps, such as numerical integration and construction of linear basis functions using barycentric coordinates were omitted here since they are computed by the well known formulas.

Let us define the following parameters, vectors and matrices that are used in a pseudocode for the c++ code realization:

Parameters	Description
$N_{\triangle,\Omega}$	the total number of triangles
$N_{\triangle,\Omega_0}$	the number of triangles in Ω_0
N_{nodes,Ω_0}	the number of nodes in Ω_0
N_{nodes,Ω_1}	the number of nodes in Ω_1
$N_{unknowns}(i)$	the total number of basis functions on the i_{th} node
$XY(i,n)$	the coordinates of the i_{th} node $n = 1, 2$
$N_{triangle}$	the number of nodes in each *triangle*
$IJK(n,m)$	for each triangle n contains the numbers of it's nodes
$N_{boundary}$	the total number of boundaries
$N_{interval}(k)$	the number of line intervals in each of the boundary k
$IJ(k,l,i)$	for each boundary k stores numbers of nodes that belong to each interval l
$U_i(l)$	the super-vector for each node i represents the vector of unknowns
$A_{ij}(k,l)$	the super-matrix contains sub-matrices for each nodes i and j

Table 5.9: Parameters of the numerical algorithm

5.5.1 Format of the mesh file

A mesh for computations can be generated inside the c++ code or read from a file having a regular text format as follows:

 # beginning of the file
$N_{nodes,\Omega}$ $N_{\triangle,\Omega}$ # the total number of nodes and triangles
$N_{boundary}$ # the number of boundaries
$N_{interval}(1)$ $N_{interval}(2)$ $N_{interval}(3)$ ... $N_{interval}(N_{boundary})$ # numbers of intervals
$XY(i,1)$ $XY(i,2)$ $N_{unknowns}(i)$ # coordinates of nodes
...
$IJK(n,1)$ $IJK(n,2)$ $IJK(n,3)$ $IJK(n,4)$ # numbers of nodes for each triangle
...
$IJ(1,l,0)$ $IJ(1,l,1)$ # numbers of nodes for each boundary element
...
$IJ(2,N_{interval}(1),0)$ $IJ(2,N_{interval}(1),1)$
...
$IJ(N_{boundary},l,0)$ $IJ(N_{boundary},l,1)$
 # end of the file

5.5.2 Pseudocode

1. Input of the initial data and the mesh generation

(001) 1.1. N_{nodes,Ω_0}, N_{nodes,Ω_1}, $N_{\triangle,\Omega}$, $N_{\triangle,\Omega_0}$, $N_{boundary}$
(002) 1.2. $N_{unknowns}(i)$, $XY(i,n)$, $IJK(n,m)$, $N_{interval}(k)$, $IJ(k,l,i)$
(003) 1.3. μ, K, S, p_{in}, p_{out}, p_m

2. Initialize the super-matrix, the super-vectors of unknowns and the right hand side

(004) **for** $i \leftarrow 0$ **to** $N_{nodes,\Omega}$
(005) $Ui \leftarrow$ *zero vector of dimension* $N_{unknowns}(i)$
(006) $Bi \leftarrow$ *zero vector of dimension* $N_{unknowns}(i)$
(007) **for** $j \leftarrow 0$ **to** $N_{nodes,\Omega}$
(008) $\bar{A}_{ij} \leftarrow$ *zero matrix of dimension* $N_{unknowns}(i) \times N_{unknowns}(j)$

3. Assembling the super-matrix

(009) **for** $t \leftarrow 0$ **to** $N_{\triangle,\Omega}$
(010) **if** $t \in \mathcal{T}_h(\Omega_0)$
(011) **for** $ii \leftarrow 0$ **to** $N_{triangle,\Omega_0}$
(012) $i \leftarrow IJK(t,ii)$
(013) **for** $jj \leftarrow 0$ **to** $N_{triangle,\Omega_0}$
(014) $j \leftarrow IJK(t,jj)$
(015) **if** $i \in v[\Omega_0]$
(016) **if** $j \in v[\Omega_0]$
(017)

$$\bar{A}_{ij} \leftarrow_{(+)} \begin{pmatrix} b_{ij|t} & c_{ij|t} & d_{ij|t} \\ c^t_{ij|t} & \mu a_{ij|t} & 0 \\ d^t_{ij|t} & 0 & \mu a_{ij|t} \end{pmatrix}$$

(018) **else**
(019)

$$\bar{A}_{ij} \leftarrow_{(+)} \begin{pmatrix} \bar{c}_{ij|t} & \bar{d}_{ij|t} \\ \mu \bar{a}_{ij|t} & 0 \\ 0 & \mu \bar{a}_{ij|t} \end{pmatrix}$$

(020) **else**
(021) **if** $j \in v[\Omega_0]$
(022)

$$\bar{A}_{ij} \leftarrow_{(+)} \begin{pmatrix} \bar{c}^t_{ij|t} & \mu \bar{a}^t_{ij|t} & 0 \\ \bar{d}^t_{ij|t} & 0 & \mu \bar{a}^t_{ij|t} \end{pmatrix}$$

(023) **else**

(024)

$$\bar{A}_{ij} \leftarrow_{(+)} \begin{pmatrix} \mu\hat{a}_{ij|t} & 0 \\ 0 & \mu\hat{a}_{ij|t} \end{pmatrix}$$

(025) **else if** $t \in \mathcal{T}_h(\Omega_1)$
(026) **for** $ii \leftarrow 0$ **to** $N_{triangle}$
(027) $i \leftarrow IJK(t, ii)$
(028) **for** $jj \leftarrow 0$ **to** $N_{triangle}$
(029) $j \leftarrow IJK(t, jj)$
(030) $\bar{A}_{ij}(0,0) \leftarrow_{(+)} b_{ij|t}$

Remark 5.5.1 *Index t in $a_{ij|t}$ means that an integral in the coefficient a_{ij} is computed only on the triangle t but not over the whole domain.*

4. Add boundary and interface conditions to the super-matrix

(031) **for** $boundary \leftarrow 0$ **to** $N_{boundary}$
(032) **for** $interval \leftarrow 0$ **to** $N_{interval}(boundary)$
(033) **for** $ii \leftarrow 0$ **to** 2
(034) $i = IJ(boundary, interval, ii)$
(035) **for** $jj \leftarrow 0$ **to** 2
(036) $j = IJ(boundary, interval, jj)$
(037) $\bar{A}_{ij}(0,2) \leftarrow_{(+)} \alpha \cdot e_{ij,interval}$
(038) $\bar{A}_{ij}(1,1) \leftarrow_{(+)} \mu Se_{ij,interval}$
(039) $\bar{A}_{ij}(2,1) \leftarrow_{(+)} \mu g_{ij,interval}$
(040) **for** $boundary \leftarrow 0$ **to** $N_{boundary}$
(041) **for** $interval \leftarrow 0$ **to** $N_{interval}(boundary)$
(042) **for** $ii \leftarrow 0$ **to** 2
(043) $i \leftarrow IJ(boundary, interval, ii)$
(044) **for** $jj \leftarrow 0$ **to** 2
(045) $j \leftarrow IJ(boundary, interval, jj)$
(046) **switch**(boundary)
(047) **case**($interval \in \Gamma_{in} \cup \Gamma_{out}$)
(048) $\bar{A}_{ij}(2, \cdot) \leftarrow 0$
(049) $\bar{A}_{ii}(2,2) \leftarrow 1$
(050) $B_i(2) \leftarrow 0$
(051) **if** $i \notin \Sigma$
(052) $\bar{A}_{ij}(0, \cdot) \leftarrow 0$
(053) $\bar{A}_{ii}(0,0) \leftarrow 1$
(054) **if** $i \in \Gamma_{in}$
(055) $B_i(0) \leftarrow p_{in}$
(056) **else**
(057) $B_i(0) \leftarrow p_{out}$
(058) **else**
(059) $\bar{A}_{ij}(1, \cdot) \leftarrow 0$
(060) $\bar{A}_{ii}(1,1) \leftarrow 1$
(061) $B_i(1) \leftarrow 0$
(062) **case**($interval \in \Gamma$)

(063) $\bar{A}_{ij}(1,\cdot) \leftarrow 0$
(064) $\bar{A}_{ii}(1,1) \leftarrow 1$
(065) $B_i(1) \leftarrow 0$
(066) $\bar{A}_{ij}(2,\cdot) \leftarrow 0$
(067) $\bar{A}_{ii}(2,2) \leftarrow 1$
(068) $B_i(2) \leftarrow 0$
(069) **case**$(interval \in M)$
(070) $\bar{A}_{ij}(0,\cdot) \leftarrow 0$
(071) $\bar{A}_{ii}(0,0) \leftarrow 1$
(072) $B_i(0) \leftarrow p_m$

5. Solve the linear super-system $\bar{\mathbf{A}} \cdot \mathbf{U} = \mathbf{B}$

5.1. Transform $\bar{\mathbf{A}}$, U and B to a regular matrix and vector form:
(073) $\bar{\mathbf{A}} \rightarrow \bar{A}$
(074) $\mathbf{U} \rightarrow \mathbf{x}$
(075) $\mathbf{B} \rightarrow \mathbf{b}$
5.2. Apply the iterative method for solving the linear system.

6. Restore vectors p, u_1 and u_2 from the solution vector x

6.1. Restore p in the whole domain Ω but u_1 and u_2 only in the domain Ω_0
Initialize unknowns p_i, $u_{1,i}$, $u_{2,i}$ and restore values
(076) $k \leftarrow 0$
(077) **for** $i \leftarrow 0$ **to** $N_{nodes,\Omega}$
(078) $p_i \leftarrow 0$
(079) $u_{1,i} \leftarrow 0$
(080) $u_{2,i} \leftarrow 0$
(081) **for** $i \leftarrow 0$ **to** $N_{nodes,\Omega}$
(082) **for** $j \leftarrow 0$ **to** $N_{unknowns}(i)$
(083) **if** $i \in v[\Omega]$
(084) **if** $j = 0$
(085) $p_i \leftarrow x_k$
(086) **if** $j = 1$
(087) $u_{1,i} \leftarrow x_k$
(088) **if** $j = 2$
(089) $u_{2,i} \leftarrow x_k$
(090) $k \leftarrow k + 1$
6.2. Find u_1 and u_2 using Darcy law equations in the domain Ω_1
Initialize the matrix M_{ij}, vectors $v_{1,i}$, $v_{2,i}$, $b_{1,i}$, $b_{2,i}$ and build a linear system
(091) **for** $i \leftarrow 0$ **to** $N_{nodes,\Omega}$
(092) $v_{1,i} \leftarrow 0$
(093) $v_{2,i} \leftarrow 0$
(094) $b_{1,i} \leftarrow 0$
(095) $b_{2,i} \leftarrow 0$

(096) **for** $j \leftarrow 0$ **to** $N_{nodes,\Omega}$
(097) $M_{i,j} \leftarrow 0$
(098) **for** $t \leftarrow 0$ **to** $N_{\triangle,\Omega}$
(099) **if** $t \notin \mathcal{T}(\Omega_0)$
(100) **for** $ii \leftarrow 0$ **to** 3
(101) $i = IJK(t, ii)$
(102) **for** $jj \leftarrow 0$ **to** 3
(103) $j = IJK(t, jj)$
(104) $M_{ij} \leftarrow_{(+)} m_{ij|t}$
(105) $b_{1,i} \leftarrow_{(+)} \sum_{j\in[\bar{\Omega}\setminus\bar{\Omega}_0]} \bar{p}_j \cdot r_{ij|t}$
(106) $b_{2,i} \leftarrow_{(+)} \sum_{j\in[\bar{\Omega}\setminus\bar{\Omega}_0]} \bar{p}_j \cdot s_{ij|t}$
(107) **else if** $t \in \mathcal{T}(\Omega_0)$
(108) **for** $ii \leftarrow 0$ **to** 4
(109) $i = IJK(t, ii)$
(110) $b_{1,i} \leftarrow_{(+)} \bar{u}_{1,i}$
(111) $b_{2,i} \leftarrow_{(+)} \bar{u}_{2,i}$
(112) **for** $jj \leftarrow 0$ **to** 4
(113) $j = IJK(t, jj)$
(114) **if** $i \neq j$
(115) $M_{ij} \leftarrow_{(+)} 0$
(116) **else**
(117) $M_{ii} \leftarrow_{(+)} 1$

6.3. Apply the iterative method for solving linear systems $M \cdot \mathbf{v}_1 = \mathbf{b}_1$ and $M \cdot \mathbf{v}_2 = \mathbf{b}_2$.

Remark 5.5.2 *$m_{ij|t}$, $r_{ij|t}$ and $s_{ij|t}$ are considered as restrictions on a particular triangle of the integrals in (4.6.4).*

Remark 5.5.3 *Particular attention is paid to the part where boundary conditions are prescribed. In lines (051)-(061) we prescribe pressure on the boundaries Γ_{in} and Γ_{out}. In the boundary-interface contact points $\partial\Sigma$ we do not prescribe boundary values p_{in} and p_{out} for the pressure but prescribe boundary value 0 for the velocity u_1. The reason why we do this comes from the model for the domain Ω_0 with extensions (2.3) where boundary-interface contact points are $\bar{\Sigma} \cap \bar{\Gamma}$. Since $u_{1|\Gamma} = 0$ then u_1 also has to be zero in boundary-interface contact points $\partial\Sigma$. In the case of the problem with the domain Ω_0 with no extensions, extra parts of the boundary Γ degenerate into the boundary-interface contact points $\partial\Sigma$. Therefore $u_{1|\partial\Sigma} = 0$ holds. We can not prescribe boundary values for the pressure in $\partial\Sigma$ because already having prescribed u_1 and u_2 it would overdefine the problem.*

5.6 Comparison of Poiseuille solutions for a symmetric mesh and a center oriented mesh

Here we consider the Stokes and the mass conservation law equations only in the channel $\Omega_0 = (0,2) \times (0,-1)$. The pressure is given on the inlet and the outlet. For this case we have an exact Poiseuille solution: the pressure is linear, the tangential velocity is quadratic and the normal velocity is zero. In Table 5.2 we present solutions that our computational method gives for each kind of mesh. We also provide some graphs to show the difference.

	Symmetric mesh		Center oriented mesh	
Parameters	**(I)**	**(II)**	**(III)**	**(IV)**
μ, K, S	1	1	1	1
p_{in}	100	100	100	100
p_{out}	0	0	0	0
N_{Ω_0,x_1}	10	20	10	20
N_{Ω_0,x_2}	10	20	10	20
N_{nodes,Ω_0}	321	1241	321	1241
$N_{\triangle,\Omega_0}$	200	800	200	800
Dim_{Matrix}	763	2923	763	2923
$\mathrm{u}_{1\Gamma_{in}}$	4.11755	4.15532	4.12043	4.15591
$\mathrm{u}_{1\Gamma_{out}}$	4.11755	4.15532	4.12043	4.15591
Order of u_2	10^{-14}	10^{-14}	10^{-2}	10^{-3}
$\int_{\partial\Omega_0} \mathbf{u_h} \cdot \boldsymbol{\nu}_0$	$-1.85037 \cdot 10^{-15}$	$-4.16334 \cdot 10^{-15}$	$1.77636 \cdot 10^{-15}$	$8.88178 \cdot 10^{-16}$

Table 5.10: Poiseuille solutions for the symmetric mesh and the center oriented mesh.

Remark 5.6.1 *Modifying the pressure finite element space by including cubic functions in the center nodes of each triangle in the channel, for the center oriented mesh, we can decrease order of the normal velocity* $\mathcal{U}_2$ *to* 10^{-13}. *In this case a condition number of the resulting matrix is of order* 10^{+17}.

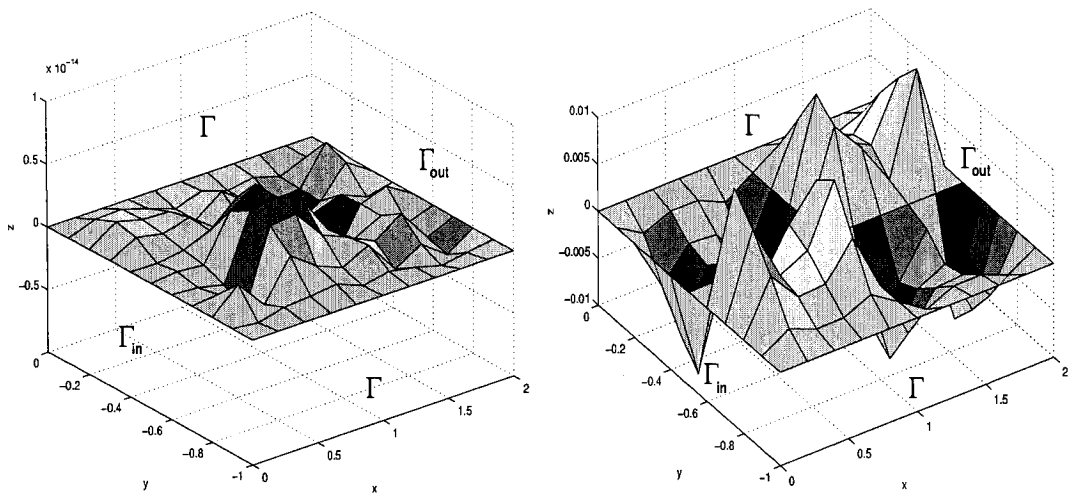

Figure 5.24: The graphs of the normal velocity u_2. The result (I) on a symmetric mesh (left). The result (III) on a center oriented mesh (right).

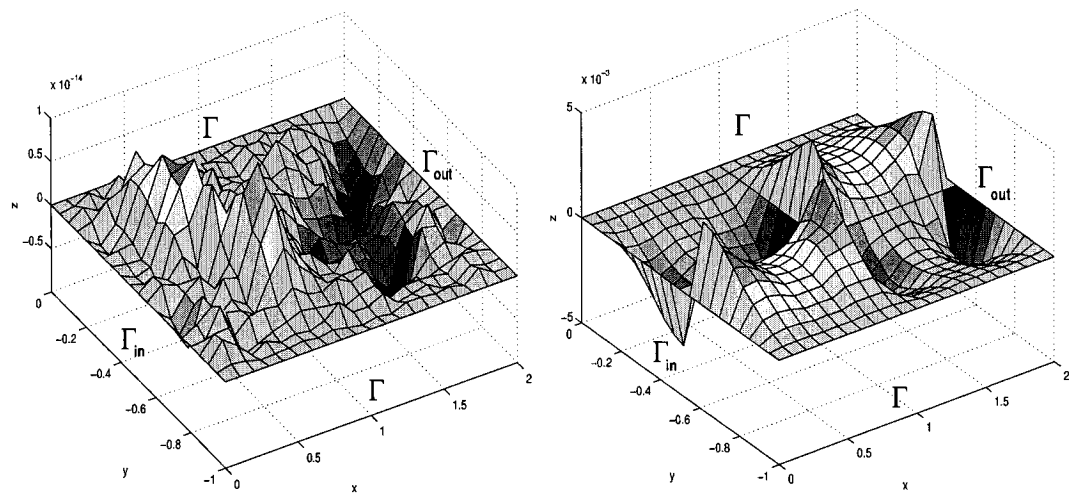

Figure 5.25: The graphs of the normal velocity u_2. The result (II) on a symmetric mesh (left). The result (IV) on a center oriented mesh (right).

6

Conclusions

6.1 Formulation of the problem

In this work we presented a model of a steady-state 2D incompressible fluid dynamics in two rectangular domains with a common boundary. The 2D model is a simplification of the Hydrogen Fuel Cell(HFC) fluid dynamics for the case of one gas component with constant molar concentration and temperature in the cross section of the cathode (or anode) of a HFC in the plane (x_2, x_3) (see on Figure 2.1). The 2D model inherits strong coupling of solutions in free air and porous domains from the full 3D HFC model. Therefore an efficient method of coupling solutions in the 2D model can be extended and applied to the full HFC model.

Our main concern here is to present a fast and efficient computational method for solving the 2D problem with real data and a coupled domain with a large aspect ratio. Our approach is not based on a domain decomposition and decoupling of solutions. Domain decomposition methods lead to many separate problems which have to be solved independently and solutions have to be coupled again, that can decrease precision. We find an approximate solution which is valid for the whole domain without preliminary decomposition and decoupling, and therefore is more accurate. Our choice is motivated by the idea to solve precisely the interface coupling.

6.2 Existence and uniqueness

We prove existence and uniqueness of the velocity solution of the problem in a weak form (see page 14). It is proved for the particular boundary conditions (3.1.2) when the velocity is prescribed on the membrane. On the interface are imposed conditions (3.1.3) with the reduced Saffman's condition $u_{1|\Sigma} = g(x_1)$. The reduced Saffman's condition includes the limit case $u_{1|\Sigma} = 0$ of the regular Saffman's condition in (2.2.7) for $S \to \infty$.

The pressure solution was excluded from the consideration by the choice of the functional space and we did not prove its existence and uniqueness.

If we use interface conditions (2.2.7) with the regular Saffman's condition instead of reduced one in (3.1.3), then we obtain the bilinear form (3.2.14) for which we cannot prove V-ellipticity. So, we cannot apply the Lax-Milgram lemma and up to this moment we do not have the existence result for the interface conditions (2.2.7).

6.3 Computational method

6.3.1 Finite element approximation

In our computational method we consider the problem (2.2.2)-(2.2.3) in the form (4.1.1) where the velocity is removed from consideration in the GDL. This approach does not require construction of a divergence free space and is simple in numerical implementation.

In our numerical implementation we use the Finite Element Method. For the finite element space in the channel we choose the velocity-pressure MINI element (see [1] D.Arnold, F.Brezzi, M.Fortin): triangle with linear basis functions which correspond to vertex nodes and a cubic basis function which corresponds to the center node. For the finite element space in the GDL we choose P_1 element: a triangle with linear basis functions corresponding to vertex nodes.

Numerical results show that this choice of the finite element space is adequate for our problem. The computational method gives an accurate numerical solution for both a model and a real domains.

Elimination of the velocity from the GDL significantly reduces overall computations. Discretization of the Darcy law equation in the GDL gives linear systems which can be solved since matrices are invertible. Therefore the velocity in the GDL can be easily restored.

We did not prove analytically that our approximation method is stable. In our case the resulting linear system, which is obtained by the finite element discretization, is complicated by boundary and interface conditions. Up to this moment we can say that only numerical results show that our method is stable.

6.3.2 Precision criterion

The criterion of how precise is our numerical solution is related to satisfaction of the mass conservation equation in the channel, in the whole coupled domain and estimation of the resulting linear system residual. After obtaining a numerical solution we compute and compare errors (4.7.2)-(4.7.3) of mass conservation in the channel and in the whole coupled domain. Numerical results show that by refining the mesh we can obtain a numerical solution with smaller error of mass conservation both in the channel and in the whole domain.

6.3.3 Boundary-interface contact points and Saffman's conditions

In order to understand the behavior of the solution in the inlet and outlet-interface contact points we also consider the same problem (2.2.2)-(2.2.3) with the same domain Ω_1 as in (2.2.1) and slightly modified domain $\Omega_0 = (0-\delta, L+\delta) \times (-H, 0)$, where $\delta > 0$ is some small constant, as it is shown on the Figure 2.3 (see page 8).

Numerical results for a model domain show that the problem with no extensions can be considered as a limit case of the problem with extensions. Particular attention is paid to the part where boundary conditions are prescribed. In the boundary-interface contact points $\partial\Sigma$ we do not prescribe boundary values p_{in} and p_{out} for the pressure but prescribe boundary value 0 for the velocity u_1. The reason why we do this comes from the model for the domain Ω_0 with extensions (2.3), where the boundary of the extended domain with $u_1 = 0$ includes points $\partial\Sigma$. So we take $u_{1|\partial\Sigma} = 0$.

Computations are made for both the regular and the reduced Saffman's interface conditions. In Remark 2.2.1 we already mentioned that the regular and reduced Saffman's conditions can be considered as "similar" if the function $g(\mathbf{x})$ in (2.2.8) is close to porosity of the GDL. In the result (II) on Figure 5.4 (see page 44) on the interface is imposed reduced Saffman's condition $u_1 = 0$. The shape of the flow is very similar to the one of the result (III) on Figure 5.5 with the regular Saffman's conditions and constant $S = 1$. The essential difference can be seen on pictures of vector field. On the vector field for the solution with the reduced Saffman's condition $u_1 = 0$ it is seen that the tangential component of the velocity is zero on the interface.

Computations were done for both cases when the pressure prescribed on the membrane is constant or it is variable. The results obtained for the model domain with a small aspect ratio show that our model and its numerical implementation is adequate, gives accurate solution and can be applied to the real domains with large aspect ratio (see pages 53 - 57).

6.3.4 Pseudocode

We present a pseudocode that is useful to trace the computational method. The pseudocode represents main steps that we use in our c++ code. Some steps, such as numerical integration and construction of linear basis functions as barycentric coordinates were omitted here since they are computed by the well known formulas. A mesh for computations can be generated inside our c++ code or read from the text file with a regular mesh format (see page 62).

6.3.5 Scaling and the mesh generation

We consider a domain which represents a cross section of a real 3D hydrogen fuel cell. So, the domain sizes, viscosity μ, the Darcy coefficient K, the Saffman's coefficient S, boundary and interface conditions are the same as those which usually are taken in

HFC models. It means that the pressure in the inlet is very large, a domain is very thin and relatively long. For these parameters it is very difficult to solve the resulting linear system because of round-off errors which are accumulated in computations and affect the numerical solution. In order to solve this problem we apply scaling.

Another problem comes from the aspect ratio of the domain. We need a finer mesh in those parts of a domain where a solution changes rapidly. In order to remove these difficulties we apply a mesh adaptation which makes it to be more appropriate for the problem (see page 51).

6.4 Iterative Gauss-Seidel overlapping block method

Our main concern here is to find a fast and efficient computational method of the problem for a domain with a large aspect ratio, at least 1:1000.

For this purpose we applied the iterative Gauss-Seidel overlapping block method for solving the resulting linear system (4.4.13). This iterative method efficiently uses block diagonal structure of the matrix (see page 32) and gives results with the same precision and much faster than the direct Gaussian Elimination method. It works for large matrices when the direct method does not work because of PC memory shortage.

We present a complete algorithm of the iterative Gauss-Seidel overlapping block method which is applied for our problem to solve the resulting linear system (see page 35). LUP decomposition with scaling reduces CPU time, PC memory consumption and is important for the precision and convergence of the iterative schemes (see page 37).

As an initial approximation in our implementation of the iterative Gauss-Seidel overlapping block method we can take: Poiseuille flow solution computed in the channel and extended to the GDL or the multigrid approximation. The multigrid approximation is obtained by assembling the resulting linear system on the coarse mesh, solving it by the direct Gaussian Elimination method and then projecting the solution to the fine mesh. On the first iteration step we apply LUP decomposition for matrix diagonal blocks and backstep substitution for solving the linear system. On the next iterations we apply only the backstep substitution method that preserves computation time.

In all our numerical experiments overlapping diagonal matrix blocks are non-singular. Iterative schemes (4.8.8) and (4.8.9) converge and give precision of the same order as the direct Gaussian Elimination method. The comparison of the iterative Gauss-Seidel overlapping block method with the direct Gaussian Elimination method shows obvious superiority of the iterative method over the direct one (see page 59). The iterative method not only provides possibility to compute faster, but also gives results for the finer mesh when the direct method does not work because of PC memory shortage.

7

Supplement

In the Supplement we present some graphs for the results from Tables 5.2, 5.3, 5.4, 5.6, 5.8. Also we present numerical results for the case when the finite element space is modified so that the basis center functions are included in the approximation for the pressure in the channel.

7.1 Graphs for a model domain

7.1.1 Graphs for a model domain with no extensions, when the pressure is constant on the membrane

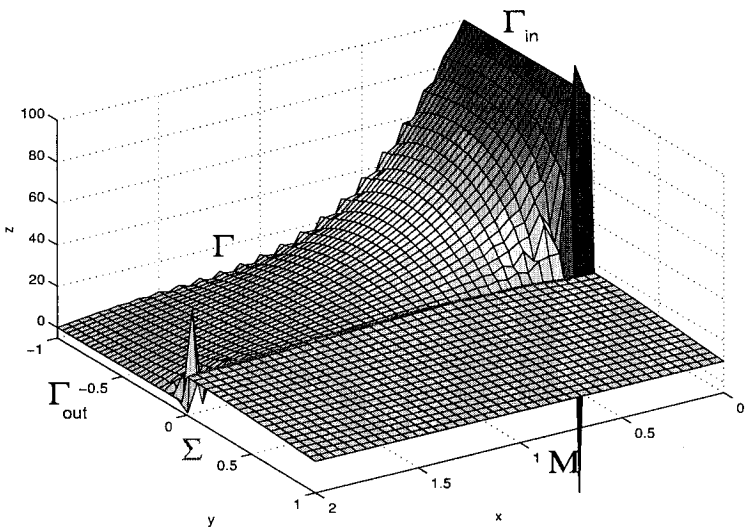

Figure 7.1: The pressure graph for the model problem for the domain with no extensions. The domain division is $N_{\Omega_0,x_1} = 40$, $N_{\Omega_0,x_2} = 28$, $N_{\Omega_1,x_2} = 20$.

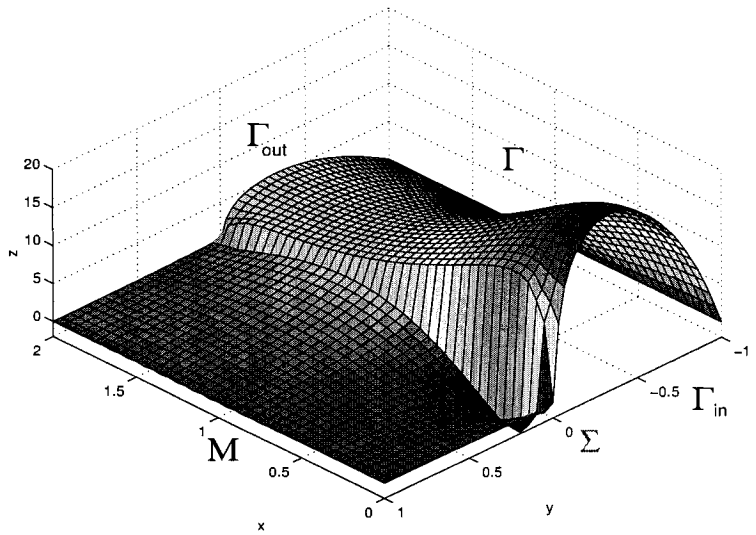

Figure 7.2: The velocity u_1 graph for the model problem for the domain with no extensions. The domain division is $N_{\Omega_0,x_1} = 40$, $N_{\Omega_0,x_2} = 28$, $N_{\Omega_1,x_2} = 20$.

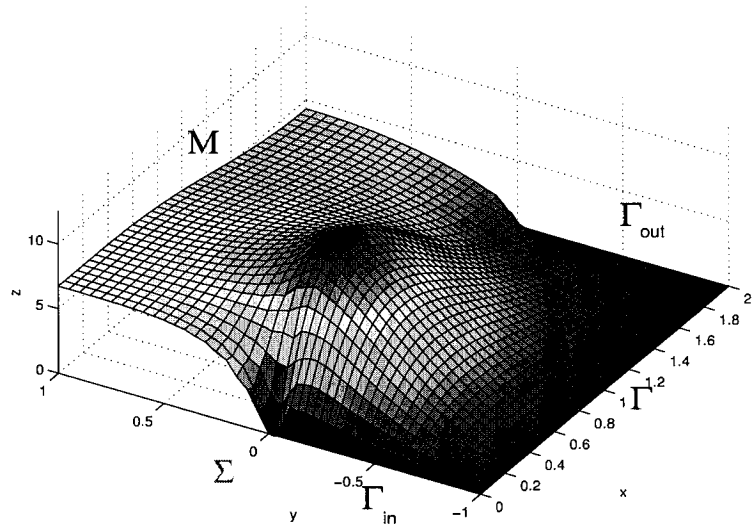

Figure 7.3: The velocity u_2 graph for the model problem for the domain with no extensions. The domain division is $N_{\Omega_0,x_1} = 40$, $N_{\Omega_0,x_2} = 28$, $N_{\Omega_1,x_2} = 20$.

7.1.2 Graphs for a model domain with extensions, when the pressure is constant on the membrane

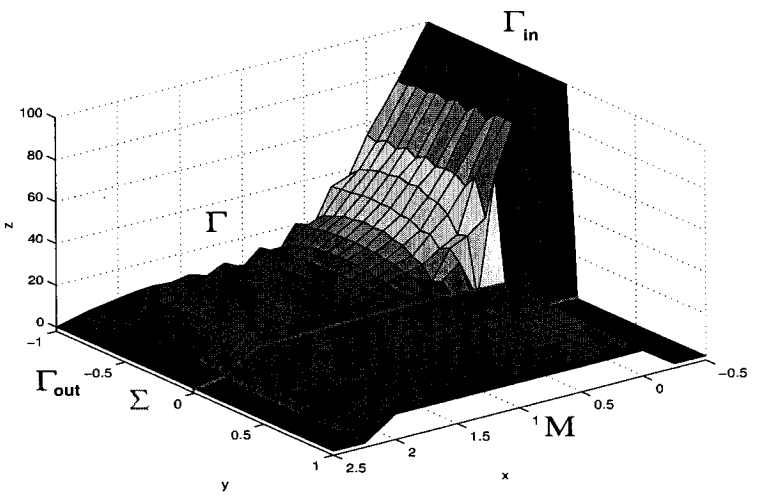

Figure 7.4: The pressure graph for the model problem for the domain with extensions. The domain division is $N_{\Omega_0,x_1} = 14$, $N_{\Omega_0,x_2} = 14$, $N_{\Omega_1,x_2} = 14$. The extensions division is $N_{ext,x_1} = 2$ and length is $L_{ext} = 0.5$.

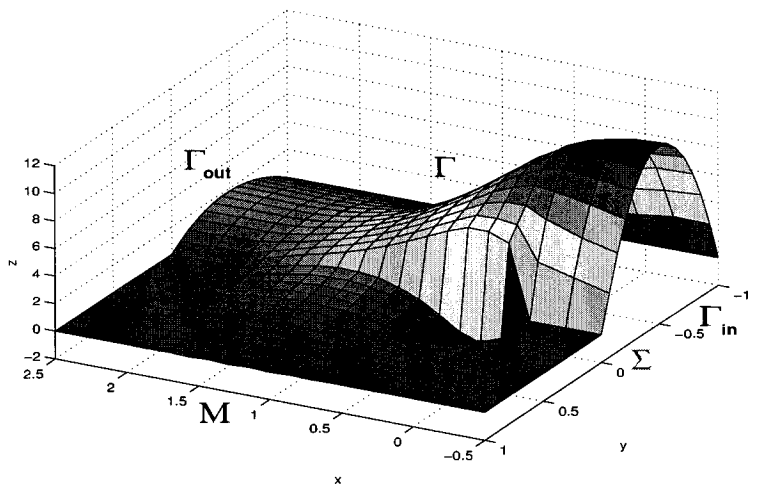

Figure 7.5: The velocity u_1 graph for the model problem for the domain with extensions. The domain division is $N_{\Omega_0,x_1} = 14$, $N_{\Omega_0,x_2} = 14$, $N_{\Omega_1,x_2} = 14$. The extensions division is $N_{ext,x_1} = 2$ and length is $L_{ext} = 0.5$.

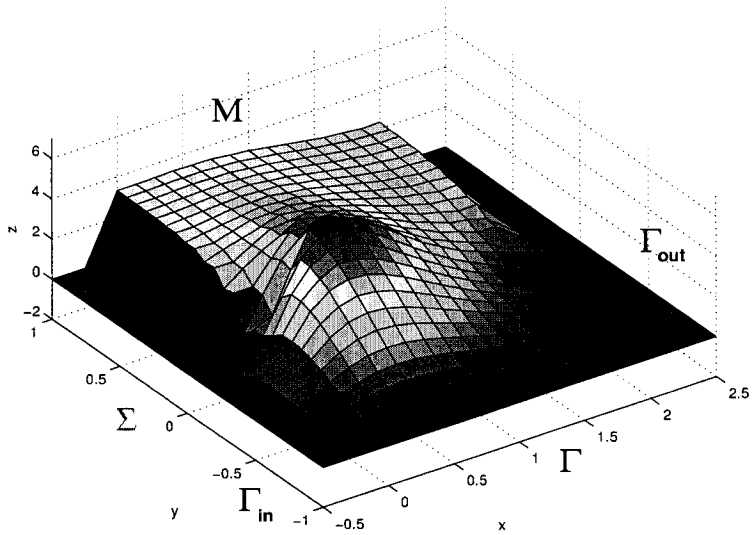

Figure 7.6: The velocity u_2 graph for the model problem for the domain with extensions. The domain division is $N_{\Omega_0,x_1} = 14$, $N_{\Omega_0,x_2} = 14$, $N_{\Omega_1,x_2} = 14$. The extensions division is $N_{ext,x_1} = 2$ and length is $L_{ext} = 0.5$.

7.1.3 Graphs for a model domain with no extensions, when the pressure is non-constant on the membrane

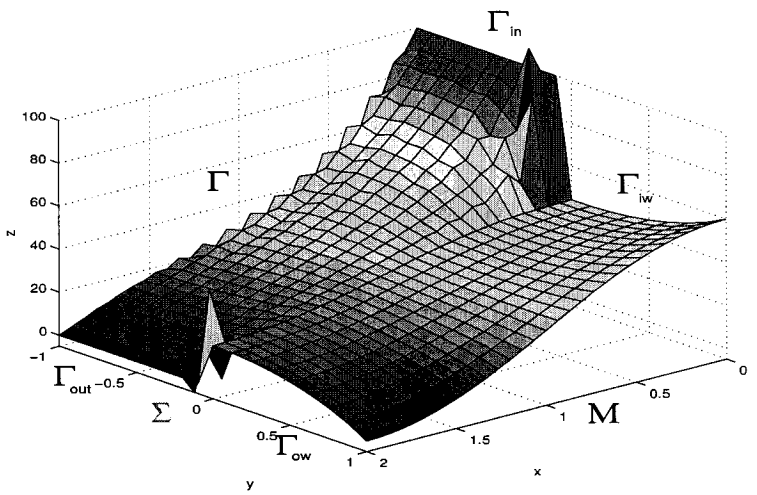

Figure 7.7: The pressure graph for the model domain with no extensions and non-constant pressure prescribed on the membrane M. The domain division is $N_{\Omega_0,x_1} = 30$, $N_{\Omega_0,x_2} = 10$, $N_{\Omega_1,x_2} = 8$. The given pressure $p_m = 30(1 + cos(\pi \frac{x_1}{l}))$ is prescribed on the membrane M.

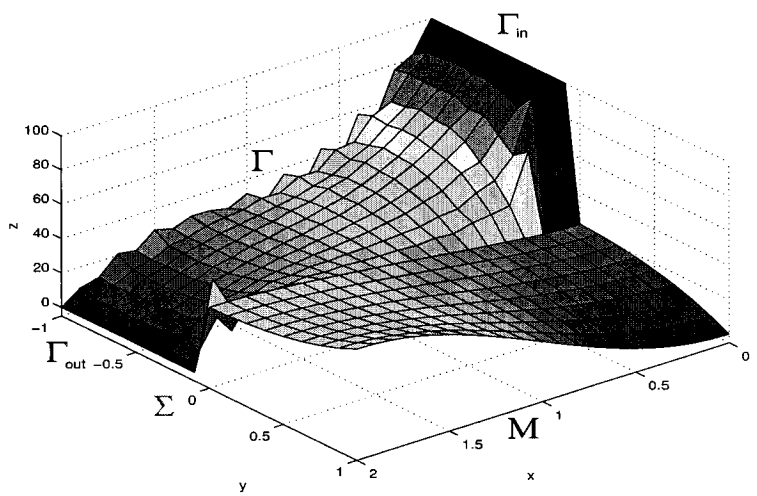

Figure 7.8: The pressure graph for the model domain with no extensions and non-constant pressure prescribed on the membrane M. The domain division is $N_{\Omega_0,x_1} = 20$, $N_{\Omega_0,x_2} = 10$, $N_{\Omega_1,x_2} = 8$. The given pressure $p_m = 30(1 - cos(\pi \frac{x_1}{l}))$ is prescribed on the membrane M.

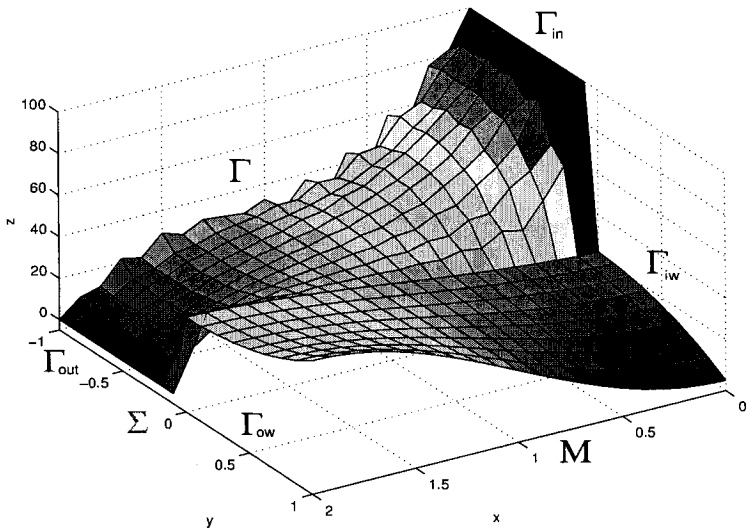

Figure 7.9: The pressure graph for the model domain with no extensions and non-constant pressure prescribed on the membrane M. The domain division is $N_{\Omega_0,x_1} = 20$, $N_{\Omega_0,x_2} = 10$, $N_{\Omega_1,x_2} = 8$. The homogeneous reduced Saffman's condition $u_1 = 0$ is imposed on the interface and the given pressure $p_m = 30(1 - cos(\pi \frac{x_1}{l}))$ is prescribed on the membrane M.

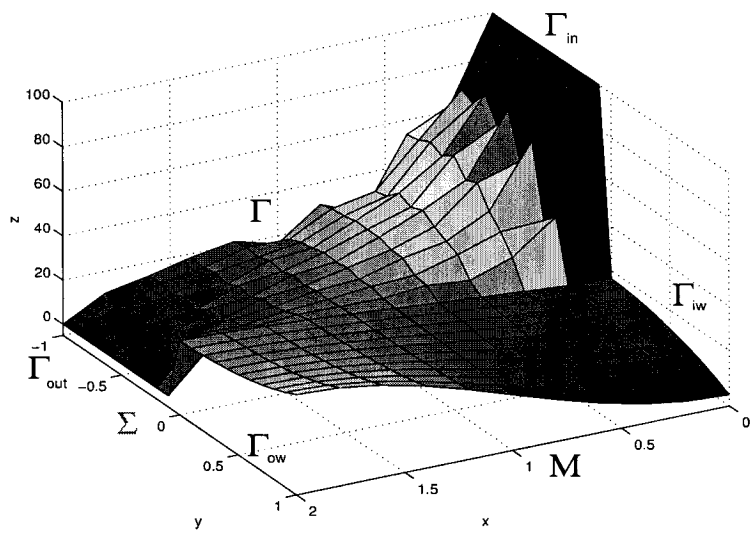

Figure 7.10: The pressure graph for the model domain with no extensions and non-constant pressure prescribed on the membrane M. The domain division is $N_{\Omega_0,x_1} = 10$, $N_{\Omega_0,x_2} = 10$, $N_{\Omega_1,x_2} = 10$. The homogeneous reduced Saffman's condition $u_1 = 0$ is imposed on the interface and the given pressure $p_m = 20(1 - cos(\pi \frac{x_1}{l}))$ is prescribed on the membrane M.

7.1.4 Graphs for a model domain when there is no flow on the membrane

Graphs of the results for a model domain with no extensions presented in Table 5.4

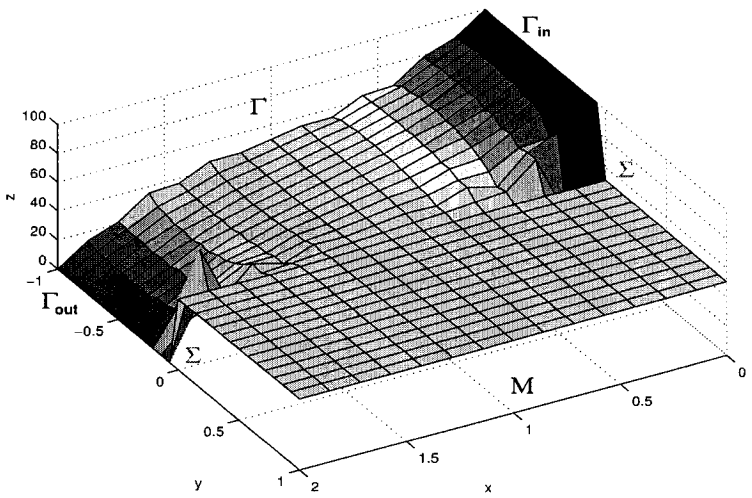

Figure 7.11: The pressure graph for the model domain with no extensions and closed boundary M. The domain division is $N_{\Omega_0,x_1} = 14$, $N_{\Omega_0,x_2} = 14$, $N_{\Omega_1,x_2} = 14$.

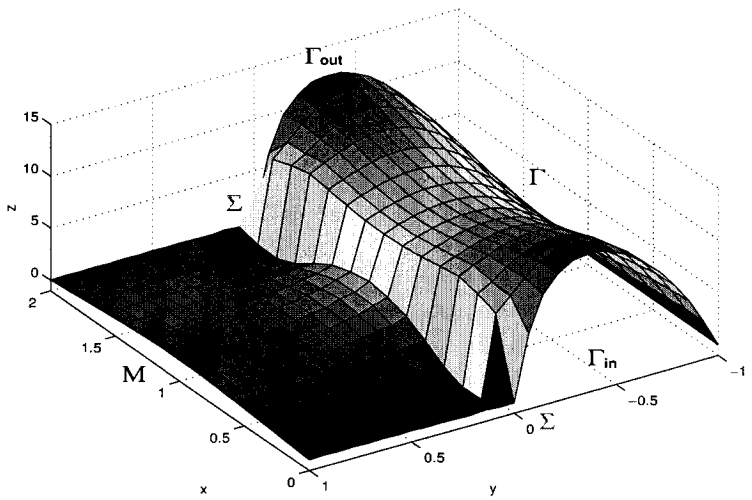

Figure 7.12: The velocity u_1 graph for the model domain with no extensions and closed boundary M. The domain division is $N_{\Omega_0,x_1} = 14$, $N_{\Omega_0,x_2} = 14$, $N_{\Omega_1,x_2} = 14$.

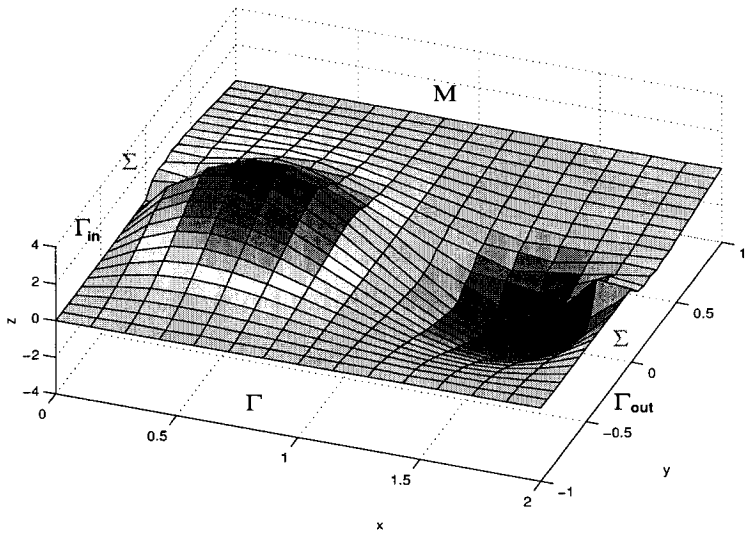

Figure 7.13: The velocity u_2 graph for the model domain with no extensions and closed boundary M. The domain division is $N_{\Omega_0,x_1} = 14$, $N_{\Omega_0,x_2} = 14$, $N_{\Omega_1,x_2} = 14$.

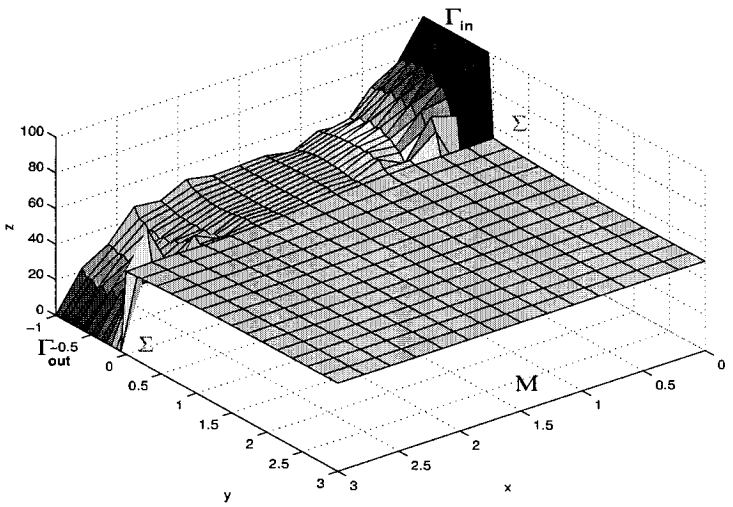

Figure 7.14: The pressure graph for the model domain with no extensions and closed boundary M. The domain division is $N_{\Omega_0,x_1} = 14$, $N_{\Omega_0,x_2} = 14$, $N_{\Omega_1,x_2} = 14$. Viscosity $\mu = 0.1$, the domain sizes are $l = 3$, $h = 3$,$H = 1$.

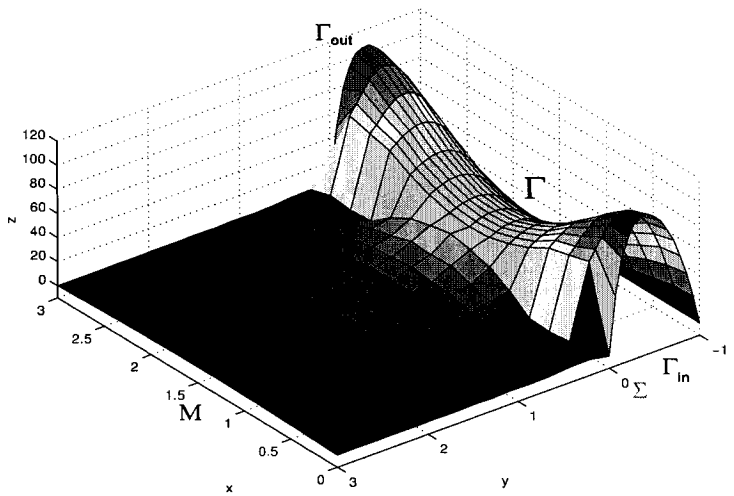

Figure 7.15: The velocity u_1 graph for the model domain with no extensions and closed boundary M. The domain division is $N_{\Omega_0,x_1} = 14$, $N_{\Omega_0,x_2} = 14$, $N_{\Omega_1,x_2} = 14$. Viscosity $\mu = 0.1$, the domain sizes are $l = 3$, $h = 3$,$H = 1$.

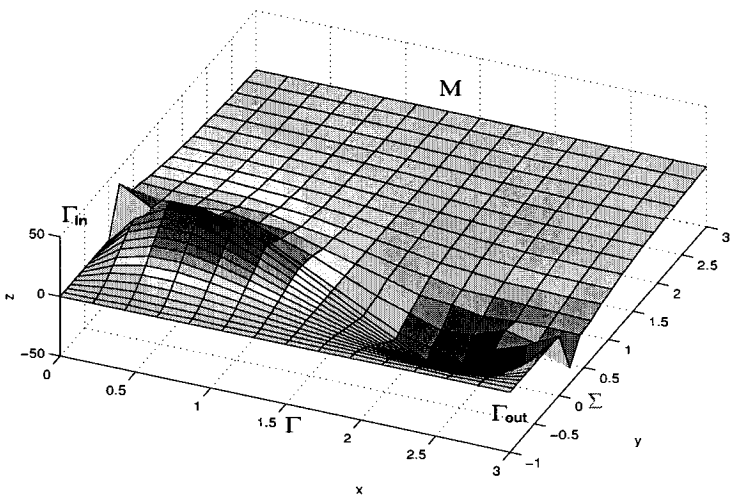

Figure 7.16: The velocity u_2 graph for the model domain with no extensions and closed boundary M. The domain division is $N_{\Omega_0,x_1} = 14$, $N_{\Omega_0,x_2} = 14$, $N_{\Omega_1,x_2} = 14$. Viscosity $\mu = 0.1$, the domain sizes are $l = 3$, $h = 3$,$H = 1$.

Graphs of the results for a model domain with extensions presented in Table 5.4

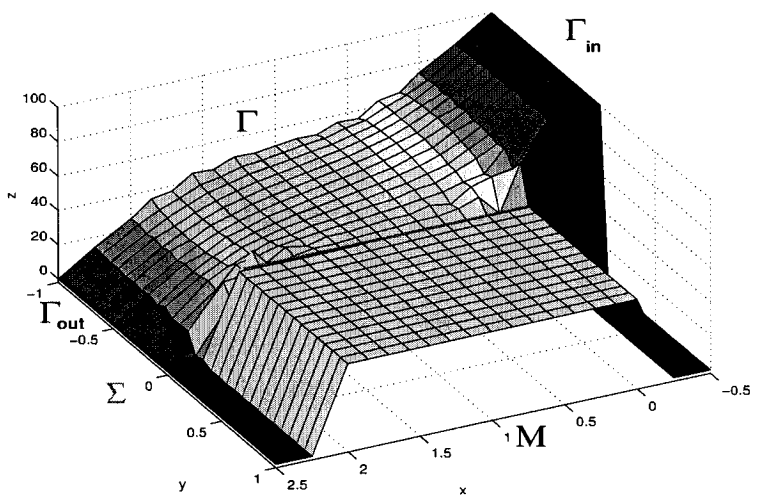

Figure 7.17: The pressure graph for the model domain with extensions and closed membrane. The domain division is $N_{\Omega_0,x_1} = 14$, $N_{\Omega_0,x_2} = 14$, $N_{\Omega_1,x_2} = 14$. Extensions division is $N_{ext,x_1} = 2$ and length is $L_{ext} = 0.5$.

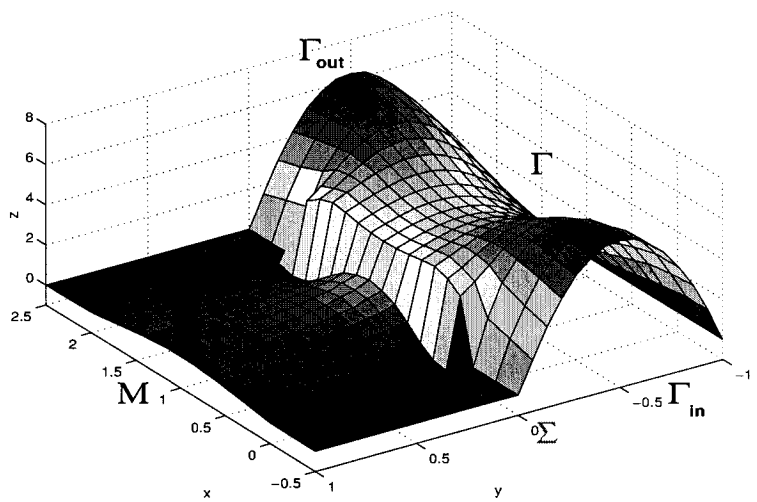

Figure 7.18: The velocity u_1 graph for the model domain with extensions and closed membrane. The domain division is $N_{\Omega_0,x_1} = 14$, $N_{\Omega_0,x_2} = 14$, $N_{\Omega_1,x_2} = 14$. The extensions division is $N_{ext,x_1} = 2$ and length is $L_{ext} = 0.5$.

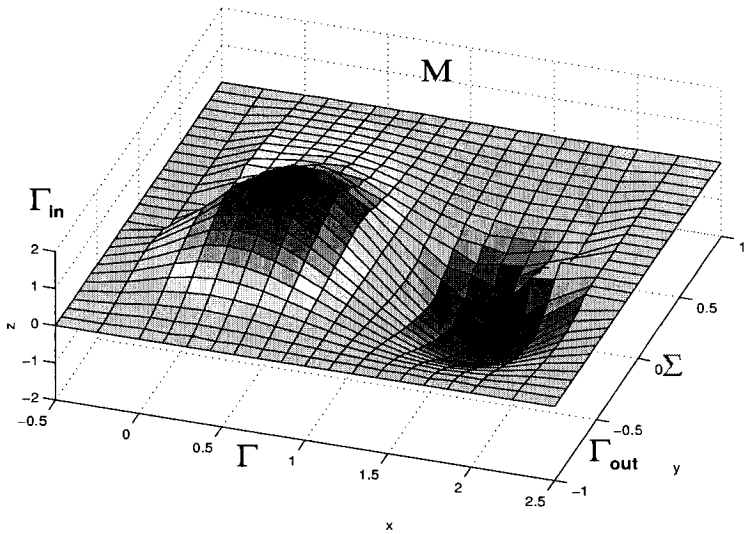

Figure 7.19: The velocity u_2 graph for the model domain with extensions and closed membrane. The domain division is $N_{\Omega_0,x_1} = 14$, $N_{\Omega_0,x_2} = 14$, $N_{\Omega_1,x_2} = 14$. The extensions division is $N_{ext,x_1} = 2$ and length is $L_{ext} = 0.5$.

7.2 Graphs for a real domain

Here we present some graphs for numerical results from Tables 5.6 and 5.7.

7.2.1 Graphs for the numerical results when the pressure is constant on the membrane

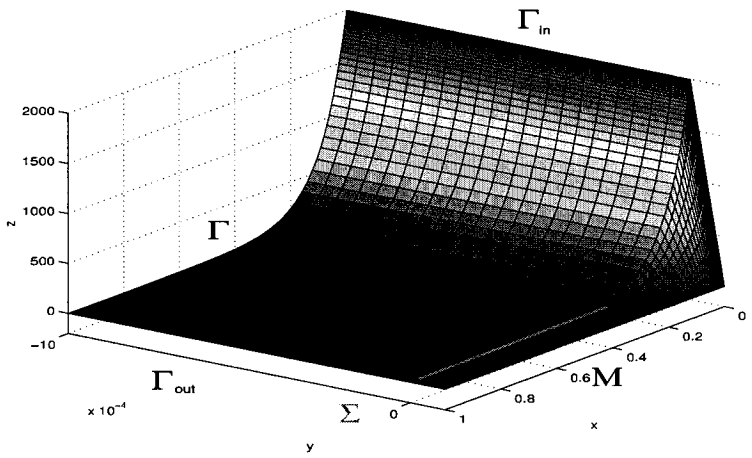

Figure 7.20: The pressure graph for the real flow. The domain division is $N_{\Omega_0,x_1} = 62$, $N_{\Omega_0,x_2} = 20$, $N_{\Omega_1,x_2} = 8$.

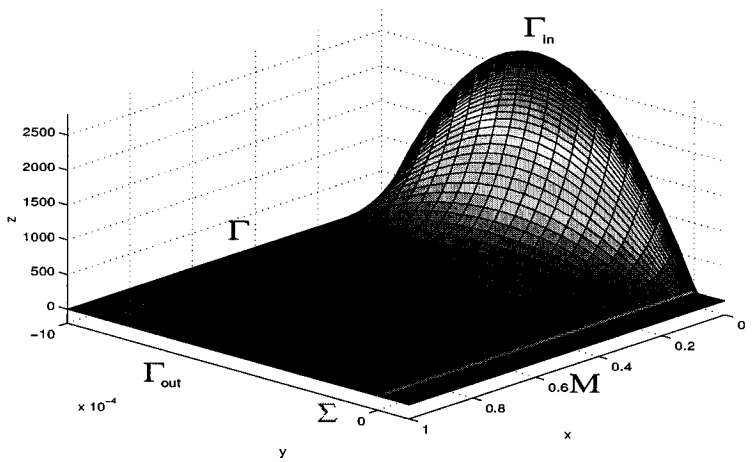

Figure 7.21: The velocity u_1 graph for the real flow. The domain division is $N_{\Omega_0,x_1} = 62$, $N_{\Omega_0,x_2} = 20$, $N_{\Omega_1,x_2} = 8$.

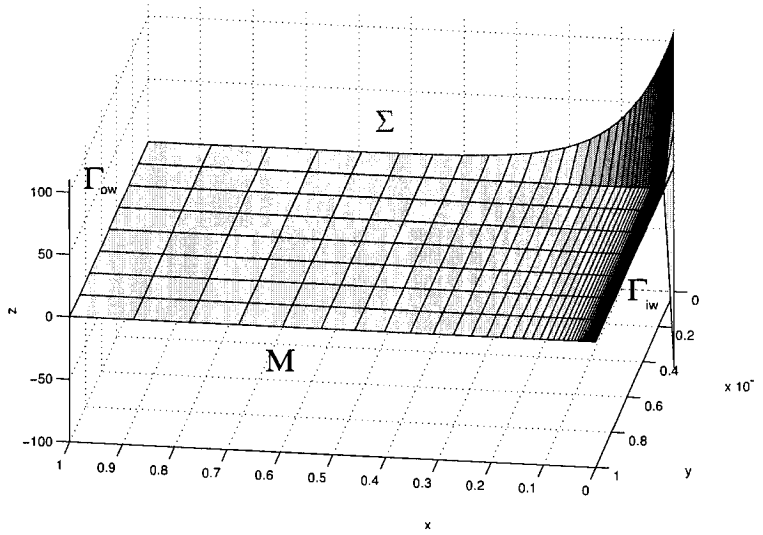

Figure 7.22: The velocity u_1 graph for the real flow in Ω_1 (GDL). The domain division is $N_{\Omega_0,x_1} = 62$, $N_{\Omega_0,x_2} = 20$, $N_{\Omega_1,x_2} = 8$.

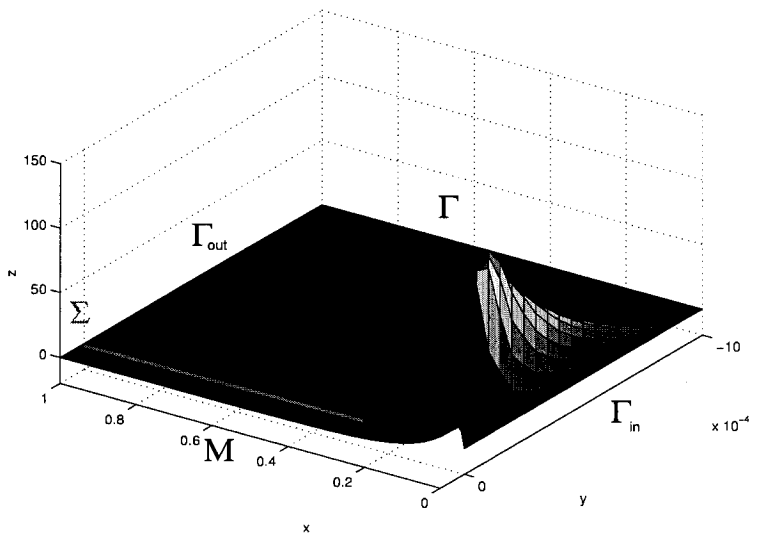

Figure 7.23: The velocity u_2 graph for the real flow. The domain division is $N_{\Omega_0,x_1} = 62$, $N_{\Omega_0,x_2} = 20$, $N_{\Omega_1,x_2} = 8$.

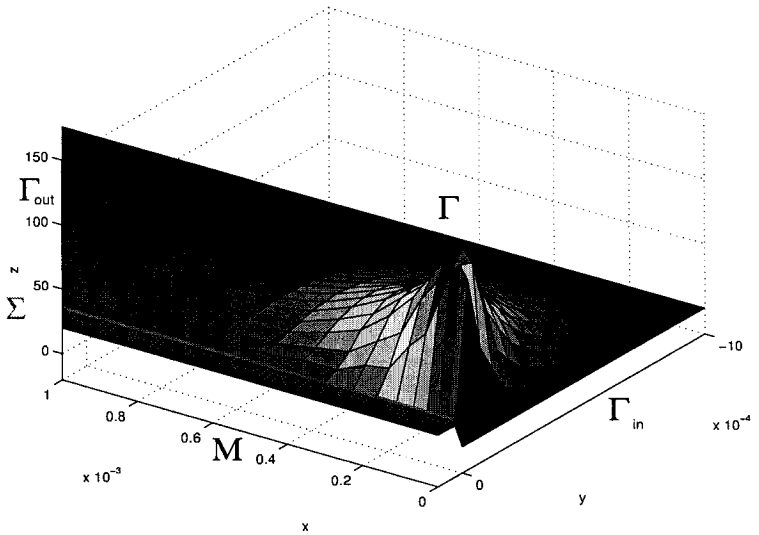

Figure 7.24: The velocity u_2 graph for the real flow with zoom close to Γ_{in}. The domain division is $N_{\Omega_0,x_1} = 62$, $N_{\Omega_0,x_2} = 20$, $N_{\Omega_1,x_2} = 8$.

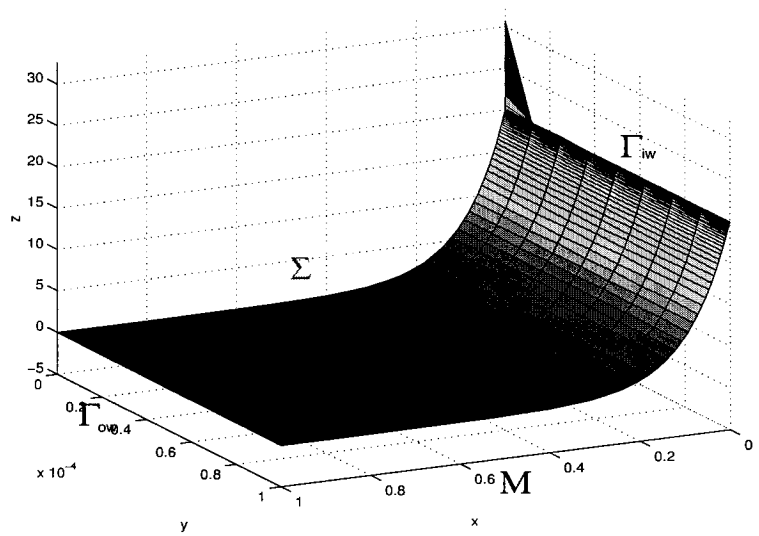

Figure 7.25: The velocity u_2 graph for the real flow in Ω_1 (GDL). The domain division is $N_{\Omega_0,x_1} = 62$, $N_{\Omega_0,x_2} = 20$, $N_{\Omega_1,x_2} = 8$.

7.2.2 Graphs for the numerical results when the pressure is non-constant on the membrane

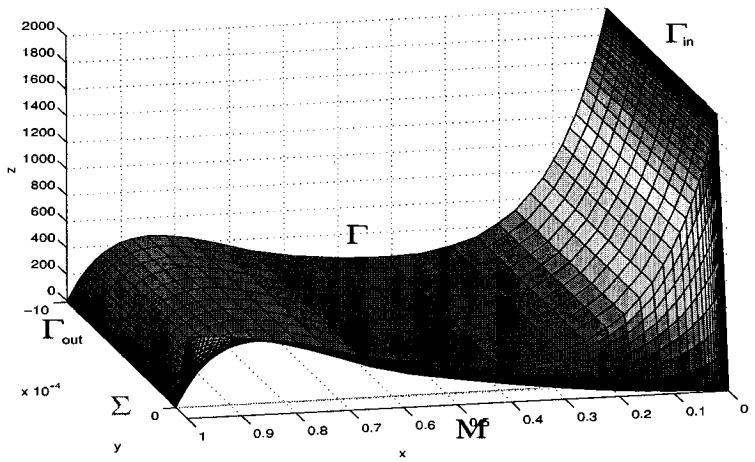

Figure 7.26: The pressure graph for the real flow. The domain division is $N_{\Omega_0,x_1} = 80$, $N_{\Omega_0,x_2} = 10$, $N_{\Omega_1,x_2} = 8$. The pressure $p_m = 300(1 - cos(\pi \frac{x_1}{l}))$ is prescribed on the membrane M.

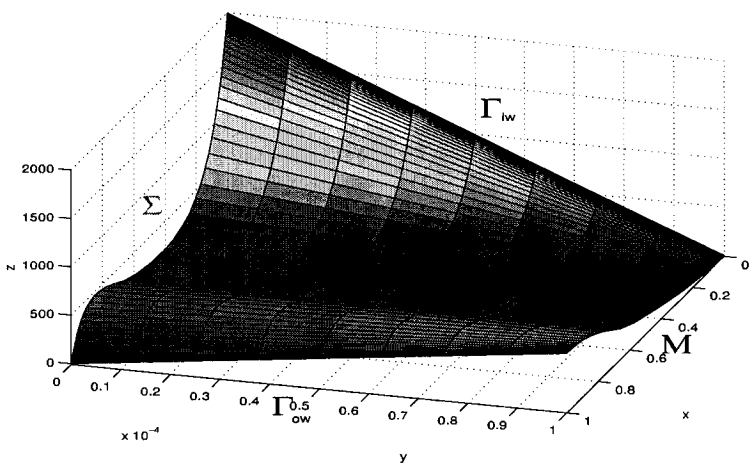

Figure 7.27: The pressure graph for the real flow in Ω_1 (GDL). The domain division is $N_{\Omega_0,x_1} = 80$, $N_{\Omega_0,x_2} = 10$, $N_{\Omega_1,x_2} = 8$. The pressure $p_m = 300(1 - cos(\pi \frac{x_1}{l}))$ is prescribed on the membrane M.

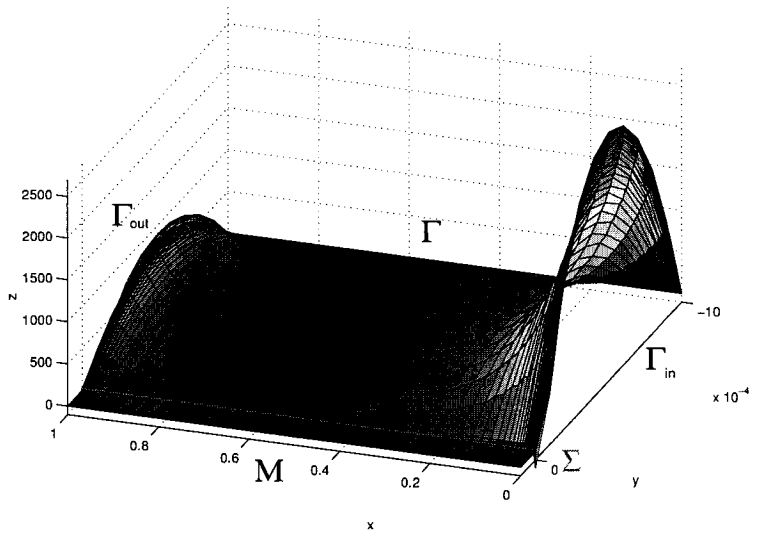

Figure 7.28: The velocity u_1 graph for the real flow. The domain division is $N_{\Omega_0,x_1} = 80$, $N_{\Omega_0,x_2} = 10$, $N_{\Omega_1,x_2} = 8$. The pressure $p_m = 300(1 - cos(\pi \frac{x_1}{l}))$ is prescribed on the membrane M.

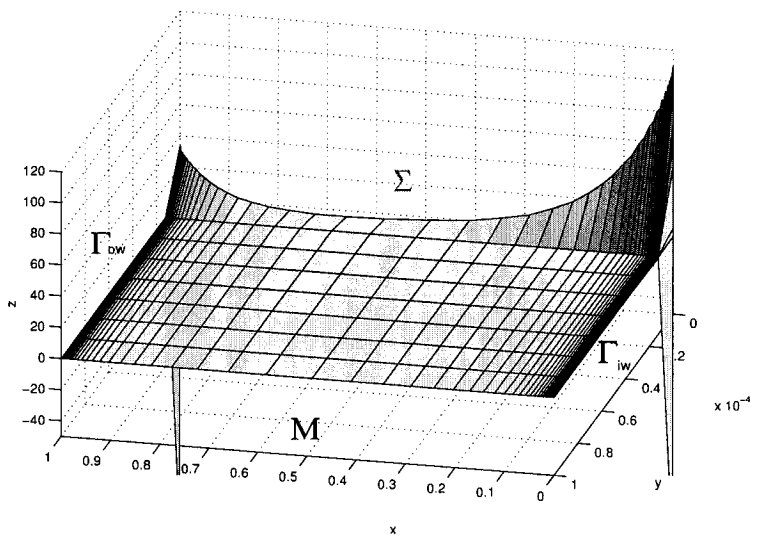

Figure 7.29: The velocity u_1 graph for the real flow in Ω_1 (GDL). The domain division is $N_{\Omega_0,x_1} = 80$, $N_{\Omega_0,x_2} = 10$, $N_{\Omega_1,x_2} = 8$. The pressure $p_m = 300(1 - cos(\pi \frac{x_1}{l}))$ is prescribed on the membrane M.

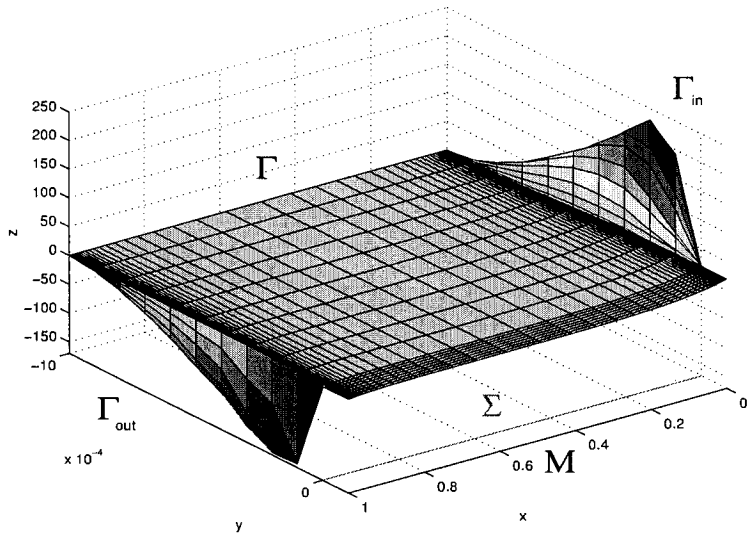

Figure 7.30: The velocity u_2 graph for the real flow. The domain division is $N_{\Omega_0,x_1} = 80$, $N_{\Omega_0,x_2} = 10$, $N_{\Omega_1,x_2} = 8$. The pressure $p_m = 300(1 - cos(\pi \frac{x_1}{l}))$ is prescribed on the membrane M.

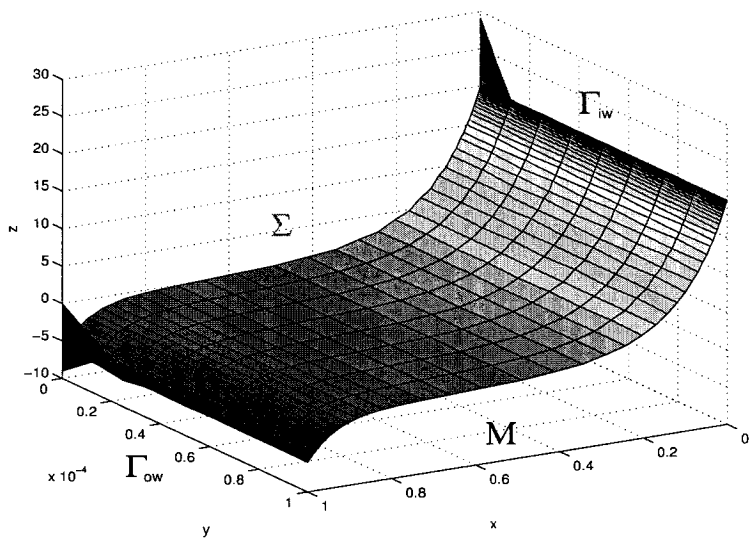

Figure 7.31: The velocity u_2 graph for the real flow in Ω_1 (GDL). The domain division is $N_{\Omega_0,x_1} = 80$, $N_{\Omega_0,x_2} = 10$, $N_{\Omega_1,x_2} = 8$. The pressure $p_m = 300(1 - cos(\pi \frac{x_1}{l}))$ is prescribed on the membrane M.

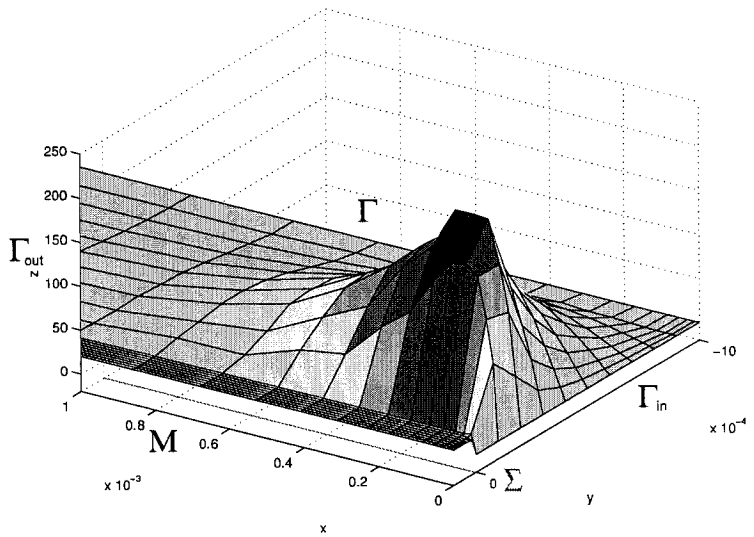

Figure 7.32: The velocity u_2 graph for the real flow with zoom close to Γ_{in}. The domain division is $N_{\Omega_0,x_1} = 80$, $N_{\Omega_0,x_2} = 10$, $N_{\Omega_1,x_2} = 8$. The pressure $p_m = 300(1 - cos(\pi \frac{x_1}{l}))$ is prescribed on the membrane M.

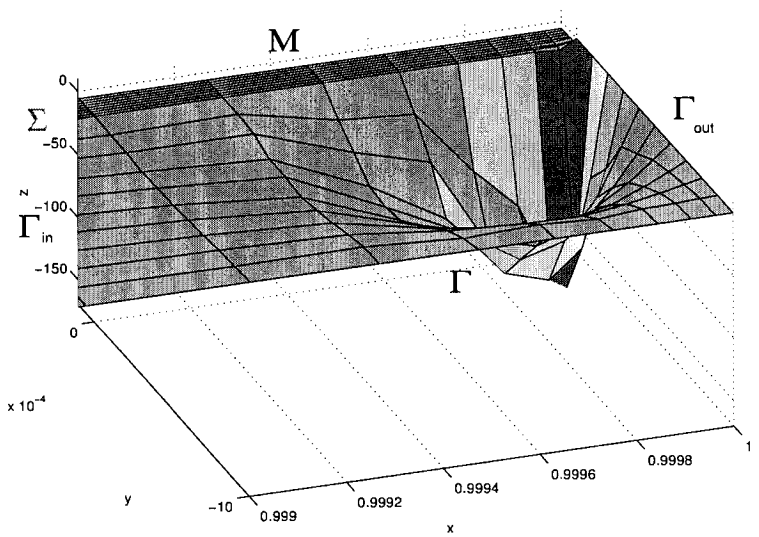

Figure 7.33: The velocity u_2 graph for the real flow with zoom close to Γ_{out}. The domain division is $N_{\Omega_0,x_1} = 80$, $N_{\Omega_0,x_2} = 10$, $N_{\Omega_1,x_2} = 8$. The pressure $p_m = 300(1 - cos(\pi \frac{x_1}{l}))$ is prescribed on the membrane M.

7.2.3 Graphs of the maximum norm of the residual and convergence ratios

Here we present graphs of the maximum norm of the residual R_n, the residual convergence ratio $\frac{R_{n+1}}{R_n}$ and the Cauchy convergence ratio $\frac{||\mathbf{X_{n+1}}-\mathbf{X_n}||}{||\mathbf{X_n}-\mathbf{X_{n-1}}||}$, for the rest of the results presented in Table 5.8 (see page 58).

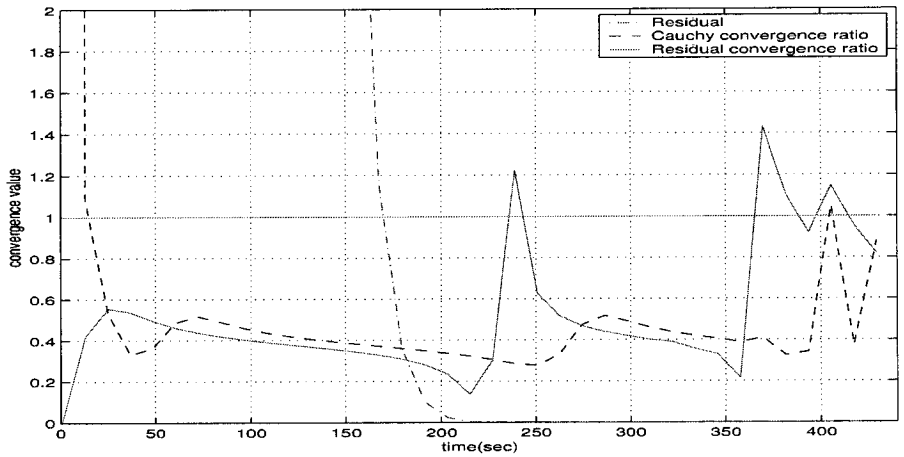

Figure 7.34: Graphs of the residual and convergence ratios for the domain division 40-12-10, N_{blocks} = 3, $N_{block,nodes}$ = 775, $N_{displ,nodes}$ = 564, Overlapping = 27 %, $N_{iterations}$ = 31, $Time_{GS}$ = 00 : 06 : 19, $Res_{GS} = 1.29 \cdot 10^{-07}$ (the result (III) in Table 5.8).

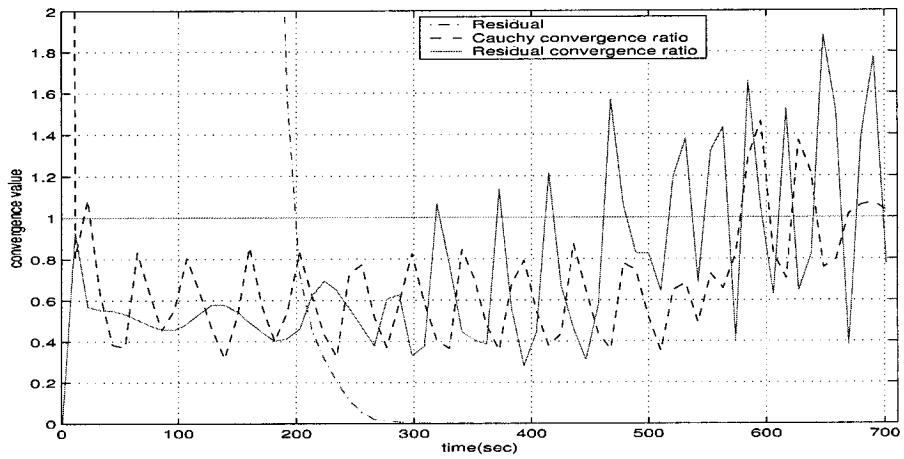

Figure 7.35: Graphs of the residual and convergence ratios for the domain division 40-12-10, N_{blocks} = 4, $N_{block,nodes}$ = 634, $N_{displ,nodes}$ = 423, Overlapping = 33 %, $N_{iterations}$ = 61, $Time_{GS}$ = 00 : 10 : 51, $Res_{GS} = 1.6 \cdot 10^{-07}$.

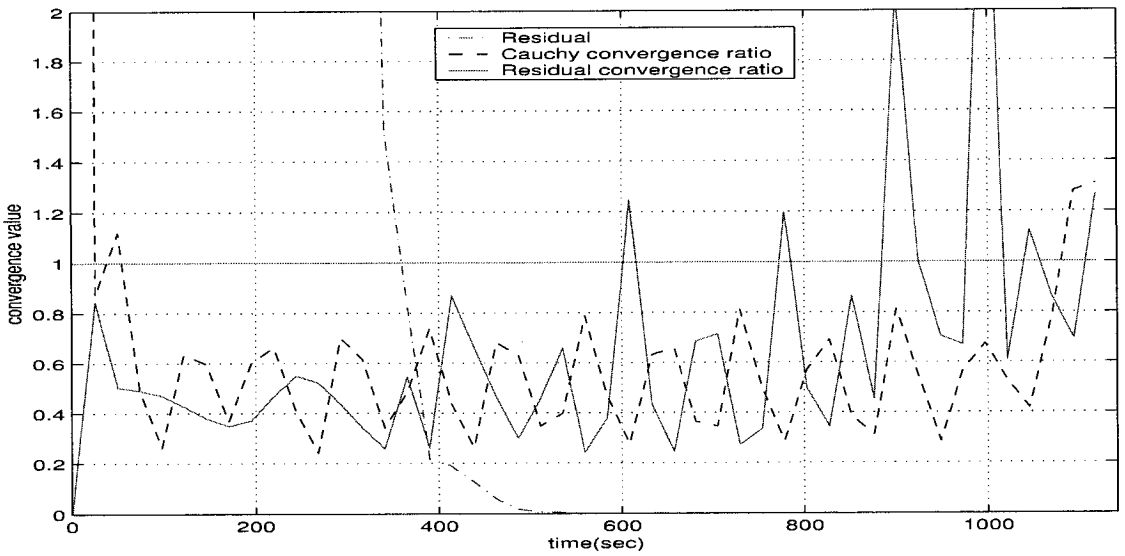

Figure 7.36: Graphs of the residual and convergence ratios for the domain division 50-14-10, $N_{blocks} = 4$, $N_{block,nodes} = 926$, $N_{displ,nodes} = 583$, Overlapping = 37 %, $N_{iterations} = 41$, $Time_{GS} = 00:16:53$, $Res_{GS} = 2.14 \cdot 10^{-07}$ (the result (IV) in Table 5.8).

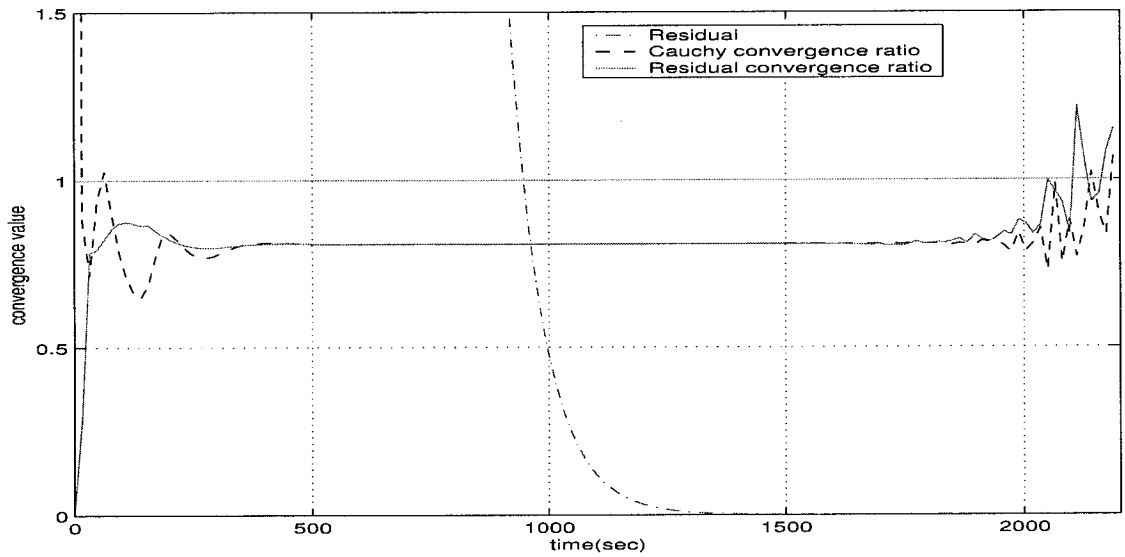

Figure 7.37: Graphs of the residual and convergence ratios for the domain division 50-14-10, $N_{blocks} = 6$, $N_{block,nodes} = 555$, $N_{displ,nodes} = 424$, Overlapping = 24 %, $N_{iterations} = 137$, $Time_{GS} = 00:35:13$, $Res_{GS} = 3.7 \cdot 10^{-07}$.

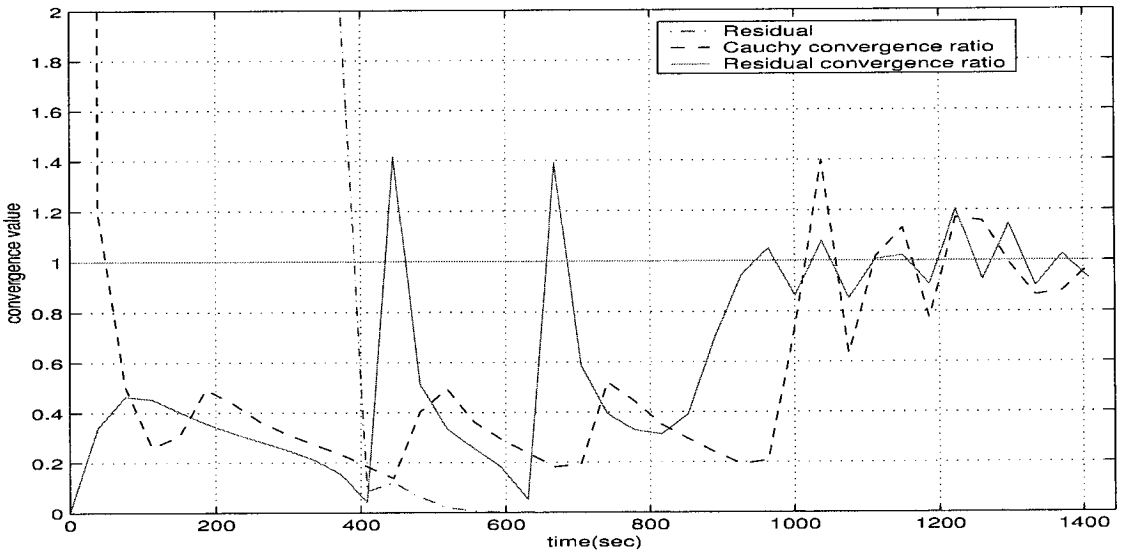

Figure 7.38: Graphs of the residual and convergence ratios for the domain division 60-14-10, $N_{blocks} = 3$, $N_{block,nodes} = 1297$, $N_{displ,nodes} = 954$, Overlapping = 27 %, $N_{iterations} = 33$, $Time_{GS} = 00:21:05$, $Res_{GS} = 3.22 \cdot 10^{-07}$ (the result (V) in Table 5.8).

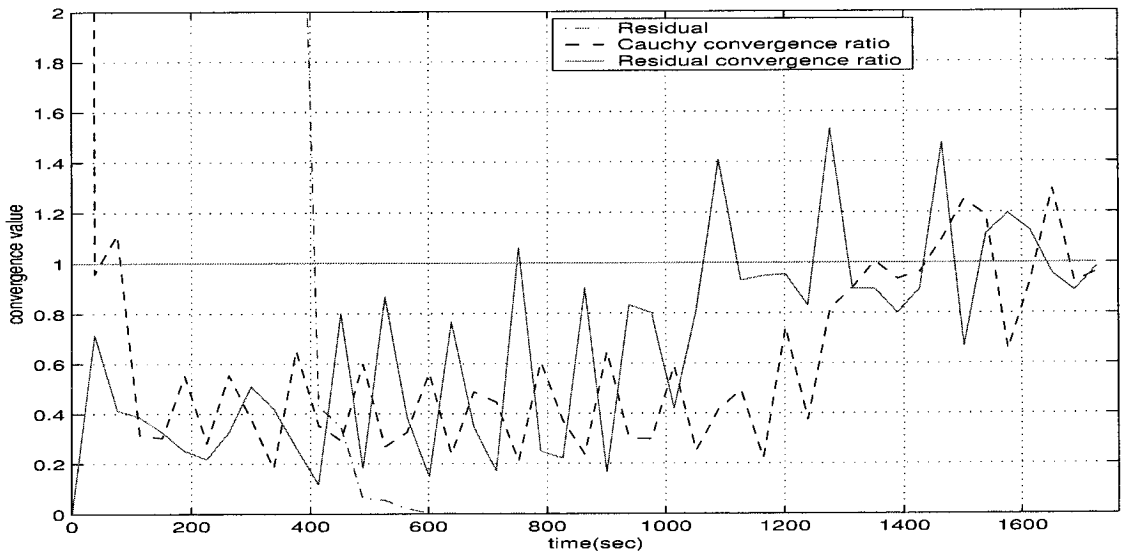

Figure 7.39: Graphs of the residual and convergence ratios for the domain division 60-14-10, $N_{blocks} = 4$, $N_{block,nodes} = 1138$, $N_{displ,nodes} = 689$, Overlapping = 40 %, $N_{iterations} = 41$, $Time_{GS} = 26:10$, $Res_{GS} = 2.3 \cdot 10^{-07}$.

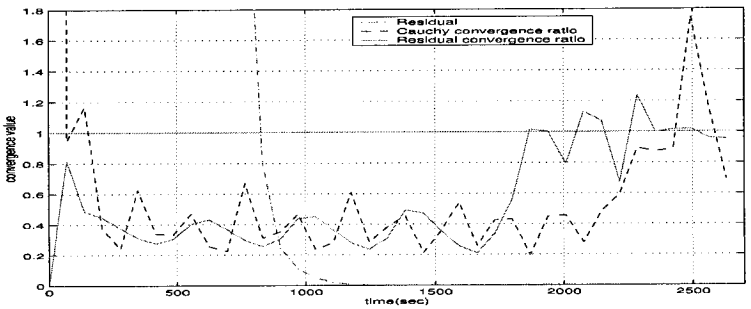

Figure 7.40: Graphs of the residual and convergence ratios for the domain division 76-16-6, $N_{blocks} = 4$, $N_{block,nodes} = 1398$, $N_{displ,nodes} = 935$, Overlapping = 33 %, $N_{iterations} = 33$, $Time_{GS} = 00:39:25$, $Res_{GS} = 1.97 \cdot 10^{-07}$ (the result (VI) in Table 5.8).

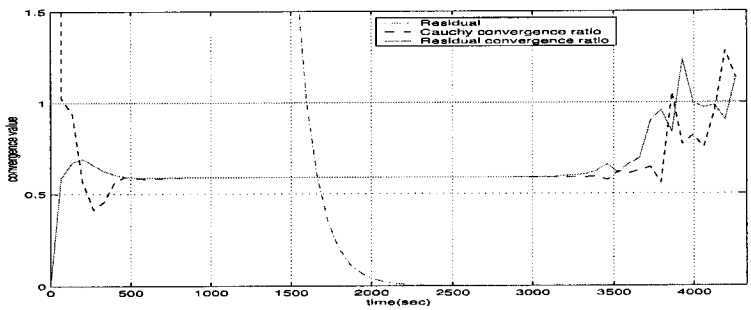

Figure 7.41: Graphs of the residual and convergence ratios for the domain division 62-20-8, $N_{blocks} = 4$, $N_{block,nodes} = 1409$, $N_{displ,nodes} = 966$, Overlapping = 32 %, $N_{iterations} = 59$, $Time_{GS} = 01:04:26$, $Res_{GS} = 9.38 \cdot 10^{-08}$ (the result (VII) in Table 5.8).

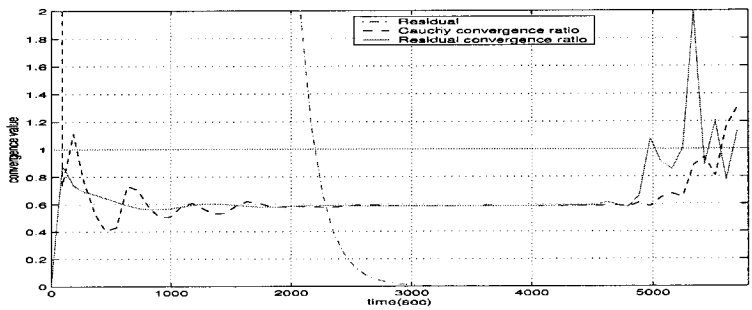

Figure 7.42: Graphs of the residual and convergence ratios for the domain division 80-16-10, $N_{blocks} = 4$, $N_{block,nodes} = 1384$, $N_{displ,nodes} = 1121$, Overlapping = 19 %, $N_{iterations} = 58$, $Time_{GS} = 01:28:52$, $Res_{GS} = 1.35 \cdot 10^{-07}$ (the result (VIII) in Table 5.8).

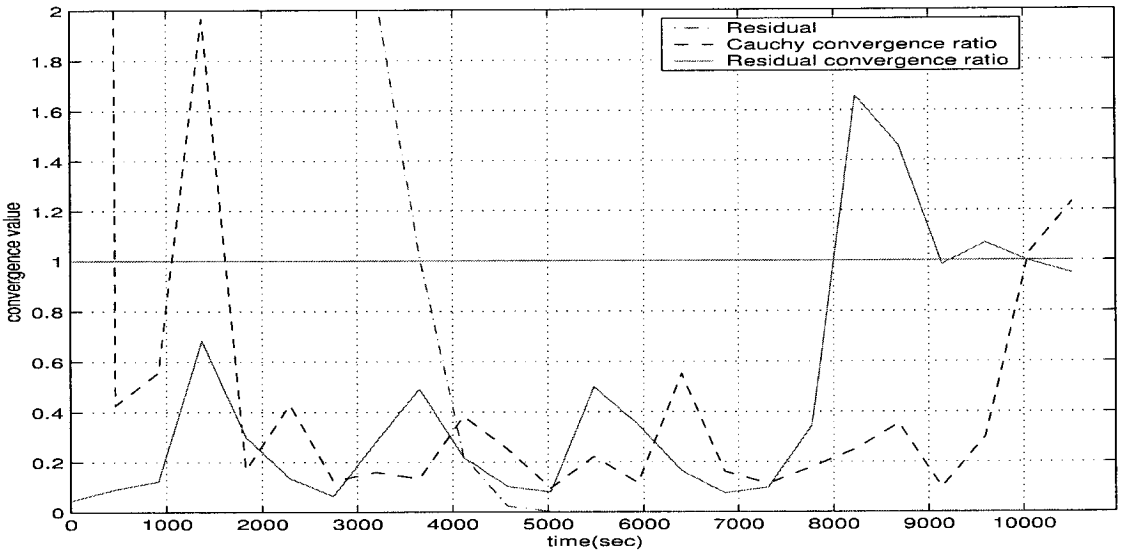

Figure 7.43: Graphs of the residual and convergence ratios for the domain division 90-16-8, $N_{blocks} = 4$, $N_{block,nodes} = 1735$, $N_{displ,nodes} = 1140$, Overlapping = 34 %, $N_{iterations} = 18$, $Time_{GS} = 02:25:05$, $Res_{GS} = 1.31 \cdot 10^{-07}$ (the result (IX) in Table 5.8).

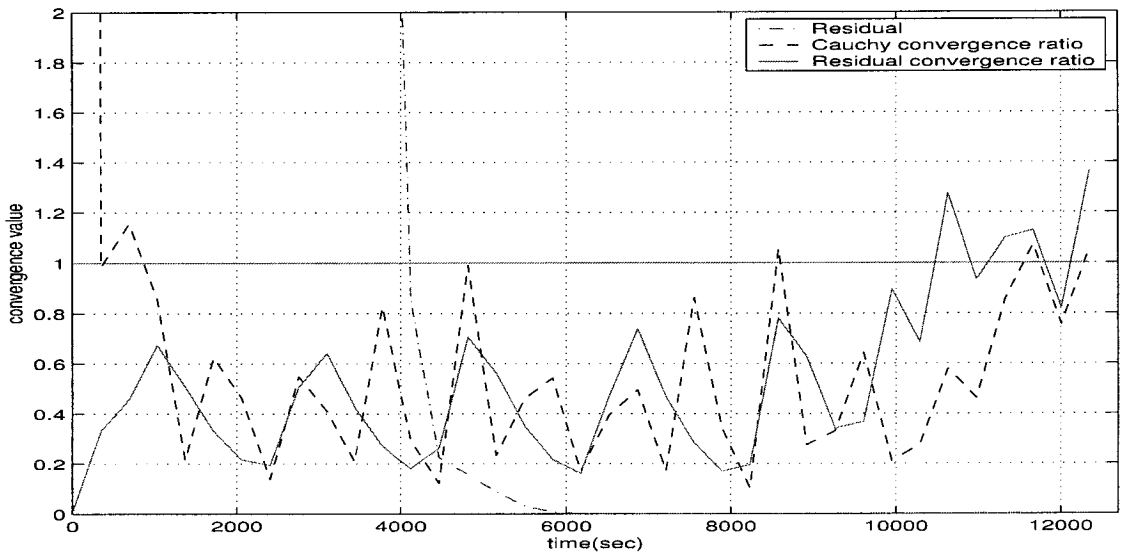

Figure 7.44: Graphs of the residual and convergence ratios for the domain division 90-16-8, $N_{blocks} = 5$, $N_{block,nodes} = 1507$, $N_{displ,nodes} = 912$, Overlapping = 40 %, $N_{iterations} = 31$, $Time_{GS} = 02:59:02$, $Res_{GS} = 6.2 \cdot 10^{-08}$.

7.3 Modification of the pressure finite element space

Here we consider the case of the finite element approximation when basis center functions are included in the approximation for the pressure in Ω_0. As it is seen on Figure 7.45 the pressure with the regular approximation is not very smooth in Ω_0, but the pressure on Figure 7.46 where center basis functions are included is smooth.

From the results in Table 7.1 it is seen that this modification of the pressure makes matrix dimension larger, very ill-conditioned and even singular. All that gives some reason to think that the source of non-smoothness of the pressure on Figure 7.45 is divergence-pressure equation in (4.1.1) which in the regular case, in a weak form, is multiplied only on linear test functions, but in the modified case it is multiplied on center basis functions also, that increases accuracy. We also compared modified and regular approximations on the "center oriented mesh" for the case of Poiseuille flow in Ω_0 and observed that deviations of the velocity u_2 from zero are of order 10^{-13} for the modified approximation and 10^{-03} for the regular one.

Divisions	$\mathbf{N}_{nodes}$	$\mathbf{N}_{triangles}$	$\mathbf{D}_{Matrix}$	$\int_{\partial\Omega_0} \mathbf{u_h} \cdot \nu_0$	**Condition number**
$3-3-3$	46	36	114	-	singular matrix
$4-4-4$	77	64	191	-	singular matrix
$5-5-5$	116	100	288	-	singular matrix
$6-6-6$	163	144	405	$-1.07288 \cdot 10^{-06}$	$2.4532559 \cdot 10^{+16}$
$7-7-7$	218	196	542	$-1.19209 \cdot 10^{-06}$	$3.2074694 \cdot 10^{+17}$
$8-8-8$	281	256	699	-	singular matrix
$9-9-9$	352	324	876	$-9.53674 \cdot 10^{-07}$	$3.3442262 \cdot 10^{+17}$
$10-10-10$	431	400	1073	$+4.76837 \cdot 10^{-07}$	$1.5233274 \cdot 10^{+17}$
$11-11-11$	518	484	1290	$-1.19209 \cdot 10^{-06}$	$6.9598013 \cdot 10^{+16}$
$12-12-12$	613	576	1527	$-4.76837 \cdot 10^{-07}$	$9.5100143 \cdot 10^{+16}$

Table 7.1: Numerical results for the model domain in the case when center basis functions are included into the finite element approximation for the pressure in Ω_0.

$\int_{\partial\Omega_0} \mathbf{u_h} \cdot \nu_0$ is the error in computation of mass conservation (4.7.1) in Ω_0 and $12-12-12$ means that $N_{\Omega_0,x_1} = 12$, $N_{\Omega_0,x_2} = 12$, $N_{\Omega_1,x_2} = 12$.

Unfortunately we do not have any results for the domain with extensions since the resulting matrices were singular.

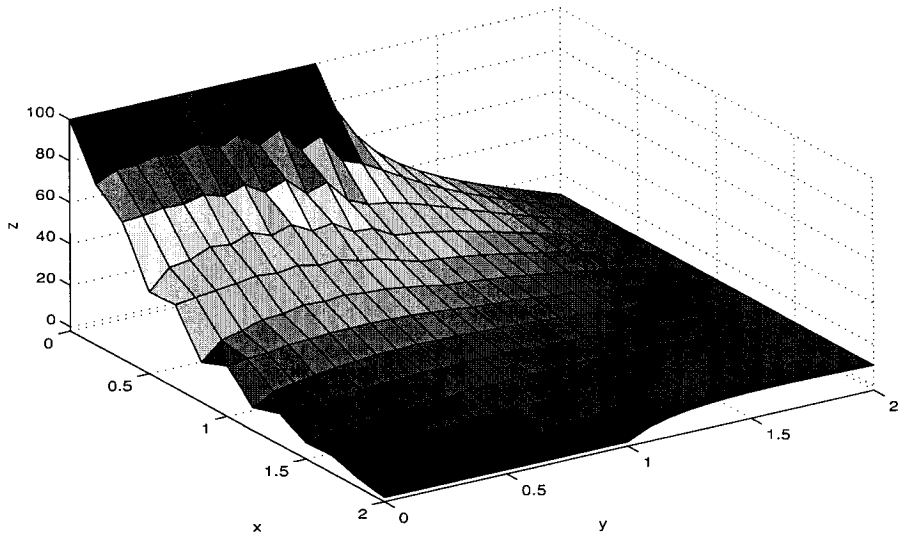

Figure 7.45: The pressure graph for the regular case when center basis functions are not included in the finite element approximation for the pressure in Ω_0. Domain division is $12-12-12$, $N_{nodes} = 613$, $N_{triangles} = 576$, *Matrix dimension* $= 1239$, $\int_{\partial\Omega_0} \mathbf{u_h} \cdot \boldsymbol{\nu}_0 = -0.074755591$, *Condition number* $= 2.505330293 \cdot 10^{+04}$.

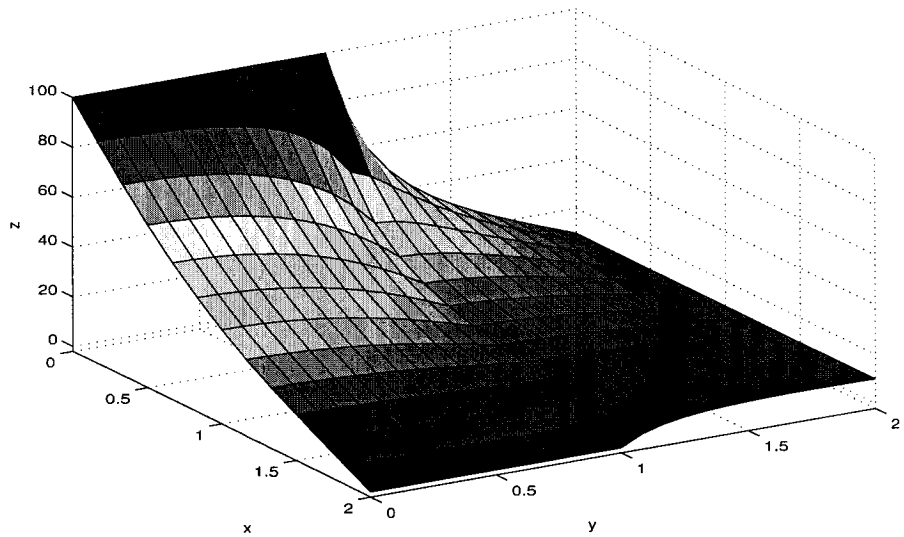

Figure 7.46: The pressure graph for the case when center basis functions are included in the finite element approximation for the pressure in Ω_0. Domain division is $12-12-12$, $N_{nodes} = 613$, $N_{triangles} = 576$, *Matrix dimension* $= 1527$, $\int_{\partial\Omega_0} \mathbf{u_h} \cdot \boldsymbol{\nu}_0 = -4.76837 \cdot 10^{-07}$, *Condition number* $= 9.51001436491 \cdot 10^{+16}$.

Bibliography

[1] D. ARNOLD, F. BREZZI, M. FORTIN. *A stable finite element for the Stokes equations.* Estratto da Calcolo Vol. XXXI, fasc. IV (Ottobre-Dicembre) 1984, pp. 337-344.

[2] K. ATKINSON, W. HAN. *Theoretical Numerical Analysis. A Functional Analysis Framework.* Texts in Applied Mathematics Vol.39, Springer-Verlag, New York, 2001.

[3] R. BRADEAN, K. PROMISLOW, B. WETTON. *Transport phenomena in the porous cathode of a proton exchange membrane fuel cell.* Heat and Mass transfer in porous fuel cell electrodes. Numerical Heat Transfer, Part A **42** (2002) 1-18.

[4] M. DELFOUR, J.-P. ZOLÉSIO. *Shapes and Geometries. Analysis, Differential Calculus and Optimization.* SIAM, Philadelphia, 2001.

[5] W. JÄGER, A. MIKELIĆ. *On the interface boundary condition of Beavers, Joseph, and Saffman.* SIAM J. Applied Mathematics, Vol. 60, No. 4, pp. 1111-1127, 2000.

[6] O.A. LADYZHENSKAYA. *The mathematical theory of viscous incompressible flow.* The series of monographs and texts. Mathematics and its Applications, V.2(1963), p.24.

[7] W. LAYTON, F. SCHIEWECK, I. YOTOV. *Coupling fluid flow with porous media flow.* SIAM J. Numerical Analysis (2003),Vol. 40, No. 6, pp. 2195-2218.

[8] A. NOVRUZI, K. PROMISLOW, B. WETTON. *3D Hydrogen Fuel Cell Fluid Dynamics Computation.* European Congress on Computational Methods in Applied Sciences and Engineering: ECCOMAS, July 2004, *Jyväskylä* 24-28.

[9] A. QUARTERONI, A. VALLI. *Numerical Approximation of Partial Differential Equations.* Springer-Verlag, New York, 1994.

[10] Y. SAAD. *Iterative Methods for Sparse Linear Systems.* Society for Industrial and Applied Mathematic, 2nd edition, April 2003.

[11] Y. SAAD, M. SCHULTZ. *GMRES: A generalized minimal residual algorithm for solving non-symmetric linear systems.* SIAM J. Sci. Statist. Comput., 7:856-869, 1986.

[12] P. G. SAFFMAN. *On the boundary Condition at the surface of a porous media.* Studies in Applied Mathematics. Vol. L, No. 2, June 1971.